Mechanical Modelling of Composites with Reinforcements in Finite Deformation

Xiaohao Shi

Thesis submitted in partial fulfilment of the requirements
of the regulations for the degree of Doctor of Philosophy

Newcastle University
Faculty of Science, Agriculture & Engineering
School of Civil Engineering & Geosciences

January 2012

Mechanical Modelling of Composites with Reinforcements in Finite Deformation

A thesis submitted in partial fulfilment for the degree of Doctor of Philosophy at Newcastle University.

By Xiaohao Shi, School of Civil Engineering & Geosciences, October 2011

ABSTRACT

Although the mechanical behaviour of particle-reinforced and fibre-reinforced composites have been studied extensively in infinitesimal deformation regime, their properties under finite deformation are still not well understood due to the complex interaction mechanisms between matrix and reinforcement, the intrinsic material and geometry nonlinearities. In this work, theoretical analysis, numerical simulation, and experimental data in the literature are employed to investigate the mechanical properties of composites with reinforcement in finite deformation.

First, a three-dimensional Representative Volume Element (RVE) is developed for neo-Hookean composite, in which the incompressible neo-Hookean matrix is reinforced with spherical neo-Hookean particles. Four types of finite deformation (i.e., uniaxial tension/compression, simple shear and general biaxial deformation) are simulated using the RVE models with periodic boundary conditions enforced. The simulation results show that the overall mechanical responses of the incompressible particle-reinforced neo-Hookean composite (IPRNC) can be well predicted by another simple incompressible neo-Hookean model. The results also indicate that the effective shear modulus of IPRNC with different particle volume fraction and different particle/matrix stiffness ratio can be well predicted by the classical linear elastic estimation.

In the second half of the study, the significance of the fibre-matrix interaction in the Human Annulus Fibrosus (HAF) is identified and analysed in detail. Based on the experimental results in the literature it is shown that the mechanical behaviour of the matrix can be well simulated by the incompressible neo-Hookean type model, but the effective stiffness of the matrix depends on fibre stretch ratio, which can only be explained by fibre-matrix interaction. Furthermore, it is found that this interaction takes place anisotropically between the matrix and the fibres distributed in different proportions in different directions. The dependence of the tangent stiffness of the matrix on the first invariant of the deformation tensor can also be explained by this fibre orientation dispersion.

Acknowledgements

Firstly, I would like to thank my supervisor Dr. Zaoyang Guo particularly for his supervision and guidance throughout my PhD. He is erudite in the research area and always patient and ready to help, I could not be able to complete my research without his support. I also want to express my thanks to Dr. Philip Harrison, Dr. Henrik Gollee, Dr. Huabing Yin, Dr. Sylvie Coupaud and Dr. Aleksandra Vuckovic from University of Glasgow for their kind advices and help during the first and second year of my PhD study, and Prof. Peter Gosling from Newcastle University for his kind support during the third year.

My parents are supporting and encouraging me all the time and they are the most important people to me. I would not be able to come here, study and finish my PhD without them on my side. I want to dedicate this thesis to my parents.

I want to thank the people who I worked with during the past three years. It is great to have you around discussing questions and problems, sharing experience and helping me out with difficulties, and I really appreciate all the help and company from you all. My thanks also go to my dearest friends, Yue Cui, Hsiu-yu Ku, Yueling Wang, Miao Wang, Lu Gan, Xiang Liu, Siyang Wang, Zhixiong Hu and Hongbin Zhang, and life could be so dull and boring without you.

I gratefully acknowledge the financial support from Chinese Scholarship Council, University of Glasgow and Newcastle University, I would not be able to come to UK and have my PhD study here without their supports. In return, I will go back to China after graduation to serve my country.

Last but not least, I also want to thank the secretaries and technicians in CeG and SAgE in Newcastle University, as well as in the Department of Mechanical Engineering and Department of Civil Engineering in University of Glasgow, only their dedicate work guaranteed the perfect research environment, which is indispensable to good research.

Contents

List of figures and tables

uniaxial compressions are plotted against $I_1 - 3$. The data is fitted by $\overline{W} = 0.7459(I_1 - 3)$ (solid line).

Figure 3.7 Average strain energy $\overline{W}$ vs. $I_1 - 3$ for the 20 uniaxial tension/compression simulations of 4 RVE models ($c = 0.2, \mu_r = 10$). The linear fitting curve is plotted in solid line.

Figure 3.8 An RVE model with 5 vol% of rigid particles (a) and its deformed shape after uniaxial tension (b).

Figure 3.9 Simulation results of an RVE model with 5 vol% of rigid particles. The theoretical nominal stress-strain curve from the effective shear modulus is plotted as a dotted line in each figure.

Figure 3.10 Average strain energy $\overline{W}$ vs. $I_1 - 3$ for 4 numerical simulations of an RVE model with 5 vol% of rigid particles. The linear fitting curve is plotted as a solid line.

Figure 3.11 The effective shear moduli computed from numerical homogenisation for IPRNC with rigid particles and the SAE, SCE, and TPM predictions.

Figure 3.12 The nominal stress-strain curves of an RVE ($c = 0.1, \mu_r = 100$) for uniaxial tension (a), uniaxial compression (b) and simple shear (c) simulations respectively, while the obtained strain energy $\overline{W}$ is plotted against $I_1 - 3$ in (d).

Figure 3.13 The effective shear moduli computed from numerical homogenisation for IPRNC with $\mu_r = 100$ and the SCE, TPM predictions.

Figure 3.14 All the $\overline{W}$ vs. $I_1 - 3$ data from 34 FE simulations (9 biaxial, 3 simple shear, 12 uniaxial tension and 10 uniaxial compression simulations) for the IPRNC $(c = 0.2, \mu_r = 10)$ are fitted by the linear relation $\overline{W} = 1.496(I_1 - 3)$ ($R^2 = 0.9998$).

Figure 3.15 The effective shear moduli computed from numerical homogenisation for IPRNC with $\mu_r = 10$ and the SCE and TPM predictions.

Figure 3.16 The nominal stress-strain curves are shown in (a), (b) and (c) for uniaxial tension, uniaxial compression and simple shear simulations respectively, while the obtained strain energy $\overline{W}$ is plotted against $I_1 - 3$ for an RVE ($c = 0.3, \mu_r = 0.5$) in (d).

Figure 3.17 The effective shear moduli computed from numerical homogenisation for IPRNC with $\mu_r = 0.5$ are compared with the SCE and TPM predictions.

Figure 3.18 Simple “one particle in the centre” unit cell model

Chapter 1 Introduction

As a fundamental problem of reinforced composite, predicting the overall mechanical behaviour of the composite based on the mechanical properties of the constituents and microstructure is very important for understanding and characterizing the material. The aim of this thesis is to model and analyse the mechanical behaviour of composites with reinforcement under finite deformation, and both particle-reinforced composite (PRC) and fibre-reinforced composite (FRC) will be discussed. The mechanical performance of incompressible particle-reinforced neo-Hookean composite under finite deformation will be investigated numerically, while the significance of the fibre-matrix interaction in the Human Annulus Fibrosus (HAF) will be identified by studying the experimental data, theoretical constitutive models and the numerical simulation results in literature. In this chapter, a broad background of composite material is introduced in section 1.1 with focus on composites with reinforcement. In section 1.2, classical models for the mechanics analysis of composites with reinforcement in infinitesimal deformation regime are briefly explored, while the literature related to mechanics of composites with reinforcement in finite deformation regime is reviewed sketchily in section 1.3. The objective and the structure of the thesis are provided in the last two sections.

1.1 Composites with reinforcement

1.1.1 General composite

In order to meet the basic and advanced needs of human living and development, various kinds of substances are acquired and extracted from the natural world by chemical reactions or physical combinations. In chemical reaction, the bonds in the molecules are broken and new chemical will be composed by reconstructing the atoms or ions; while the physical combination just combine two or more substances into a new material without any change on the molecular level of each substance.

Composite material is a concept with respect to simple material, and it is not easy to define it adequately due to the structural complexity. Generally speaking, a material system, which consists of a mixture or a combination of two or more distinctly differing materials which are insoluble in each other and differ in form or chemical composition, is defined as composite material. Figure 1.1 presents the schematic diagram of a composite material with 2 different phases [1], one of which is usually discontinuous (and stiffer and stronger), and is called the reinforcement phase. The other phase is called the matrix phase, which is usually continuous (and less stiff and weaker).

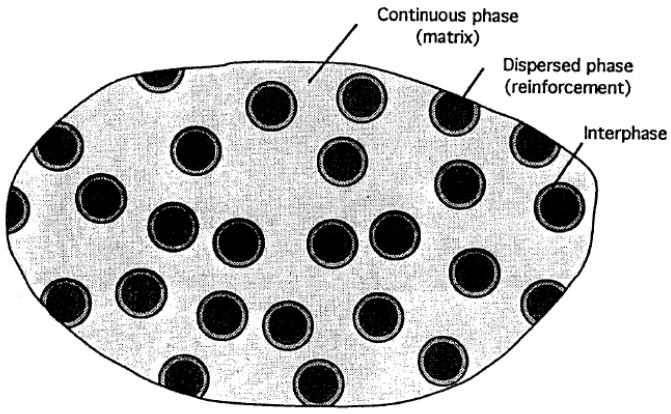

Figure 1.1 Schematic diagram of the composite phases [1].

Dating back to the ancient Egyptians, the application of fibre-reinforced materials has experienced a really long development in human history. People used mud, clay and straw to build bricks, which can be considered as the primary application of fibre-reinforced composite in the structural field [1, 2]. In Roman times, mortar and concrete were produced on large scale to construct vaults, domes and foundations [2]. The modern steel concrete originated from the 1800s, when iron rods were put into masonry as reinforcements [1]. The great development of composite materials started in the 20th century. In 1940s, the fibreglass and reinforced plastics were first developed and put into practice. Later on, filament winding, carbon fibres, metal matrix composites were introduced, and till the end of the 1970s, composites had been widely applied in many areas, such as aircraft, automotive, sporting products and biomedical devices [1]. Nowadays, large civil aircrafts, automotive industry, turbine blades and ground transportation facilities become the new hotspots for composite applications [3], and those developments are pushing forward the development of composite. Many natural materials, such as soft tissue and wood, can be considered as composite materials.

According to different criteria, composite can be classified into different categories, such as structural composite and functional composite based on their functions; resin-based, metal-based and ceramic-based composite based on the different ground (matrix) materials. Another way to categorize composite is grounded on the microstructures of the composite. The constituents compose separate phases of composite, and usually one of the components is the ground base material (matrix phase), inside which other materials (reinforcement phase(s)) are randomly or sequentially distributed. Some molecular force or chemical interactions will form the bond between inclusions and matrix material, and sometimes it is considered as a separate phase and referred as interphase. There are several important aspects in the microstructure of a composite such as the inclusion's shape, the dispersion condition and the volume fraction of inclusions. The volume fraction, the inclusion distribution pattern and the properties of each phase have significant influence on the mechanical performance of the composite.

Composites with single material reinforcement phase inside the matrix are considered to have two phases. Various two-phase composites have been widely used in industry. Because the geometry of inclusions varies from one composite to another, the two-phase composite can be roughly categorised into three groups according to the inclusion geometry, type, and orientation, which are particulate filler reinforced material, discontinuous fibre or whisker reinforced material and continuous fibre-reinforced material. Normally, composites with different types of inclusions would present distinct mechanical behaviours. The particle-shaped inclusions, such as sphere, ellipsoid and platelet, will normally enhance the strength and stiffness of the composite. Normally, the volume fraction of inclusions is smaller comparing to that of the matrix and the inclusions are distributed inside the matrix, so the matrix material is exposed to the main load and contributes more to the stiffness of the composite. On the other hand, long and continuous inclusions, such as fibres, are the main support of the composite, while the matrix material becomes the protection substance to the relatively flexible fibres. The particle-reinforced composite (PRC) and the fibre-reinforced composites (FRC) will be the main focus of the thesis: a simple PRC is modelled in chapter 3, while soft tissue investigated in chapter 4 is considered as a type of FRC.

Consisting of two or more solid phases, composites usually have some advantages over monolithic materials, including high strength, high stiffness, low density, environmental stability, better fatigue properties, more flexible, anti-corrosion, biocompatibility,

superior thermal and electrical properties, being adaptable to desired functional requirement of the structure (e.g., can make the composite strong in a particular direction). For example, in industry, rubber particles are added into brittle materials, like polymers, to improve their tensile strength; fibre reinforcements are adopted in polymers to increase the bulk modulus. Due to the advanced performances, composite have been widely adopted in many engineering areas (e.g., aeronautics and astronautics, biomaterials, automobile, etc.) and new composite materials are developed to satisfy new requirements in industry.

Except for those advantages mentioned above, composites have their own limitations and shortcomings. Composites are the combination of two or more materials and are usually anisotropic, which makes it complicated to identify and model the mechanical behaviours comparing with the conventional materials. The common methods are not good enough to measure and represent the composite's properties and behaviours accurately, which may limit the application of composites. Due to its superior properties, composite is always used in critical circumstances, which makes it important to monitor the conditions of the material. Sometimes it is not simple to detect internal changes in composites and extra techniques are adopted to detect damages and potential material failure. In addition, high cost, complex manufacturing techniques and tools for composite may affect the applications as well.

1.1.2 Composites with reinforcement

As mentioned above, modelling, characterisation and analysis of the mechanical properties of composite materials (particularly the anisotropic composite materials) are very challenging. The focus of this work is to model and analyse the mechanical behaviours of the PRC and the FRC under finite deformation. In this subsection, the concepts of PRC and FRC will be further discussed.

Particle-reinforced composite (PRC)

The reinforcement is treated as particle when all its dimensions are similar. Particle-reinforced materials have been extensively used in industry in the past few decades, and one of the common applications is rubber tire, which has carbon-black particles added to normal rubber matrix. From the structural point of view, the dispersed particles

obstruct the deformation of the whole composite, and could enhance the stiffness of the composite, but the matrix will bear the main deformation because normally the stiffness ratio between particles and matrix is far bigger than 1. We note that the rubber tire can undergo large deformation and this type of composite's mechanical behaviour will be investigated in Chapter 3.

The mechanical performance of the PRC is closely related to the volume fraction of the inclusions, the size, shape and distribution of the particles, and the stiffness ratio between the inclusions and the ground matrix. For example, for the incompressible matrix with rigid particles, the overall effective modulus of the composite only depends on the stiffness of matrix and volume ratio [4], if the influence of the size, shape and distribution of the rigid particles are reasonably ignored.

Fibre-reinforced composite (FRC)

As a very important material in engineering applications, the use of fibre-reinforced materials has been growing rapidly in the last few years [5]. This type of material has been applied into many fields, including aircraft, automobile, boat, chemical, furniture, equipment, electrical product and sport products. Take helicopter rotor blade for example, the blades of helicopter rotor were made of wood and fabric originally; later, the adoption of steel and aluminium greatly improved the performance of the previous design, but the fatigue resistance and the strength/density ratio are not satisfactory among many other deficiencies. Then, carbon fibre-reinforced composite brings many advantages compared to metal, such as easy to manufacture, high strength/density, as well as low cost.

Due to the wide application of the FRCs, it is crucial to characterise its mechanical performance in order to better exploit it. There are several parameters which will affect the mechanical properties of the FRC, such as the volume fraction, the length and orientation of the fibres, the effective diameter of fibre cross section, the stiffness ratio between the fibres and the matrix. According to the fibre length, FRC can be divided into two categories, namely the discontinuous fibre-reinforced composite and the continuous fibre-reinforced composite. For both types of FRCs, the fibre orientation can be unidirectional or randomly distributed. Composites with fibres of randomly distributed orientation may be considered as quasi-isotropic because from the

macroscopic point of view, the overall mechanical properties of the composite are the same regardless the measuring directions. Meanwhile, composites with unidirectional fibres, no matter they are continuous or discontinuous, the material is usually anisotropic, which means the mechanical behaviour of the material depends on the measuring direction. Normally, the stiffness and the strength can be quite different from the along-fibre direction and the direction perpendicular to the fibre direction. Generally, fibres are used to improve the mechanical performance of the matrix phase, so the stiffness ratio between the fibres and the ground matrix is normally greater than 1. In this case, larger stiffness ratio will lead to larger changes in the stiffness and strength of the composite comparing to the original ground matrix material based on the same geometry. For the same reason, larger fibre volume ratio will enhance the stiffness of the composite more significantly. However, the volume ratio should be controlled within certain range due to the composite stability requirements. Biological soft tissues, such as muscle, ligament, tendon, skin and human annulus fibrosus, are modelled as fibre-reinforced materials in order to study their mechanical performance due to their similar structures (e.g. [6, 7]).

1.2 Mechanics of composites with reinforcement in infinitesimal deformation

The major aim of composite mechanics is to characterise, model and analyse the mechanical behaviours of composite materials. The methods used in composite mechanics can be categorised into three types: theoretical methods, numerical methods and experimental methods.

One important objective of composite mechanics is to predict and model the mechanical behaviours of composite materials provided that the properties of each constituent are known. Many theoretical methods have been developed to estimate the overall macroscopic mechanical behaviours of composites (sometimes named as “effective mechanical properties” or “average mechanical properties”) based on the properties of the constituents. Here only the following classical theoretical approaches are briefly discussed: the mechanics of materials approach, variational methods, direct prediction models, and semi-theoretical, semi-empirical approach.

The so-called “mechanics of materials” approach assumes either uniform strain or uniform stress in the solid phases and leads to two simple models, i.e., the parallel

(Voigt) model (assuming uniform strain field) and the series (Reuss) model (assuming uniform stress distribution). Because these two models do not consider the microstructure of the composites, their predictions of composite stiffness are usually not close to the real behaviours of composites. However, it can be derived that the stiffness obtained by series model (the load direction is vertical to the material layer so the stress field is homogeneous) is a lower bound, while the parallel model (the load direction is parallel to the material layer so the strain field is homogeneous) predicts an upper bound.

To get better bounds on effective properties of composite material, different variational methods based on energy principles have been proposed in the literature [8-11]. Because the microstructure of the composites can be considered in these variational methods, for some properties (e.g., effective longitudinal modulus E_1 for unidirectional fibre-reinforced composites), the upper and lower bounds obtained by variational methods are close to each other, which implies that they provide a good estimation of properties of the composite materials. But for some properties like the effective transverse modulus E_1, the difference between the bounds estimated by variational methods is quite large and neither of them provides a good approximation to the properties of the real composites. Nevertheless, the bounds derived from variational methods can be used to check the validity of the effective properties of composites predicted by other theoretical methods.

Because variational methods can only provide bounds rather than the direct estimation of the effective properties of composites, other theoretical models have been developed in the literature to obtain direct predictions of the effective properties of composites. Hill [12-16] proposed the famous self-consistent model for composites with reinforcement, and it was soon adopted by other researchers (e.g., [17]). Christensen and Lo [18, 19] improved the self-consistent model to the so-called “three phase model”, in which the composite element (with reinforcement phase and matrix phase) is embedded in an infinite homogeneous medium whose properties are identical to the effective properties of the composite (i.e., the properties to be obtained). Classical elasticity theory is used in these self-consistent type models to derive closed-form solutions for the effective properties of composite materials. Mori and Tanaka [20] estimated the effective elastic properties of the PRC based on mean-field approximation. Theocaris and Sideridis [21] used a composite-unit cell model to investigate the static

and dynamic elastic moduli of PRC with isotropic-elastic particles and linear viscoelastic matrix phase. Ravichandran [22] approximated a two-phase composite with discontinuous reinforcements by a unit cell model incorporating isostrain and isostress elements to estimate the effective elastic moduli and the Poisson's ratios of the composite. Bourkas et al. [23] predicted the static and dynamic elastic constants of PRC using a theoretical cube-within-cube model. Torquato [24, 25] derived the third-order approximation for effective elastic properties of PRC. Recently, Jiang et al. [26] proposed a three-phase confocal elliptical cylinder model to predict the effective elastic properties of the FRC. In their models, the variations in fibre section shapes and randomness in fiber section orientation are taken into consideration by a generalised self-consistent method. Ju and Yanase [27] developed a micromechanical framework to estimate the effective elastic moduli of PRC. In their analysis, the near-field particle interactions are accounted, and the anisotropy of reinforced particles can be considered.

The direct prediction models sometimes lead to very complex formulae for effective properties of composite materials and these results are usually difficult to use in engineering. To circumvent this difficulty, Halpin and Tsai [28] proposed a consistent form to estimate all effective properties of composite materials with different microstructures. This famous Halpin-Tsai formula represents a judicious interpolation between the series and parallel models (that is, the upper and lower bounds), which provides the formula solid theoretical basis. Only one parameter is employed in the Halpin-Tsai formula to consider various effects such as the influence of the reinforcements' shape, distribution, and the reinforcing efficiency. Because this parameter can be determined by experimental data, this approach is usually named as semi-theoretical, semi-empirical approach.

Simplifications of the microstructure are usually assumed in the theoretical approaches to make the closed-form solutions possible in the related elastic problems. Therefore it is difficult for the theoretical models of composites to fully consider the effect of complex microstructures in real composite materials. For example, the interaction effects between fibres in FRC are usually neglected by most theoretical models, which lead to the underestimation of the effective properties for the FRCs with higher fibre volume fractions. Similarly, it is also very difficult to consider the nonlinear behaviours of the constituents in theoretical models. To overcome these problems, numerical approaches using finite difference, finite element, or boundary element methods have

been adopted by researchers to simulate the mechanical behaviours of composites. For example, Jaensson and Sundstorm [29] determined the Young's modulus and the Poisson's ratio for WC-Co alloys using finite element method (FEM). Tessier-Doyen et al. [30] used four FEM software to simulate the mechanical responses of the PRC and found that the obtained numerical predictions are close to the lower bound of the Hashin and Shtrikman's model [10]. Llorca and Segurado [31] developed a modified random sequential adsortion algorithm to generate three-dimensional cubic unit cell models with particle volume fractions up to 50%. The mechanical responses of the representative volume element (RVE) models were simulated by FEM using periodic boundary conditions and the effective elastic properties of the PRC were obtained. They found that both the third-order approximation [25] and the three-phase model [18] match the numerical results very well. The concept of Representative Volume Element (RVE) was first proposed by Hill [14]. According to his description, the particular microstructure of the composite is essential and important to carry out the calculation and define RVE [32]. As an idealized volume from a material, piled RVEs should be able to regain the material structure both microscopically and macroscopically as a special case.

One of the important problems in numerical approaches is to find the required size of the RVE in FEM simulations to obtain accurate results. Drugan and Willis [33, 34] proved that a small size RVE model can well predict the effective mechanical properties of linear elastic PRC. The size of RVE was also studied by analysing the composite with randomly distributed non-overlapping similar particles. The results indicated that only twice of the inclusion diameter size could be enough for a RVE to gain accurate estimation of effective modulus of the whole material. Comparing to the theoretical models, the numerical approach is able to consider various complex situations such as realistic complex microstructures of the composites, the complex matrix-reinforcement interaction, nonlinear mechanical responses of solid phases in the composites, and damage/fracture behaviours of the composite materials, etc. The numerical methods usually lead to accurate prediction of the composites' mechanical behaviours provided the RVE models represent the features of the composites correctly. However, there are also some disadvantages of the numerical approach. First, in numerical methods, the closed-form formula usually cannot be obtained (the results are normally represented by a series of curves). An accurate numerical model of composites can be very complex and the simulation can be time-consuming even on super-computers.

In the experimental approaches, various testing facilities and experimental techniques are utilised to measure and characterise the mechanical properties of composites directly (or indirectly via theories of micromechanics and macromechanics). Experiments can be performed on composite materials at three scales: micromechanical, macromechanical and structural [35-38]. Experimental study is important to the mechanics analysis of composites. It is required not only to validate the theoretical and numerical predictions of the effective properties of composites, but also to provide input data (e.g., the properties of the constituents, interactions between different phases, etc.) for the theoretical and numerical models. For example, the effective elastic properties of different kind of PRCs (e.g., WC-Co cermet [29, 39, 40], polymer-based dental composites consisting of silica particles [41], metal matrix based on Al-SiC [42], polymer embedded with glass particles [43, 44], glass-alumina based composites [45, 46], epoxy-silica composites [47]) are reported in the literature and they are collected to validate theoretical models (e.g., [22]). The properties of single fibres were characterised to obtain input data for related FRC modelling[48]. Measuring the properties of composites is more complex than that of the traditional materials and many new techniques and new facilities are designed. For example, fibre-push-out technique was proposed by Singh and Sutcu [49]. Although the experimental methods provide accurate and usually direct measurements of the mechanical behaviours of composite materials, they are normally expensive and limited by the experimental procedures and facility availability. The accuracy of the mechanical methods is sometimes affected by the complex microstructure of composite materials and the nature of existing imperfection in composites. Besides, some properties are extremely difficult to measure directly even if it is possible. For instance, there is no technique available in the literature to measure transverse coefficient of thermal expansion of FRC directly [1].

1.3 Mechanics of composites with reinforcement in finite deformation

As discussed in the previous section, the mechanical behaviours of composites with reinforcement in infinitesimal deformation have been studied extensively and many models have been developed in the literatures. However, the mechanical responses of composites with reinforcement in finite deformation regime have not been well understood due to the intrinsic difficulties from the nature of geometrical and material nonlinearities. Hill [50] considered the transition from microscopic to macroscopic

levels for composites under finite deformation. He defined a set of constitutive macro-variables and volume averages of micro-fields over a representative sample under finite strain. Using these macro-variables, Ogden [51] estimated the bulk modulus of a PRC consisting of dilute spherical inclusions embedded in a matrix of second-order elastic solid under finite strain. Hashin [52] derived the strain field in the hyperelastic PRC under hydrostatic loading. Castaneda [53] developed a self-consistent scheme for hyperelastic composites and derived an approximate model for particle reinforced neo-Hookean composite. Imam et al. [54] derived a second order elastic field of an incompressible infinite matrix with dilute inclusions. Castaneda and Tiberio [55] suggested a "linear comparison" homogenisation technique to approximate the effective behaviour of hyperelastic composites. Castaneda and co-workers have used this technique to model different composites [56-60]. The resulted models are very complex but not necessarily accurate [61]. Bergstrom and Boyce [62] examined the uniaxial compression behaviour of Chloroprene rubber filled with carbon black particles (volume fraction 7%, 15%, and 25%) up to true strain of about -1.0. They proposed an approximate model based on the strain amplification concept. Some simple FE simulations were performed to verify the model. Khisaeva and Ostoja-Starzewski [63] investigated the size of RVE needed for composite modelling in FE simulations in finite elasticity.

1.4 Objective

In this thesis, the mechanical behaviours of composite with reinforcements under finite deformation will be investigated. The PRC and the FRC will be studied separately by theoretical analysis and numerical simulation. Experimental data from the literature will also be employed to justify the theoretical models and numerical results when possible.

The first part of the study will focus on the mechanical modelling of the PRC in finite strain based on numerical homogenisation. The planned objectives are presented as follows:

- To develop three-dimensional representative volume element (RVE) models with periodic boundary conditions to investigate the mechanical behaviours under general finite deformation;

- To investigate the RVE simulation results and to develop a theoretical constitutive model based on the numerical homogenisation results;
- To compare the effective modulus of the hyperelastic composite obtained from the numerical homogenisation with the theoretical models in the literature and the classical linear elastic estimation.

The second part of the research aims to identify the significance of the fibre-matrix interaction in the FRC under finite deformation by analysing the theoretical constitutive models, the numerical simulation results, and the experimental data presented in literature. The following objectives will be investigated:

- To identify the fibre-matrix interaction by investigating the strain energy contribution from the ground matrix of the human annulus fibrosus (HAF) with collagen fibres under contraction and various stretch ratios;
- To analyse the significance of the identified fibre-matrix interaction by comparing the finite element simulations of the uniaxial test of the HAF along the circumferential direction with the experimental data in the literature;
- To discuss the potential physical mechanisms related to the identified fibre-matrix interaction and various constitutive models considering fibre-matrix interaction.

1.5 Outline

In chapter 2, the classical results of composite mechanics in infinitesimal and finite deformation regimes are reviewed in detail, in which the mechanics of the FRC and the PRC will be discussed separately. Chapter 3 is devoted to the mechanical modelling of the incompressible particle-reinforced neo-Hookean composite under finite deformation based on a numerical homogenisation approach. In Chapter 4, the significance of the fibre-matrix interaction in the HAF is identified and analysed in detail by investigating the theoretical models, the numerical simulations results, and the experimental data available in the literature. At last, conclusions of the research and some remarks are provided in Chapter 5, while some potential further research is suggested in Chapter 6.

Chapter 2 Basics of Composite Mechanics

Before the mechanical behaviours of the advanced composites with reinforcement under finite deformation are investigated, some classical results of composite mechanics are briefly reviewed in this chapter as they serve as a solid basis of the research work in this thesis. First, the classical theories of composite mechanics in infinitesimal deformation are discussed in section 2.1. Then the literature related to composite mechanics in finite deformation is explored in section 2.2. Because there is only few researches to study the mechanical behaviours of reinforced composite under finite deformation, models developed for linear elastic reinforced composite are paid much attention to. In this thesis, the research mainly focuses on hyperelastic composites with reinforcement (pseudo-hyperelastic biomaterials are modelled by hyperelastic models mathematically), therefore only the elasticity results are discussed.

2.1 Classical results of composite mechanics in infinitesimal deformation

2.1.1 General theories

For mechanics of composite under infinitesimal deformation, the focus lay on the linear elastic models and the concept of effective material properties (e.g., the effective Young's modulus and the effective Poisson's ratio for isotropic composite) is proposed to represent the mechanical behaviour of the composite.

The material is macroscopically isotropic and its mechanical behaviours are characterized by effective moduli, which are not applicable from the microscopic point of view. Under this condition, the composite is assumed to be an equivalent simple material, and the effective material properties come from the mechanical behaviours of this simple material. This concept is based on the representative volume element, which could represent the mechanical characteristics of the composite.

Many theoretical approaches have been developed to estimate/predict the effective parameters of different composites. Among them, parallel model and series model are probably the simplest models, which are used to roughly predict the effective elastic moduli of the reinforced composite under infinitesimal deformation. In these two models, two phases are usually considered separately and piled up, with the uniaxial tensile load applied. Figure 2.1 shows the two model systems with the uniaxial tensile load applied [1].

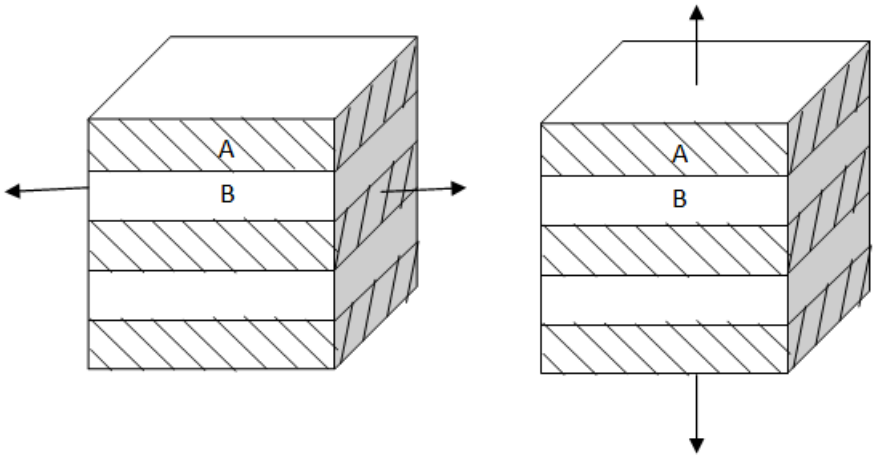

(a) (b)

Figure 2.1 Parallel model (a) and series model (b) [2]

For the parallel model, the strain field is homogeneous and the Young's modulus of the composite E_c can be expressed as

$$E_c = E_1 V_1 + E_2 V_2 , \tag{2.1}$$

Where E_1 and E_2 represent the Young's Moduli of each phase, and V_1 and V_2 denote the volume fractions of each phase, respectively. For a two-phase composite, we have $V_1 + V_2 = 1$. For the series model, the stress field is homogeneous and the Young's modulus of the composite E_c can be derived as

$$E_c = \frac{E_1 E_2}{E_1 V_2 + E_2 V_1} . \tag{2.2}$$

Eq.s (2.1) and (2.2) give a rough estimate of the Young's modulus for a two-phase composite. Based on the energy principles it can be derived that the series model gives a lower-bound prediction of the effective Young's modulus of the composite, while the parallel model predicts an upper-bound for the effective modulus of the composite [1, 2].

Hashin and Shtrikman [10] worked out more strict bounds of the effective moduli by adopting the variational principles and there was no certain presupposition about the geometry of each phase. Sometimes the estimation is quite close to the experimental results based on the assumption that each component is isotropic, elastic and homogeneous. The lower bound is derived from the minimum complementary energy theorem and the upper bound is calculated according to the minimum potential energy theorem. By comparing the results to the experimental data, Hashin's estimation was proved to give good predictions to the effective shear and bulk modulus of the composite with two phases [64].

Based on Hill's self-consistent model, Halpin and Tsai [28] proposed the following unified semi-empirical, semi-theoretical expression to predict the effective parameters of the composite:

$$\frac{\overline{p}}{p_m} = \frac{(1+\zeta\eta v_f)}{(1-\eta v_f)}, \tag{2.3}$$

where the scalar η is defined as

$$\eta = (p_f / p_m - 1)/(p_f / p_m + \zeta). \tag{2.4}$$

Here $\overline{p}$ is the effective modulus of the composite; p_f is the modulus of the filler (i.e., the reinforcement); p_m is the modulus of the matrix; the parameter ζ is related to the microstructure of the composite which relates to loading conditions. By applying the geometry factor ζ, the Halpin-Tsai semi-empirical equation considered the influence of the inclusions' shapes on the stiffness of the composites by examining a series of geometries from sphere (aspect ratio is one) to long fibre (aspect ratio increases to infinity), and the predictions are well consistent to the experimental results.

2.1.2 Theories for particle-reinforced composite (PRC)

The results given in the previous subsection usually do not consider the microstructure of the composites and the geometry of the inclusions. In this subsection, some classical results derived for PRC will be discussed. In the early 1900s, A. Einstein [65] investigated the viscosity of a Newtonian viscous fluid with rigid-spherical nonsolvated particles. The result was extended to the PRC to estimate the Young's modulus of the rigid particle reinforced composite as [66]

$$E_c/E_m = 1 + 2.5v_f\,, \tag{2.5}$$

where E_c and E_m are the Young's moduli of the PRC and the matrix, respectively, and v_f represents the volume fraction of the fillers (i.e., particles).

Guth [4] extended Einstein's approach to consider higher order terms and the prediction of the Young's modulus of the rigid particle reinforced composite was given by

$$E_c/E_m = 1 + 2.5v_f + 14.1v_f^2\,. \tag{2.6}$$

To consider deformable particle reinforced composites, Eshelby's result [67] was employed to approximate the effective elastic properties of the composites based on the moduli of individual components. Kerner [68] is one of the pioneers who gave out the solutions of the effective shear and bulk moduli of the PRC by applying the averaging method. Later, a self-consistent model was brought forward by Hill [13] aiming to predict the effective shear modulus of the PRC. In this model, the composite was placed in an arbitrary homogeneous substance, and the effective modulus of the composite was assumed to be equal to the surrounded medium. So the mechanical properties of the composite could be gained through calculating the properties of the surrounding substance.

Christensen and Lo [18] improved the self-consistent model to a three phase model, in which the geometrical model of PRC comprises three parts, the spherical inclusion, the matrix around the reinforcement and the equivalent medium surrounding the single particle model. In their model, the effective shear modulus of the PRC is predicted by

(the results were proved to be consistent to Eshelby's dilute suspension results [67] when the volume fraction is set small)

$$\left(\frac{\mu}{\mu_m}\right)^2 A+\left(\frac{\mu}{\mu_m}\right)B+D=0\,, \tag{2.7}$$

where

$$\begin{aligned}A=&8[\mu_i/\mu_m-1](4-5\nu_m)\eta_1 c^{10/3}-2[63(\mu_i/\mu_m-1)\eta_2+2\eta_1\eta_3]c^{7/3}\\&+252[\mu_i/\mu_m-1]\eta_2 c^{5/3}-50[\mu_i/\mu_m-1](7-12\nu_m+8\nu_m{}^2)\eta_2 c\\&+4(7-10\nu_m)\eta_2\eta_3\end{aligned}\,, \tag{2.8}$$

$$\begin{aligned}B=&-4[\mu_i/\mu_m-1](1-5\nu_m)\eta_1 c^{10/3}+4[63(\mu_i/\mu_m-1)\eta_2+2\eta_1\eta_3]c^{7/3}\\&-504[\mu_i/\mu_m-1]\eta_2 c^{5/3}+150[\mu_i/\mu_m-1](3-\nu_m)\nu_m\eta_2 c\\&+3(15\nu_m-7)\eta_2\eta_3\end{aligned}\,, \tag{2.9}$$

$$\begin{aligned}D=&4[\mu_i/\mu_m-1](5\nu_m-7)\eta_1 c^{10/3}-2[63(\mu_i/\mu_m-1)\eta_2+2\eta_1\eta_3]c^{7/3}\\&+252[\mu_i/\mu_m-1]\eta_2 c^{5/3}+25[\mu_i/\mu_m-1](\nu_m{}^2-7)\eta_2 c\\&-(7+5\nu_m)\eta_2\eta_3\end{aligned}\,, \tag{2.10}$$

$$\eta_1=[\mu_i/\mu_m-1](49-50\nu_i\nu_m)+35(\mu_i/\mu_m)(\nu_i-2\nu_m)+35(2\nu_i-\nu_m)\,, \tag{2.11}$$

$$\eta_2=5\nu_i[\mu_i/\mu_m-8]+7[\mu_i/\mu_m+4]\,, \tag{2.12}$$

$$\eta_3=(\mu_i/\mu_m)(8-10\nu_m)+(7-5\nu_m)\,, \tag{2.13}$$

$$c=(a/b)^3\,. \tag{2.14}$$

Here μ, μ_m and μ_i represent the effective shear moduli of the composite, the matrix and the spherical inclusion phase respectively; ν_m and ν_i denote the Poisson's ratios of the matrix and the spherical inclusion phase respectively; and c is the volume fraction of the inclusion phase. Although this model was developed for particle reinforced composite under infinitesimal deformation, the simulation results obtained in the following chapter proved that this model could be able to provide the precise approximation to the numerical results for PRC under finite deformation.

Ravichandran [22] proposed a unit cell incorporating isostrain and isostress type elements to simulate the microstructure of two-phase composites with discontinuous

reinforcements. Then simple expressions can be derived as the lower bound E_c^l and the upper bound E_c^u of the effective modulus of the composite:

$$E_c^l = \frac{(cE_f E_m + E_m^2)(1+c)^2 - E_m^2 + E_f E_m}{(cE_f + E_m)(1+c)^2}, \tag{2.15}$$

$$E_c^u = \frac{[E_f E_m + E_m^2(1+c)^2 - E_m^2](1+c)}{(E_f - E_m)c + E_m(1+c)^3}, \tag{2.16}$$

where E_m, E_f are the Young's modulus of the matrix and the filler, respectively; c is the volume fraction of the filler. Comparing to the experimental data, the expressions above gave much better predictions than the commonly used Hashin and Shtrikman bounds, particularly for composites with large stiffness contrast between the particles and the matrix. By adopting a new approximation approach, Torquato [24, 25] worked out third-order accurate expressions to estimate the shear and bulk moduli of the PRC, in which the phase arrangement information is included in the formula.

Most of the models for estimating the mechanical properties of the PRC assume that the PRC is macroscopically isotropic with randomly distributed inclusions rather than paying attention to the specific arrangement of the particles. For this reason, a new numerical approach was proposed to study the overall mechanical behaviours of the PRC, which is to solve the boundary value problems of a representative volume element (RVE) of the material [69]. The influence of the RVE size on the moduli estimation was studied by Drugan and Willis [33, 34], and their results indicate that a small size RVE is sufficient to represent the composite and it can be employed to predict the mechanical behaviours of the whole PRC. Following this approach, Segurado and Llorca [31] developed their linear elastic PRC model with 30 similar-sized spheres randomly distributed in a cube, and elastic, shear and bulk moduli were obtained by analysing the numerical simulation results from various loading conditions.

2.1.3 Theories for fibre-reinforced composite (FRC)

Hashin and Rosen [9] estimated the elastic moduli of unidirectional fibre reinforced composite (UFRC) using variational approach in 1964. Hill [12, 15, 16] developed a self-consistent model to predict the mechanical behaviours of UFRC. Christensen and

Lo [18] improved it to a three phase model to predict the effective transverse shear modulus of the UFRC. The form of the equation is quite similar to that of the PRC, and only the coefficients A, B and D are defined differently.

The effective shear modulus of the UFRC is predicted by

$$\left(\frac{\mu}{\mu_m}\right)^2 A+\left(\frac{\mu}{\mu_m}\right)B+D=0, \tag{2.17}$$

Where A, B, and D are parameters relating to volume ration c, effective shear moduli of fibre (μ_f) and matrix (μ_m), Poisson's Ratio of fibre (ν_f) and matrix (ν_m), transverse shear and plane strain bulk moduli of the "overall" composite μ_{23} and K_{23}. By comparing the predicted results to the existing models, this approach avoids the discontinuity conditions.

2.2 Basics of composite mechanics in finite deformation

2.2.1 General theories

In the infinitesimal regime, the relation between the microstructure and macro mechanical behaviours has been extensively investigated and the results fit the experimental observations well. However, the same problem seems much more difficult when the strains applied to the composite model go beyond infinitesimal regime. The fundamental work on composites under large deformations was first presented by Hill [50]. He derived some relations between the microstructure and macro mechanical properties of the composite by considering arbitrary strain distributions in a representative volume under finite deformation. Later, Castaneda and Tiberio [55] proposed a "linear comparison" homogenization technique to model hyperelastic composite.

2.2.2 Theories for particle-reinforced composite (PRC)

Based on Hill's macroscopic average definition of variables for composite under finite deformation, Ogden estimated the bulk modulus of a PRC consisting of dilute spherical

inclusions embedded in a matrix of second-order elastic solid under finite strain. Castaneda [53] predicted the shear modulus of incompressible nonlinear particle-reinforced composite by working out the first order and second order bounds of the macro mechanical properties. Polyconvexity was applied throughout the work for its advantages in expressing the minimum potential energy mathematically [70] and tightening the general convex envelops [71, 72]. The results from the research proved that the theories can be used to predict the overall mechanical behaviours of nonlinear elastic materials with multi-phases, and the self-consistent estimation is capable of estimating the shear modulus of the incompressible particle-reinforced neo-Hookean composites (IPRNC), though we will show that this prediction significantly overestimate the shear modulus of IPRNC with moderate reinforcement volume fraction (e.g., >10%).

Bergstrom and Boyce [62] studied how the reinforced particles affect the overall behaviours of the composite by comparing the theoretical models available in the literature with the experimental data. In order to avoid the drawbacks of available models for their limited application in the small deformation regime, and investigate the behaviours of the reinforced composite under large strain, a method called strain amplification [73] was adopted.

$$\Lambda = 1 + X(\lambda - 1), \tag{2.18}$$

where Λ is the stretch, and X is a constant which is decided by the volume fraction v_f. Because it is not clear about how to amplify the existing strain and there are different ideas towards this question, a new approach was proposed in [62]. The first invariant $I_1 = (\lambda_1^2 + \lambda_2^2 + \lambda_3^2)^{1/2}$ was chosen as the variable to amplify, and the strain energy function was given out for a special case, neo-Hookean matrix embedded with rigid particles:

$$W = (1 - v_f)\frac{\mu_m}{2}\left(1 + 3.5v_f + 30v_f^2\right)[I_1 - 3], \tag{2.19}$$

where the v_f expression comes from Smallwood[74], Einstein [75], Guth [4] and Guth-Gold [76]. The comparisons between the experimental data and the prediction from Guth [4], Guth-Gold [76], Govindjee-Simo [77], Ponte Castaneda [53] and Bergstrom-

Boyce [62] indicated that the newly developed Bergstrom-Boyce model gives relatively better estimation to the effective modulus of multiphase composites both in infinitesimal deformation and finite deformation.

Moreover, finite element (FE) methods were introduced to obtain homogenised properties of the particulate composites in [62]. The two dimensional analysis first examined an RVE with one particle inside, and the results showed that one particle model would underestimate the overall modulus of the composite. Then a two dimensional RVE model with many particles was studied, and both the models predicted smaller effective moduli of the composite according to the experimental results, which suggested that the two dimensional model is not suitable for the evaluation of multiphase composites. The three dimensional RVE model with many particles (not in spherical shape) was also simulated, and the results gave a fairly good approximation to the composite modulus when the volume fraction of particles was small (7% and 15%), but the approximation went higher when the volume fraction was 25%, which would overestimate the stiffness of the composite.

2.2.3 Theories for fibre-reinforced composite (FRC)

In order to investigate the mechanical behaviours of unidirectional fibre-reinforced composite, the structure of the FRC is simplified as a bundle of unidirectional fibres embedding in the isotropic matrix, and the material is treated as transversely isotropic. The fibre direction is the preferred direction of the material, and the plane which is perpendicular to the fibre direction is the isotropic plane. There are two main approaches to describe the mechanical performances of the FRC under finite deformation, Fung's approach and Spencer's invariant framework for anisotropic materials.

Fung type model

For fibre-reinforced composite under finite deformation, one important application is the soft tissue modelling, where the soft tissue is treated as collagen fibre reinforced composite. Fung et al. [78] studied the biomechanical behaviours of arteries under finite strain condition and proposed the so-called "Fung type" model which adopts strain components directly to express the strain energy. In general, most biological soft tissues

are macroscopically anisotropic and nonlinear. For example, the mechanical behaviours of the human annulus fibrosus (HAF) in the circumferential direction are very different from its mechanical behaviours in the longitudinal and radical directions. A typical Fung type model for the arteries uses the following strain energy function to simulate its mechanical behaviour [78]:

$$\rho_o W^{(2)} = \frac{C}{2}\exp[a_1(E_{\theta\theta}^2 - E_{\theta\theta}^{*2}) + a_2(E_{zz}^2 - E_{zz}^{*2}) + 2a_4(E_{\theta\theta}E_{zz} - E_{\theta\theta}^* E_{zz}^*)]. \quad (2.20)$$

Here the exponential form is used for strain energy, C, a_1, a_2 and a_4 are constants determined by the material's mechanical behaviour, and $S_{\theta\theta}^* = \frac{\partial W}{\partial E_{\theta\theta}^*}$ and $S_{zz}^* = \frac{\partial W}{\partial E_{zz}^*}$ are the selected pairs of stress related to strain components $E_{\theta\theta}^*$ and E_{zz}^*. Sometimes the polynomial form of strain energy function is adopted as follows for soft tissues [78]:

$$\rho_o W^{(2)} = Aa^2 + Bab + Cb^2 + Da^3 + Ea^2 b + Fab^2 + Gb^3, \quad (2.21)$$

where $a = E_{\theta\theta}$, $b = E_{zz}$, and A to G are material constants. For both strain functions, the parameters, such as a_1 , a_2 , a_4 and A to G, are simply constants fitted from experimental data without any clear physical meanings. The pseudo strain energy function was validated by fitting the experimental data, and the exponential expression was proved to be superior to the polynomial form for most soft tissues [78].

The general shear deformation is not included in the previous two strain energy functions and their capability to predict the soft tissue's behaviour under general deformation is questionable. Nevertheless, Fung type model has been widely adopted in the later researches. Recently it is found that this approach has convexity problem [79, 80]. By fitting the experimental data to the Fung type model, Bass's results [81] showed that Fung's approach would lead to some boundary condition problems.

Spencer's framework for FRC

For isotropic hyperelastic materials, the strain energy can be expressed by the three invariants I_1, I_2 and I_3 of $\boldsymbol{C}$, where $\boldsymbol{C} = \boldsymbol{F}^T\boldsymbol{F}$ is the Cauchy-Green deformation tensor

and $\boldsymbol{F} = \partial \boldsymbol{x} / \partial \boldsymbol{X}$ is the deformation gradient (**X** and **x** represent the position of a material point in the original (undeformed) configuration and the current (deformed) configuration, respectively). Here the invariants are defined as

$$I_1 = tr\boldsymbol{C}, \tag{2.22}$$

$$I_2 = [(tr\boldsymbol{C})^2 - tr\boldsymbol{C}^2]/2, \tag{2.23}$$

$$I_3 = \det \boldsymbol{C}. \tag{2.24}$$

When the matrix material is reinforced with unidirectional fibres, the composite is usually treated as transversely isotropic. In Spencer's framework, two additional invariants I_4 and I_5 are introduced to represent the physical condition of the unidirectional fibres

$$I_4 = \bar{\boldsymbol{N}} \cdot \boldsymbol{C}\bar{\boldsymbol{N}} = \lambda_F^2, \tag{2.25}$$

$$I_5 = \bar{\boldsymbol{N}} \cdot \boldsymbol{C}^2 \bar{\boldsymbol{N}}, \tag{2.26}$$

where $\bar{\boldsymbol{N}}$ is the preferred direction of the composite (i.e., the direction of the unidirectional fibre reinforcement), and $\lambda_F = \left\| \boldsymbol{F}\,\overline{\boldsymbol{N}} \right\|$ represents the stretch ratio of fibres.

Although the five invariants approach is capable of representing the mechanical behaviours of the transversely isotropic materials, the construction of strain energy function W based on experimental data is difficult. The reason is that it is practically impossible to change one invariant while other four invariants are kept constant during an experiment. For the sake of better presenting the mechanical behaviours of transversely isotropic materials, Criscione [82] proposed a set of physically based strain invariants to express the transversely isotropic behaviours. The every parameter has physical meaning, such as β_1 represents the dilatation strain, β_2 is the distortion fibre stretch, β_3 is the cross-fibre shear strain, β_4 is the along-fibre shear strain and β_5 is the angular measurement.

Uncoupled models

Holzapfel et al. [83] studied the mechanical behaviours of artery walls by considering the artery's multi-layer structure. In their model, each layer is treated as separate isotropic matrix reinforced by two families of aligned fibres. The strain energy function for every layer is written as:

$$\overline{\psi}(\overline{\boldsymbol{C}}, \boldsymbol{a_{01}}, \boldsymbol{a_{02}}) = \overline{\psi}_{iso}(\overline{\boldsymbol{C}}) + \overline{\psi}_{aniso}(\overline{\boldsymbol{C}}, \boldsymbol{a_{01}}, \boldsymbol{a_{02}}) . \tag{2.27}$$

Here $\boldsymbol{a_{01}}$ and $\boldsymbol{a_{02}}$ represent the preferred directions of two families of fibres; and the strain energy function is split into two parts: $\overline{\psi}_{iso}$ is the strain energy contribution from the matrix and $\overline{\psi}_{aniso}$ represents the strain energy contribution from the fibres. According to the assumption from Holzapfel's work, the strain energy contribution from fibres is negligible when fibres are under contraction, but it will make important contribution to the strain energy when fibres are under stretch.

Quapp and Weiss [84] worked on human ligaments to identify their mechanical properties in both longitudinal and transverse directions. In their model, the soft tissue is treated as an incompressible transversely isotropic hyperelastic composite, and the strain energy was written as follows:

$$W = F_1(I_1, I_2) + F_2(\lambda) + F_3(I_1, I_2, \lambda), \tag{2.28}$$

where F_1 indicates the contribution from the matrix; F_2 represents the contribution from the fibres; F_3 is the contribution from the fibre-matrix interaction; and λ is the stretch along the fibre direction. The fibre-matrix interaction is finally ignored and F_3 is omitted from the model.

Both the Holzapfel and Quapp models are categorized as uncoupled (or decoupled) models, because they treat matrix and fibres as separate parts without considering the fibre-matrix interaction. Although these approaches simplified the form of strain energy and simplified the problem researchers found out later that the classic decoupled models cannot always well predict the experimental results. Peng et al. [7] discovered that the

fibre-fibre angle changes computed from the numerical simulations of the uniaxial testing of the Human Annulus Fibrosus along the circumferential direction based on uncoupled models are very different from the experimental observation. Similar phenomenon was also reported by Gasser et al. [85]. These suggest that the fibre-matrix shear interaction should be taken into account.

Coupled models

Inspired by Criscione's physically based strain invariants model, along-fibre shear and cross-fibre shear are considered in Blemker's muscle model [86]. Both shear moduli are assumed constants and represented through $\bar{I}_1$, $\bar{I}_4$ and $\bar{I}_5$ [82] (which are defined on deviatoric deformation gradient $\bar{\mathbf{F}} = (\det \mathbf{F})^{-1/3}\mathbf{F}$):

$$\psi_{iso}(\bar{I}_1, \bar{I}_4, \bar{I}_5, \alpha) = W_1(B_1(\bar{I}_4, \bar{I}_5)) + W_2(B2(\bar{I}_1, \bar{I}_4, \bar{I}_5)) + W_3(\lambda(\bar{I}_4), \alpha), \qquad (2.29)$$

where

$$B_1 = \sqrt{\frac{\bar{I}_5}{\bar{I}_4} - 1}, \qquad (2.30)$$

$$B_2 = \cosh^{-1}\left(\frac{\bar{I}_1\bar{I}_4 - \bar{I}_5}{2\sqrt{\bar{I}_4}}\right), \qquad (2.31)$$

$$\lambda = \sqrt{\bar{I}_4}. \qquad (2.32)$$

Here the two strain invariants B_1 and B_2 represent the shears along and cross the fibre direction, respectively; λ is the stretch ratio and α indicates the muscle active level. The results show that the shear between fibres is very important, and it will affect the final results of strain energy.

In Peng's study of the mechanical properties of HAF [7], the strain energy function based on Spencer's framework [87] for fibre reinforced materials is divided into three parts, contributions from matrix, fibres and fibre-matrix shear interaction.

$$W = W(\boldsymbol{C}, \boldsymbol{a_0}) = W^M + W^F + W^{FM}, \qquad (2.33)$$

where W^M and W^F represent the strain energy contribution from the ground matrix and the fibre reinforcement respectively, and W^{FM} is the strain energy contribution from the fibre-matrix interaction. In their paper, the proposed interaction energy W^{FM} depends on the fibre stretch ratio and the shear angle between the fibre direction and the transverse matrix plane.

Guo et al. [6] proposed a composites-based hyperelastic constitutive model to describe the mechanical behaviours of soft tissue. The inhomogeneous deformation of the composite is considered to be the main reason for fibre-matrix shear interaction due to the difference between constituents' material properties inside the composite. The deformation is then decomposed multiplicatively into uniaxial deformation along fibre direction and shear deformation, and the conventional composite theories are applied to estimate the strain energy stored in the composite. The developed transversely isotropic hyperelastic model is then used to examine the mechanical behaviours of HAF. Their simulation results show that the proposed model can accurately predict the mechanical behaviours of the HAF. Moreover, they also illustrated that the composite model is compatible with the phenomenological model in [7].

Fibre orientation distribution

All the models mentioned above assume the fibres embedded in the matrix are unidirectional. However, there will always be some dispersion on fibre orientations in real soft tissues. Holzapfel et al. [88] studied the fibre directions inside the human lumbar annulus fibrosus, and the results show that the fibre orientations are similar and independent of the position in the annulus. Also, the fibre angles in different lamellae have no obvious difference, and there is no observed correlation between fibre orientation and donors' age. In each lamella, the fibre angle increases from about 20° on the ventral side to approximately 50° on the dorsal side, which means the fibre angle mainly depend on the circumferential position rather than radial and vertical positions.

Caner et al. [89] adopted the microplane model to study the consequences of fibre orientation dispersion in HAF. It is found that in some cases the experimental data could be fitted and reproduced by considering the contribution from directional distributed fibres only (that is, without explicit consideration of the fibre-matrix shear interaction).

Numerical work

Based on the numerical approach for FRC in the infinitesimal regime, deBotton et al. [90] extended the research to examine the material properties of FRC under finite strain. A numerical model of a hexagonal unit cell is proposed in the chapter, which intends to represent the basic repeatable block for composite material. Although the composite built with such unit cells is not transversely isotropic, the general structure of the composite can be represented well to some extent. The comparison results show that the FE simulation results support the analytical predictions for in-plane and axial stresses very well.

Guo et al. [91] studied hyperelastic fibre-reinforced composites under finite strain theoretically and numerically. In order to identify the fibre-matrix interaction, a numerical model of a representative unit cell was presented in the paper, which contains a cylindrical fibre inside a cube. Periodic boundary conditions were applied in order to obtain a better prediction of the overall mechanical behaviours of the composite material [92]. Five combined loading cased were simulated (i.e., uniaxial tension combined with along fibre shear, uniaxial tension combined with transverse shear, along fibre shear combined with transverse shear, along fibre shear in two directions and uniaxial tension combined with along fibre and transverse shear). The results presented an excellent agreement between the analytical analysis and numerical simulation. The assumption, that the energy from along fibre, along fibre shear and transverse deformation were independent of each other, was corroborated by the FE simulations.

Experimental work

In order to validate whether the theoretical or numerical model of FRC is suitable to represent the mechanical behaviours of real soft tissue, experimental data are necessary and crucial.

Adams and Green [93] tried to identify the fibre-matrix interactions by investigating the tensile properties of the annulus fibrosus. 6 lumber spines were harvested and totally 37 specimens were investigated in the experiments. Each specimen was obtained from lateral and tailored into a vertical slice of about 5mm thick and 30mm wide. Tensile strain was applied vertically on the sample after preconditioning, and the size effect of

specimen was studied later by cutting the original sample into smaller ones schematically. The new sample was geometrically similar to the original one but only with smaller size. The mechanical behaviours of the soft tissue were proved to be size-dependent by Adams and Green's study, and the stiffness of the material would reduce when the sample size decreases.

Bass et al. [81] carried out a series of uniaxial and biaxial tensile tests to characterise the mechanical responses of HAF. Healthy human spines were obtained from autopsy, properly stored and later cut into the required shape for experiments following strict procedures. The outer annulus was kept with the vertebra bones attached on both sides, which helped to maintain the physiological loading condition and the maximum height of specimen For biaxial tests, the circumferential strains were held at six constant values (0.0, ±0.0125, ±0.025 and +0.0375) while the tension was applied on the orthogonal direction on the specimen plane. Based on Fung's approach [78], strain data from experiments were directly used to fit the strain energy functions. By comparing the constitutive models obtained from different data set, the results showed that the strain energy functions obtained from uniaxial tension data cannot be applied to estimate the material responses in biaxial tensile tests, and vice versa. Due to the multi-axial loading condition for annulus, as well as the nonlinearity and anisotropy of HAF, they concluded that uniaxial data is insufficient to predict the mechanical behaviours of HAF under general deformation state.

Chapter 3 Mechanical Modelling of Incompressible Particle-Reinforced neo-Hookean Composites Based on Numerical Homogenisation

Objective

- To develop three-dimensional representative volume element (RVE) models to simulate the microstructure of composites with randomly distributed spherical particles;
- To generate periodic boundary conditions for the RVEs to simulate the mechanical behaviour of the particle-reinforced composites;
- To simulate the mechanical behaviour of the RVEs under finite deformation;
- To investigate the RVE simulation results and to develop a theoretical constitutive model based on the numerical homogenisation results;
- To compare the effective modulus of the hyperelastic composite obtained from the numerical homogenisation with the classical linear elastic estimation.

Summary

In this Chapter, the mechanical responses of incompressible particle-reinforced neo-Hookean composites (IPRNC) under general finite deformation are investigated numerically. Three-dimensional representative volume element (RVE) models containing 27 non-overlapping identical randomly distributed spheres are created to represent the neo-Hookean composite which consists of one incompressible neo-Hookean elastomer embedded with randomly distributed equal-sized spherical incompressible neo-Hookean particle reinforcements. Four types of finite deformation (i.e., uniaxial tension, uniaxial compression, simple shear and general biaxial deformation) are simulated using the RVE models with periodic boundary condition (PBC) enforced. The simulation results show that the overall mechanical responses of

the IPRNC can be well predicted by another simple incompressible neo-Hookean model. It is also shown that the effective shear modulus of the IPRNC with different particle volume fraction and different particle/matrix stiffness ratio can be well predicted by the classical linear elastic estimation.

3.1 Introduction

A fundamental problem for particle-reinforced composites (PRC) is to predict the overall mechanical behaviour of the composite based on the mechanical properties of the constituents and the microstructure of the composites. Guth [4] extended Einstein's linear estimate originally developed for viscous fluid and proposed a second order polynomial to predict the small strain Young's modulus of (rigid) particle-filled solids. Kerner [68] designed an averaging procedure to estimate the effective shear modulus and bulk modulus of the PRC. Hill [13] proposed a self-consistent model to estimate the effective shear modulus of the PRC. The three-phase model developed by Christensen and Lo [18] gives a very good prediction of the PRC's effective shear modulus [31]. Torquato [25] derived accurate expressions for the bulk and shear moduli of the PRC based on a third-order approximation. Although a few studies investigated some special microstructures such as cubic arrays of spheres [e.g., 94], most papers in the literature have focused on macroscopically isotropic composites with randomly distributed particles. Besides the direct estimation of the effective moduli of the PRC, some rigorous bounds for the elastic properties of the PRC have been obtained from variational principles [e.g., 10]. Another approach to investigate the "overall" mechanical behaviour of the PRC is to solve the boundary value problems for a representative volume element (RVE) model of the composite numerically [69]. Drugan and Willis [34] showed that a small size RVE model can predict accurately the mechanical response of the PRC. Segurado and Llorca [31] provided a comprehensive numerical study of the mechanical properties of the linear elastic PRC using multi-particle RVE models.

Although the mechanical properties of the PRC in infinitesimal strain have been investigated extensively, their mechanical behaviour in the finite deformation regime is still not well-understood due to the intrinsic difficulties related to the geometrical and material nonlinearities. Hill [50] proposed a set of macroscopic variables for constitutive modelling of composites in finite deformation. Based on that, Ogden [95]

derived an approximate expression for the overall bulk modulus of the PRC with second-order isotropic compressible elastic constituents under finite strain. Hashin [52] studied the response of hyperelastic PRC under hydrostatic loading. Imam et al. [54] derived the second order elastic field for incompressible hyperelastic composites with dilute inclusions, which was then employed to estimate the overall moduli of the PRC. Although recently several research groups have investigated hyperelastic composites with inclusions in two dimension (which physically implies composites with aligned fibre reinforcement) and some related boundary value problems are solved analytically [e.g., 6, 90, 96, 97], exact solutions for three-dimensional PRC model under general homogeneous displacement boundary conditions are still not available in the literature. Nevertheless, Castaneda [53] proposed a self-consistent approach to predict the shear modulus of incompressible particle-reinforced neo-Hookean composites (IPRNC). Bergstrom and Boyce [62] used the concept of strain amplification under large strain to estimate the shear modulus of incompressible neo-Hookean composites filled with rigid particles. Because these two models are not based on an accurate approximation of the elastic fields, it is not surprising to find that they don't provide good estimates of effective shear modulus of IPRNC with moderate particle volume fractions. The numerical studies of hyperelastic composites available in the literature are also mainly limited to two-dimensional problems of composites with aligned fibres or voids [e.g., 61, 97, 98], though Bergstrom and Boyce [62] used simple 2D axisymmetric models to simulate IPRNC under uniaxial deformation. Three-dimensional RVE modelling in finite deformation is only investigated for single-fibre unit cell [91]. To the best of the authors' knowledge, there is no comprehensive numerical study of the PRC under finite deformation published in the literature.

Because it is difficult to predict the mechanical response of the PRC under general finite deformation theoretically due to the related geometrical and material nonlinearities, this study employs the numerical homogenisation approach to investigate the mechanical behaviour of the simplest hyperelastic PRC under general finite deformation, in which the mechanical properties of both the matrix and the reinforcement are described by an incompressible neo-Hookean model. In this chapter, three-dimensional RVE models are created to represent the neo-Hookean composite which consists of one incompressible neo-Hookean elastomer embedded with the other randomly distributed equal-sized spherical incompressible neo-Hookean particle reinforcement. Four types of finite deformation (i.e., uniaxial tension, uniaxial compression, simple shear and general

biaxial deformation) are investigated using the RVE models with periodic boundary condition (PBC) enforced. The simulation results show that the overall mechanical responses of the IPRNC can be well predicted by another simple incompressible neo-Hookean model. The numerical results also suggest that the classical linear elastic estimation [18] can be used to predict the effective shear modulus of the IPRNC with different particle volume fraction and different particle/matrix stiffness ratio.

The structure of the chapter is as follows: In section 3.2, the IPRNC to be investigated is described and the theoretical basis of the numerical homogenisation in finite deformation [50, 95] is also introduced. In section 3.3, the RVE models are developed for numerical simulations using finite element method (FEM) and some related issues (e.g., isotropy of the RVE models, FEM mesh) are discussed. The results of the RVE simulations are presented and investigated in section 3.4. The effective modulus of the hyperelastic composites is also compared with classical linear elastic estimation. Some concluding remarks are given in section 3.5.

3.2 Particle-reinforced neo-Hookean composites and theoretical basis of numerical homogenisation

As mentioned in Chapter 2, for a continuum solid, the deformation gradient is defined as $\mathbf{F} = \partial \mathbf{x} / \partial \mathbf{X}$, where $\mathbf{X}$ and $\mathbf{x}$ denote the positions of a typical material point respectively in the original (undeformed) and deformed configuration of the solid. The mechanical behaviour of an isotropic hyperelastic material can be determined by its strain energy function (per unit volume in the original configuration) $W = W(\mathbf{F})$. If the material is compressible, the nominal stress $\mathbf{P}$, which means the average stress on the area, can be obtained as

$$\mathbf{P} = \frac{\partial W(\mathbf{F})}{\partial \mathbf{F}}, \quad P_{ij} = \frac{\partial W}{\partial F_{ij}}, \tag{3.34}$$

while for incompressible material, it reads

$$\mathbf{P} = -p\mathbf{F}^{-T} + \frac{\partial W(\mathbf{F})}{\partial \mathbf{F}}, \tag{3.35}$$

where p is the pressure. The simplest model for hyperelastic materials is the incompressible neo-Hookean model, as follows

$$W(\mathbf{F}) = \frac{1}{2}\mu(I_1 - 3), \tag{3.36}$$

where the only material constant μ is the shear modulus of the material; $I_1 = tr(\mathbf{C})$ is the first invariant of the right Cauchy-Green deformation tensor.

In the chapter, the interest will focus on the mechanical behaviour of the simplest hyperelastic PRC, the so-called "incompressible particle-reinforced neo-Hookean composite" (IPRNC), in which both the matrix and the particle reinforcement are incompressible neo-Hookean materials and they are perfectly bonded on the surface. Let μ_m and μ_r denote the shear moduli of the matrix and the reinforcement respectively. If the mechanical properties of the composite are assumed to be macroscopically isotropic and homogeneous, only two parameters need to be considered, the stiffness ratio μ_r/μ_m and the volume fraction of the reinforcement c. Hence the shear modulus of the matrix μ_m can be set as 1 (one unit) without losing any generality.

The macroscopic mechanical behaviour of the (microscopically inhomogeneous) hyperelastic composite can be characterised by the constitutive macro-variables defined in Hill [50]. A representative volume of the inhomogeneous hyperelastic material is considered here, which occupies volume V in the reference configuration. The volume average (denoted by an over-bar) of the deformation gradient $\mathbf{F}$, the nominal stress tensor $\mathbf{P}$, and the strain energy W are given by [50, 95]

$$\bar{\mathbf{F}} = \frac{\int_V \mathbf{F} dV}{V}, \bar{\mathbf{P}} = \frac{\int_V \mathbf{P} dV}{V}, \overline{W(\mathbf{F})} = \frac{\int_V W(\mathbf{F}) dV}{V}. \tag{3.37}$$

Using the divergence theorem, it can be derived that

$$\bar{F}_{ij} = \frac{\int_S x_i n_j dS}{V}, \tag{3.38}$$

where S is the surface of the volume V; $\mathbf{n} = n_j \mathbf{e}_j$ is the outward unit vector normal to the surface S. Here $\mathbf{e}_j$ is the unit vector in the direction of the X_j axis. That means the average deformation gradient $\bar{\mathbf{F}}$ can be computed in terms of the displacement on the surface S.

Similarly, if the continuum body is in equilibrium, the average nominal stress $\bar{\mathbf{P}}$ can be obtained as

$$\bar{P}_{ij} = \frac{\int_S X_i P_{kj} n_k dS}{V}, \tag{3.39}$$

which implies that the average nominal stress $\bar{\mathbf{P}}$ can be computed in terms of the nominal stress $\mathbf{P}$ on the surface S. Hill [50] showed that

$$\bar{\mathbf{P}} = \frac{\partial \overline{W(\mathbf{F})}}{\partial \bar{\mathbf{F}}} \tag{3.40}$$

for compressible composites. If the material is incompressible, it reads

$$\bar{\mathbf{P}} = -p\bar{\mathbf{F}}^{-T} + \frac{\partial \overline{W(\mathbf{F})}}{\partial \bar{\mathbf{F}}}, \tag{3.41}$$

Hence $\overline{W(\mathbf{F})}$ can be treated as a potential (strain energy) for the volume V and a function of $\bar{\mathbf{F}}$. The mechanical behaviour of the overall composite can be determined by $\overline{W} \equiv \overline{W}(\bar{\mathbf{F}})$. However, because of the fundamental difficulties caused by the related geometrical and material nonlinearity, even for the simplest PRC defined above, it is still impossible to derive strain energy field in the volume V under general deformation state analytically. To the best of the authors' knowledge, there is no accurate approximation of $\overline{W}(\bar{\mathbf{F}})$ reported in literature for this simple IPRNC.

To overcome the theoretical difficulty, numerical homogenisation methods have been proposed to estimate the effective properties of microscopically inhomogeneous composites [69, 92]. In order to determine the mechanical behaviour of hyperelastic

composites under any given "overall" deformation (represented by the average deformation gradient $\overline{\mathbf{F}}$) based on the macro-variables defined in Hill [50], appropriate displacement boundary conditions, which satisfy Eq. (3.38), are applied to a geometrical representative model, and the corresponding stress/strain fields can then be computed numerically (usually by finite element mechanics). The macroscopically defined nominal stress tensor $\overline{\mathbf{P}}$ can be obtained based on Eq. (3.40) and the related strain energy $\overline{W}\left(\overline{\mathbf{F}}\right)$ can also be computed numerically.

For macroscopically homogeneous and isotropic incompressible hyperelastic material, any general deformation can be treated as a biaxial deformation in its principal directions. Hence any general deformation can be represented by principal stretches λ_1 and λ_2 (the third principal stretch can be determined by the incompressibility constraint as $\lambda_3 = 1/(\lambda_1\lambda_2)$). If the principal stretches are further sorted as $\lambda_1 \geq \lambda_2 \geq \lambda_3$, then only the region $\left\{(\lambda_1,\lambda_2)\middle|\lambda_1 \geq 1, \lambda_1 \geq \lambda_2 \geq \lambda_1^{-1/2}\right\}$ needs to be investigated numerically. Now the overall strain energy function can be written as $\overline{W} \equiv \overline{W}(\lambda_1,\lambda_2)$. When the invariant approach is used, the overall strain energy function can be represented by I_1 and I_2 as $\overline{W} \equiv \overline{W}(I_1,I_2)$, where $I_2 = \frac{1}{2}\left[(tr\mathbf{C})^2 - tr\mathbf{C}^2\right]$ is the second invariant of the right Cauchy-Green deformation tensor $\mathbf{C}$, which is defined as $\mathbf{C} = \overline{\mathbf{F}}^T\overline{\mathbf{F}}$ here. If sufficiently many values of $\overline{W}$ are computed numerically, for some simple composites, the data might suggest a simple function $\overline{W}(\lambda_1,\lambda_2)$ or $\overline{W}(I_1,I_2)$, as illustrated later in this chapter.

3.3 RVE models and finite element simulations

The first step of numerical homogenisation is to generate a set of appropriate RVE models which can statistically represent the composite. In the chapter, the IPRNC is geometrically simulated by three-dimensional representative cubic unit cell with 27 non-overlapping identical spheres randomly distributed inside. Because the PBC will be applied to the RVE models in the FEM simulations, it is required that the RVE models have periodic microstructures, or else it would not be proper and possible to use periodic boundary condition. That is, if a particle intersects the RVE surface, it has to be

split into an appropriate number of parts and copied to the opposite sides of the cube. Figure 3.1 explains the concept of an RVE model with periodic microstructure.

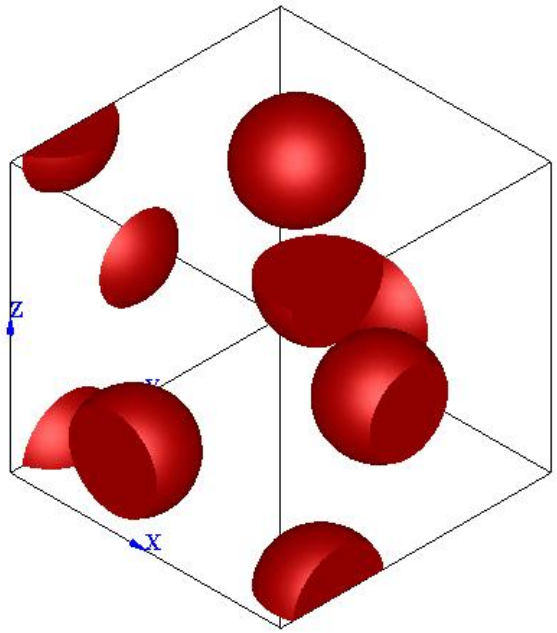

Figure 3.1 Schematic diagram of a RVE.

Therefore the RVE model can be used as a unit block to build composite models with correct periodic microstructure. The software DIGIMAT 4.1 (http://www.e-xstream.com/) is used to generate RVE models with periodic microstructure. To investigate the effect of different particle volume fraction c, RVE models with various particle volume fractions (i.e., c = 5%, 10%, 20% and 30%) are generated. For each volume fraction value, 4 different RVE samples are created to study the variation of the predictions.

There are 27 spheres inside a RVE and the diameter of the particles d in each RVE can be determined by the particle volume fraction c.

$$V_{RVE} \times c = 27 \times V_p \tag{3.42}$$

$$V_p = \frac{4}{3}\pi(\frac{d}{2})^3 \tag{3.43}$$

Here V_{RVE} is the volume of the RVE and V_P is the volume of a sphere. Here the RVE is considered as a unit cubic cell, the length of each edge is $L=1$ and the volume of RVE $V_{RVE}=1$.

Combining Eq. (3.42) and Eq. (3.43), the diameter of the embedded spheres is calculated by

$$d = 2\times\left(\frac{V_{RVE}\times c}{27\times\frac{4}{3}\pi}\right)^{\frac{1}{3}} \tag{3.44}$$

The particle volume ratios and the corresponding diameters of the embedded spheres are listed in Table 3.1.

c	5%	10%	20%	30%
d	0.1524	0.1920	0.2418	0.2768

Table 3.1 Particle volume ratios and the corresponding sphere diameters.

In order to prevent severely distorted finite element mesh in the matrix necking zone between particles, the distance between spheres and sphere- surface should be restricted. In this study, the distance should be larger than $0.1d$ when the particle volume ratio is no more than 20%, and $0.05d$ when the volume ratio is 30%.

For every RVE cube, the length of each edge is 1, which is 3.6 times of the biggest diameter (when the volume fraction of inclusion is 30%). According to Drugan and Will's research [34], the RVEs are big enough in size to represent the general mechanical behaviours of the composites in the linear elastic regime.

The interfaces between spheres and matrix are presumed to be perfectly bounded initially and throughout the simulation. If the microstructure is damaged, those RVEs are no longer applicable to represent the composite because the broken interfaces would change the mechanical performance of the material and certain rearrangement of particles might show great effects on the stiffness in certain direction of the composite .

In this work, the mechanical behaviours of RVEs are studied under large deformation but damage is not considered, because the stability of the composite no longer exists and RVEs lose their meanings in this condition. Although it is impossible to identify if the microstructures of deformed RVEs are damaged or not, the simulation results show that the mechanical behaviours could be represented by the neo-Hookean model, which in the other way around proves that the RVEs are not damaged during the deformations.

To correctly predict the mechanical response of the macroscopically isotropic IPRNC, it is important to make sure that the generated RVE models are close to isotropic. The isotropy of the particle distribution in the16 RVE models is analysed by computing the positions of the centroid of the particles and their moment of inertia in relation to the three axes which are parallel to the three axes of the coordinate system and pass through the centre of the RVE unit. The results are plotted in Figure 3.2. When the particles are ideally randomly distributed, the moment of inertia is $I = cL^2/6$ [31]. This is also plotted in Figure 3.2 for comparison. The results in Figure 3.2 show that, for all RVE samples, the centroid is always close to $L/2$, and the value of the moment of inertia is also close to the ideal value $cL^2/6$ (the moment of inertia of the particles in an RVE model is usually slightly smaller than the ideal value because the partition of the particles leads to smaller contribution of the particles to the overall moment of inertia). This implies that there are no axial preferential directions identified in the 16 RVE samples. An alternative method to verify the isotropy of an RVE model is to simulate directly the response of the RVE model under uniaxial tension/compression along various directions, which will be discussed in the next section.

For a given average deformation gradient $\bar{\mathbf{F}}$, based on (3.38), it is obvious that the choice of boundary condition is not unique. Usually three types of boundary condition are used for general RVE models:

(i) The prescribed displacement boundary condition (PDBC);
(ii) The prescribed traction boundary condition (PTBC) (or sometimes named as “mixed boundary condition (MBC)”);
(iii) The periodic boundary condition (PBC) [64].

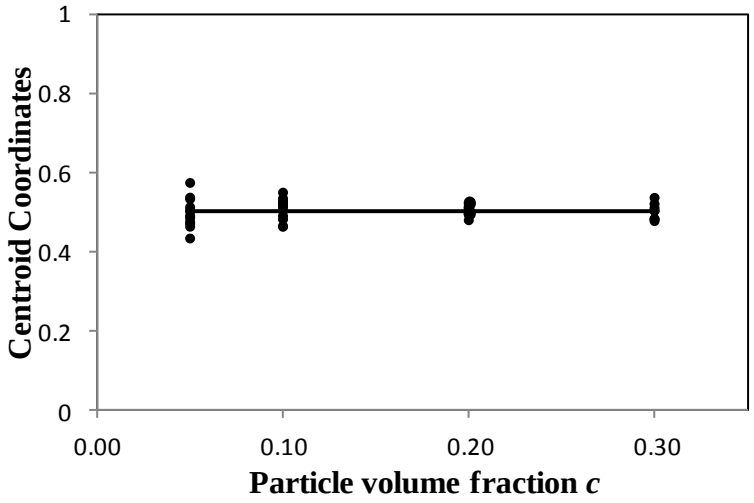

(a) Coordinates of the centroid of the spherical particles vs. the particle volume fraction c. For each value of c, there are 4 RVE samples, which produce 12 coordinate values (x, y, z coordinate values for every RVE sample)

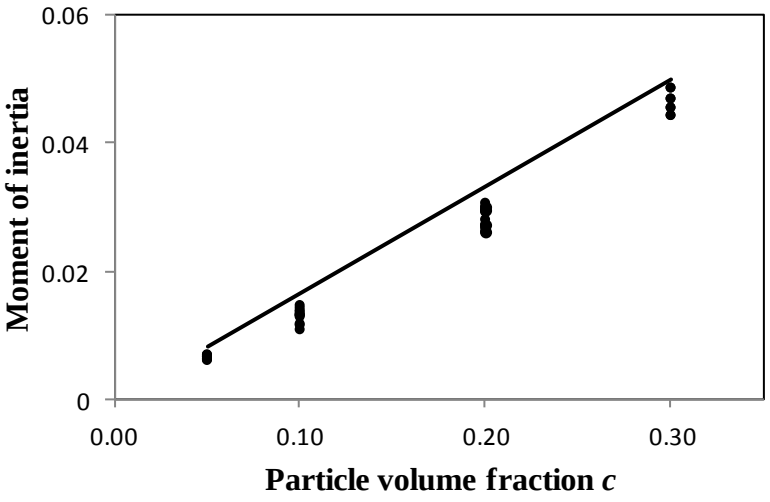

(b) Moment of inertia, I, of the spherical particles vs. the particle volume fraction c. $I = cL^2/6$ for ideally randomly distributed particles is also plotted in solid line for comparison. Similarly, there are 12 values of I for each value of c (there are I_x, I_y, I_z for every RVE sample).

Figure 3.2 Centroid coordinates and moment of inertia of spherical particles.

Chen et al. [64] investigated the effects of these three types of boundary condition on predictions of RVE models and their results showed that the PBC provides the best performance, while the PDBC and the MBC over and underestimate the effective modulus respectively. Under the prescribed displacement boundary condition, the deformed Representative Volume Elements need extra restraints to form the material, which would increase the overall stiffness of the material; while the prescribed traction boundary condition does satisfy the balance requirements, but when the deformed RVEs are piled up to form the material, gaps between RVEs result in lower effective modulus. For periodic boundary condition, RVE is put under an ideal loading condition, so the predicted modulus stay between the high and lower bounds and is more close to the real value. This observation has also been verified by many other researchers (e.g., Hohe and Becker [99] and Demiray and Becker[100]).

Because of this, the PBC is applied to all FEM simulations of RVE models in the chapter. For any given average deformation gradient $\bar{\mathbf{F}}$ applied to the RVE model, the PBC can be represented as the following general format [91]

$$\begin{aligned} &\mathbf{x}(Q_1)-\mathbf{x}(Q_2)=\bar{\mathbf{F}}\left[\mathbf{X}(Q_1)-\mathbf{X}(Q_2)\right] \\ &\mathbf{V}(Q_1)=-\mathbf{V}(Q_2) \end{aligned} \tag{3.45}$$

where Q_1 represents a general node on a face of the RVE cube and the corresponding node Q_2 is at the same location of the opposite face of the RVE model. $\mathbf{V}$ is the force applied on the nodes. Here again $\mathbf{X}$ and $\mathbf{x}$ denote the position of a material point respectively in the original (undeformed) and deformed configuration. The first equation in Eq. (3.45) represents the periodic displacements, while the second equation represents the antiperiodic traction condition.

The Periodic Boundary Condition is implemented by “Equation” type of constraints in ABAQUS 6.10 [101]. PBC was imposed on three pairs of paralleled surfaces and three sets of paralleled edges of RVEs. When the RVE deforms due to the given strain, the PBC can be described according to displacement ($\vec{u}$). If the displacement $\vec{u}$ is applied on surface $X_1 = L$ ($X_1X_2X_3$ is a coordinate system defined by three concurrent edges of the unit cube), the distance between the corresponding nodes on surfaces $X_1 = 0$ and

$X_1 = L$ will be decided according to U, which relates to the specific loading conditions applied on RVE, e.g., for a uniaxial tensile deformation, $\overrightarrow{U_1} = (1,0,0)$, $\overrightarrow{U_2} = (0,u_2,0)$ and $\overrightarrow{U_3} = (0,0,u_3)$, while for a simple shear deformation, $\overrightarrow{U_1} = (0,0,0)$, $\overrightarrow{U_2} = (1,0,0)$ and $\overrightarrow{U_3} = (0,0,0)$. Details are given in Appendix B: Boundary conditions. To implement the PBC, it is good to have periodic meshes (i.e., identical meshes on each pair of faces of the RVE cube) for the RVE models. The same procedure proposed by Segurado and Llorca [31] is employed here to mesh the RVE models to guarantee that all the meshes are periodic.

The FEM simulations of all RVE models are performed with ABAQUS/Standard 6.10 within the framework of finite deformation [101]. The matrix is modelled as incompressible neo-Hookean material with $\mu_m = 1$. The particles are also modelled as incompressible neo-Hookean material and different particle/matrix stiffness ratios are considered, i.e., $\mu_r = 100, 10, 0.5$ ($\mu_r = 0.5$ implies a softer particle reinforcement), and the case of rigid particle (which corresponds to $\mu_r = \infty$) is also investigated. In a standard mesh of an RVE model, there are about 60,000 elements for the matrix phase and about 20,000 elements for the particles. Quadratic tetrahedral elements (element type C3D10MH in ABAQUS) are used and around 120,000 nodes are defined. Because of the material and geometric nonlinearity, as well as the severe meshing distortion in the matrix necking zone between spherical particles, convergence is usually very challenging in the numerical simulations (particularly when the stiffness contrast between the particles and the matrix is large) and a typical simulation on an RVE with the standard mesh takes about 4-7 days on a HP Z600 workstation with 16 GB of RAM and 12 CPU cores. Implicit approach was adopted when the FEM simulation was carried out, so the material geometry nonlinearity would lead to the convergence problem. Moreover, the high stiffness contrast between matrix and inclusions could make the system matrix ill-conditioned, which makes the convergence difficult.

To check if this standard mesh is good enough or not to predict accurately the response of the RVE models, an RVE model with $c = 0.2$ is meshed with a refined mesh containing more than 170,000 elements and 200,000 nodes. The uniaxial tension along the X_1 axial direction is simulated for the RVE model with standard and refined meshes respectively. The nominal stress vs. nominal strain (defined as $\varepsilon = \lambda - 1$, where λ

denotes the stretch ratio) curves for both meshes are plotted in Figure 3.3. The two curves are practically superposed, which implies that the standard mesh is able to predict the mechanical response of the RVE model at almost the same level of accuracy as the refined mesh (though the model with the refined mesh can simulate larger value of uniaxial tensile stretch). Hence the standard mesh is used in all the numerical simulations in the chapter due to the limitation of the computing resources.

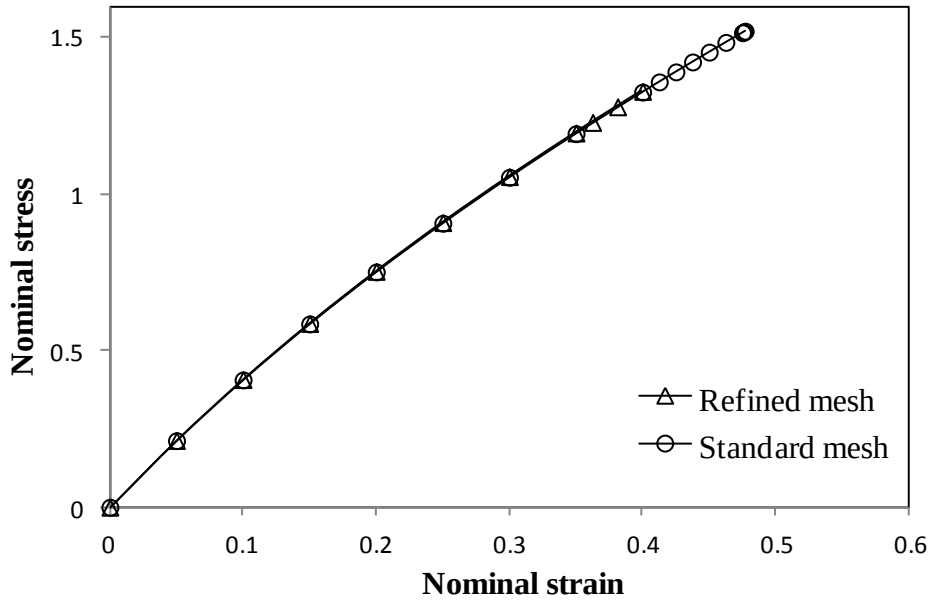

Figure 3.3 Results of the FEM simulations of an RVE model ($c = 0.2, \mu_r = 10$) subjected to uniaxial tension along the X_1 axial direction with standard (denoted by circles) and refined meshes (denoted by triangles). The curves show the nominal stress and the nominal strain $\varepsilon = \lambda - 1$.

As pointed out in the previous section, any general deformation can be represented by a biaxial deformation provided the model is "overall" isotropic. Therefore the following four types of finite deformations are simulated: uniaxial tension, uniaxial compression (along the coordinate axial directions and random directions), simple shear and general biaxial deformation. For all FEM simulations carried out in this study, the deformation is applied until convergence is not achieved by ABAQUS with minimum strain increment setting as 0.001.

3.4 Results and Discussion

3.4.1 Size of the RVE in finite deformation

Based on homogenisation theory, an RVE model should be sufficiently large to be statistically representative of the composite [34]. But because of the limitation of computing resources, the size of an RVE model should be chosen for the purpose of predicting the overall response of the composite with desired accuracy [34]. According to Drugan and Willis [34]'s study, a small size RVE model can well represent the macroscopic behaviour of many composites with reinforcement within the framework of linear elasticity: for example, the minimum RVE size required to obtain "overall" modulus of the composite with less than 5% error is just about twice of the reinforcement diameter. This is verified by the numerical simulation of RVE model for the linear elastic PRC [31]. For composites with nonlinear phase(s), although there is no theoretical estimates for the minimum RVE size, various numerical investigations showed that similar size of RVE models can be used to obtain predictions with the same degree of accuracy [102, 103].

For hyperelastic composites, however, as pointed out by Moraleda et al. [61], there is no critical size of the RVE because of the instabilities coming from the non-convexity of the local strain energy functions [104]. The numerical simulations of fibre-reinforced composites in finite deformation [61, 63] suggested that the edge length of RVE should be 16 times as much as the sphere diameter, which is $L/d \geq 16$. However, for the RVE models created here, L/d is ranging from 3.61 ($c = 0.3$) to 6.56 ($c = 0.05$). If the ratio L/d was increased to 16, more than 390 spheres would be contained inside the RVE and obviously the corresponding computing cost is beyond the practical limit. On the other hand, as will be illustrated in the following sections, the simulation results show that the variations of predictions between various RVE models are well below 5% in general, which implies that the small RVE size used in the chapter is able to obtain exact responses (to a few percent) of the IPRNC under general three-dimensional finite deformation. That is, similar accuracy can also be obtained for the IPRNC in the finite deformation regime with small size RVE models comparing to the results in the infinitesimal deformation regime.

3.4.2 Isotropy of the RVE models

After the random distribution of the particles in the 16 RVE models is verified in the previous section, the isotropy of the mechanical behaviour of the RVE models is double-checked by direct simulations of the responses of the RVE models subjected to uniaxial tension/compression along various directions. For an RVE model with $c = 0.2$, $\mu_r = 10$, the nominal stress vs. nominal strain curves for uniaxial tension along the three coordinate axial directions are plotted in Figure 3.4. For the three uniaxial tension simulations, convergence problem occurs when the stretch ratio λ reaches about 1.5 ~ 1.7. The ultimate stretch ratio obtained by ABAQUS depends on the particle/matrix stiffness ratio, the RVE geometry, the mesh, as well as the stretch direction. The response of the same RVE model subjected to uniaxial tension along a random direction represented by the unit vector $(-0.6461, -0.1411, 0.7501)$ is also simulated and plotted in Figure 3.4 (all random directions and numbers used in the study are generated in MATLAB prior to the ABAQUS simulation). The four curves are practically superposed (relative difference less than 0.85%, which is within the error of the FEM simulation itself). The nominal strains in the two transverse directions are also examined for the four simulations against the isotropic solution $\varepsilon_2 = \varepsilon_3 = \lambda^{-1/2} - 1 = (1+\varepsilon_1)^{-1/2} - 1$ (Figure 3.4). The eight curves from numerical simulation results are very close to the theoretical solution (maximum relative variation less than 1.5%). This indicates that the uniaxial tensile behaviour of this RVE model (in the undeformed configuration) is very close to isotropic. Similarly, the FEM simulation results of this RVE model subjected to uniaxial compression along the three coordinate axial directions and a random direction $(0.6366, 0.6433, 0.4253)$ are plotted in Figure 3.5. Uniaxial compression can be simulated until about $\lambda = 0.55$. It is clear that the uniaxial compression behaviour of this RVE model is also very close to isotropic because the maximum variation between the four simulations is well below 0.9%.

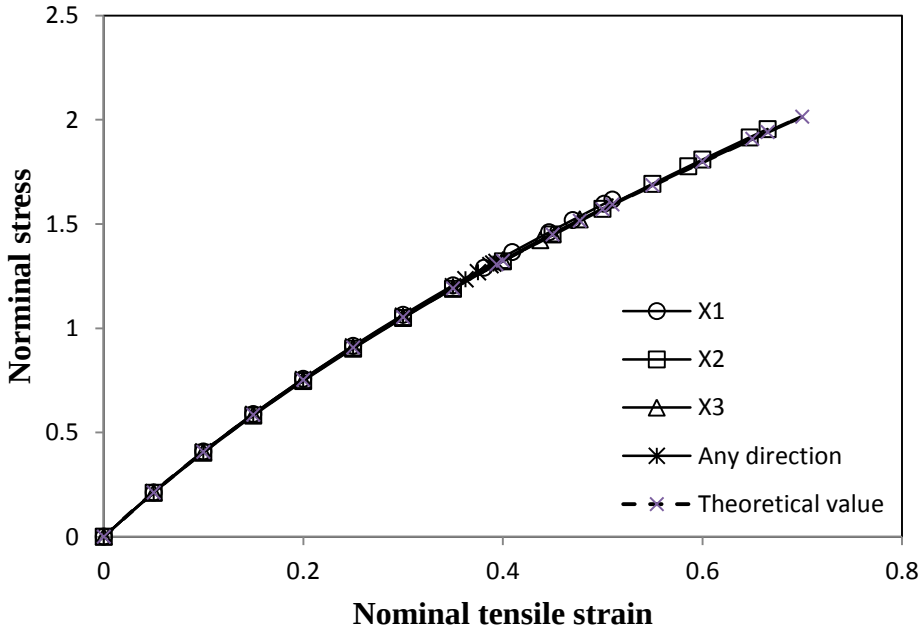

(a)

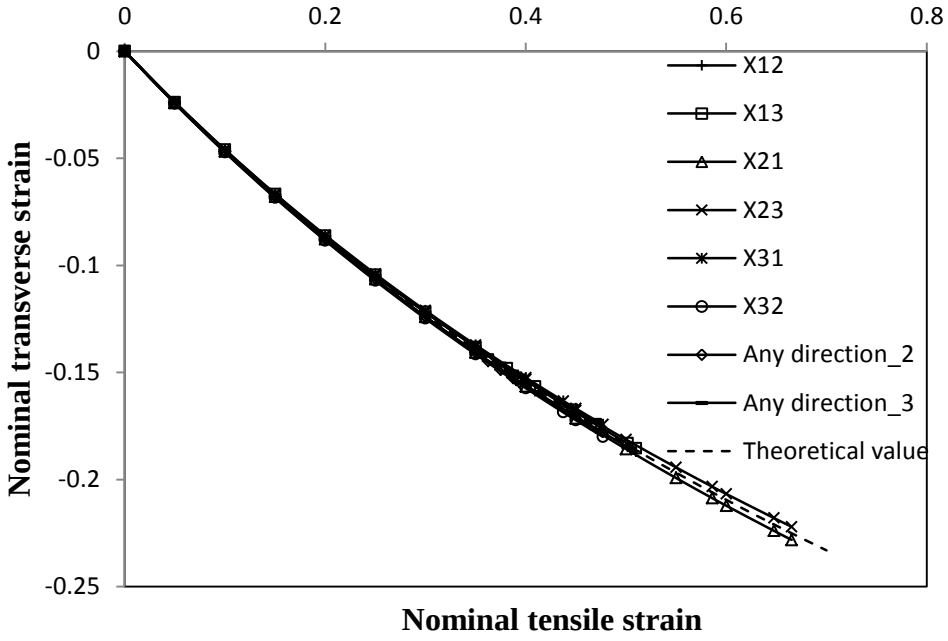

(b)

Figure 3.4 (a) Nominal stress vs. nominal strain curves of an RVE model ($c = 0.2$, $\mu_r = 10$) subjected to uniaxial tensions along the three axial directions and a random direction $(-0.6461, -0.1411, 0.7501)$. The theoretical nominal stress vs. nominal strain curve from the fitted strain energy function is plotted as a dotted line. (b) The corresponding nominal strains in the transverse directions are also plotted against the nominal tensile strain. The isotropic solution $\varepsilon_2 = \varepsilon_3 = \lambda^{-1/2} - 1 = (1+\varepsilon_1)^{-1/2} - 1$ is plotted as a dotted line.

Since both Castaneda [53] and Bergstrom and Boyce [62] proposed the use of an incompressible neo-Hookean model to estimate the response of an IPRNC, the strain energy results $\overline{W}$ computed from the FEM simulations of the uniaxial tension are plotted against $I_1 - 3$ in Figure 3.6. A clear propositional relation is observed and the data is well fitted by $\overline{W} = 0.7441(I_1 - 3)$ using MS Excel 2007 (the coefficient of determination $R^2 = 0.9999$ indicates an excellent fit), which implies the effective shear modulus of the IPRNC is $\mu_c = 1.4882$ for the loading case of uniaxial tension. The theoretical nominal stress-strain curve computed from the fitted strain energy function is plotted as a dotted line in Figure 3.4, which is practically identical to the numerical results. The strain energy results $\overline{W}$ computed from the uniaxial compression simulations are also fitted as $\overline{W} = 0.7459(I_1 - 3)$ in Figure 3.6 ($R^2 = 0.9998$ in MS Excel 2007). The corresponding theoretical nominal stress-strain curve obtained from this fitted strain energy function is plotted in dotted line in Figure 3.5, which is again practically superposed with the numerical results. The difference between the effective shear moduli of the IPRNC predicted by uniaxial tension and uniaxial compression is less than 0.24%, which suggests that a unique incompressible neo-Hookean model might be capable of predicting the mechanical behaviour of the IPRNC under general finite deformation. Similar procedure is applied to all 16 RVE models to examine their isotropy. The simulation results show that, for any RVE model, its responses under uniaxial tension or compression along different directions can all be well described by a unique incompressible neo-Hookean model. The differences between the effective shear moduli predicted by various tension or compression simulation cases for one model is well below 4.6%. Therefore the isotropy of the 16 RVE models is confirmed directly by the FEM simulations.

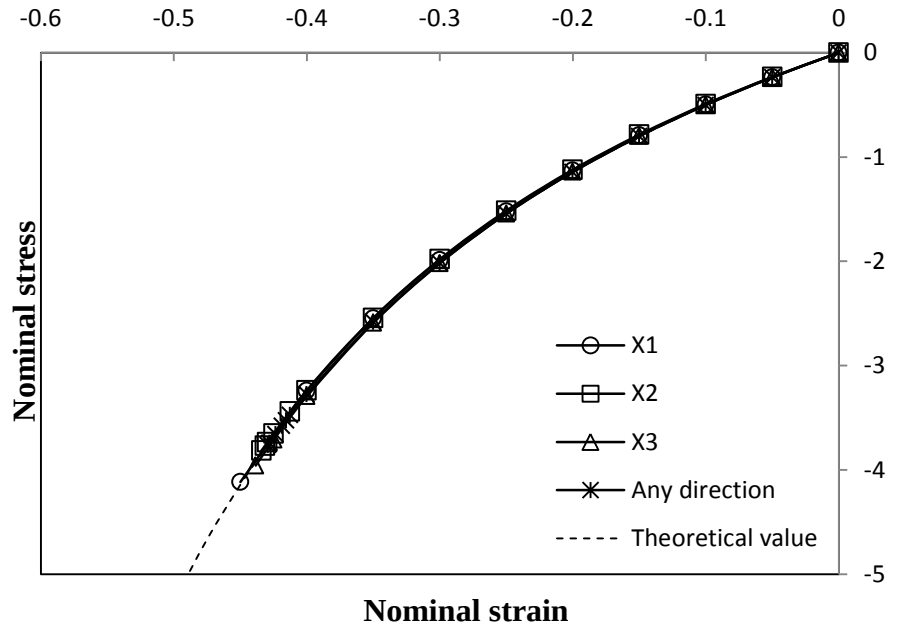

(a)

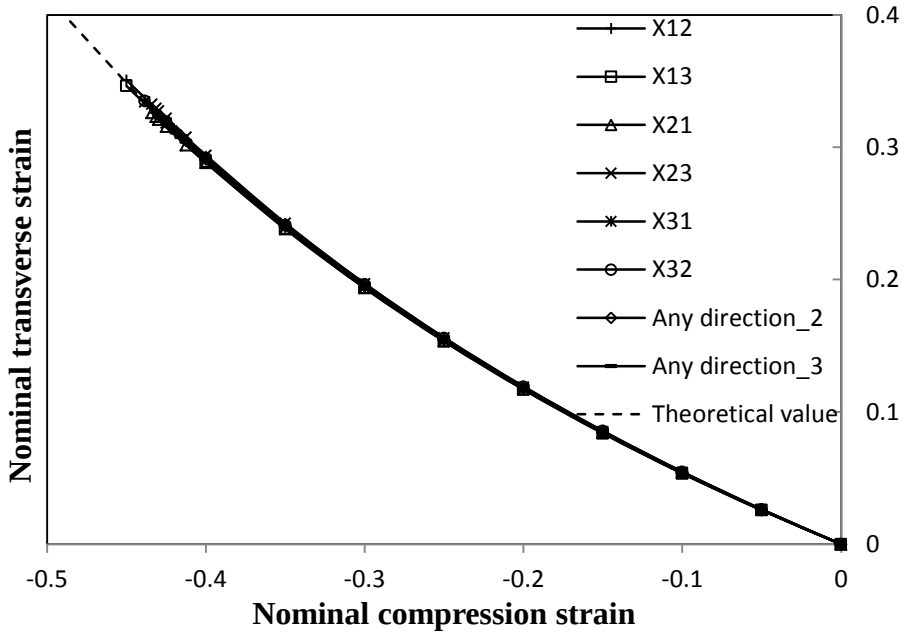

(b)

Figure 3.5 (a) Nominal stress vs. nominal strain curves of an RVE model ($c = 0.2$, $\mu_r = 10$) subjected to uniaxial compressions along the three axial directions and a random direction $(0.6366, 0.6433, 0.4253)$. The theoretical nominal stress vs. nominal strain curve from the fitted strain energy function is plotted in dotted line. (b) The corresponding nominal strains in the transverse directions are also plotted against the nominal compression strain. The isotropic solution $\varepsilon_2 = \varepsilon_3 = \lambda^{-1/2} - 1 = (1+\varepsilon_1)^{-1/2} - 1$ is plotted as a dotted line.

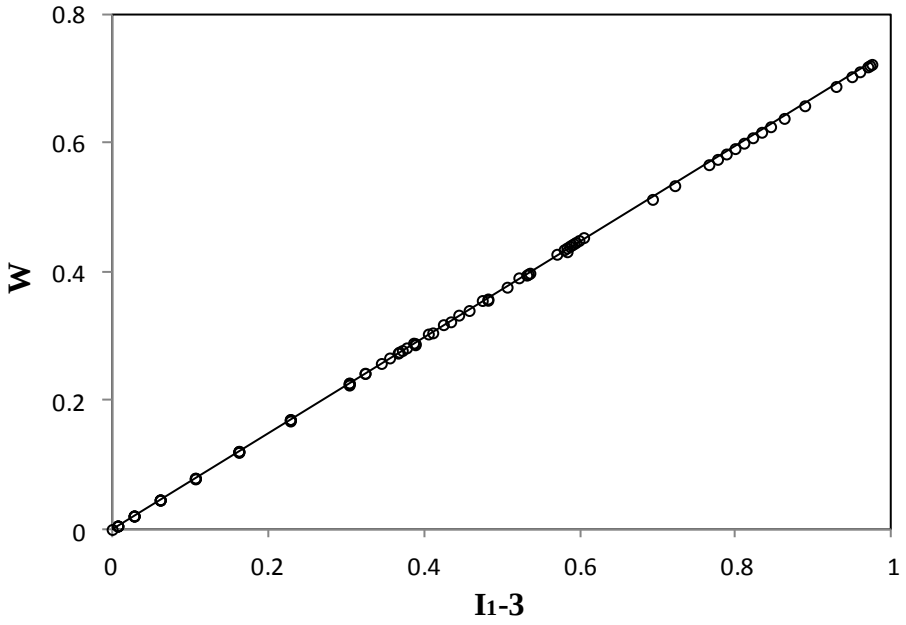

(a) $\overline{W}$ vs. $I_1 - 3$ for uniaxial tension simulations

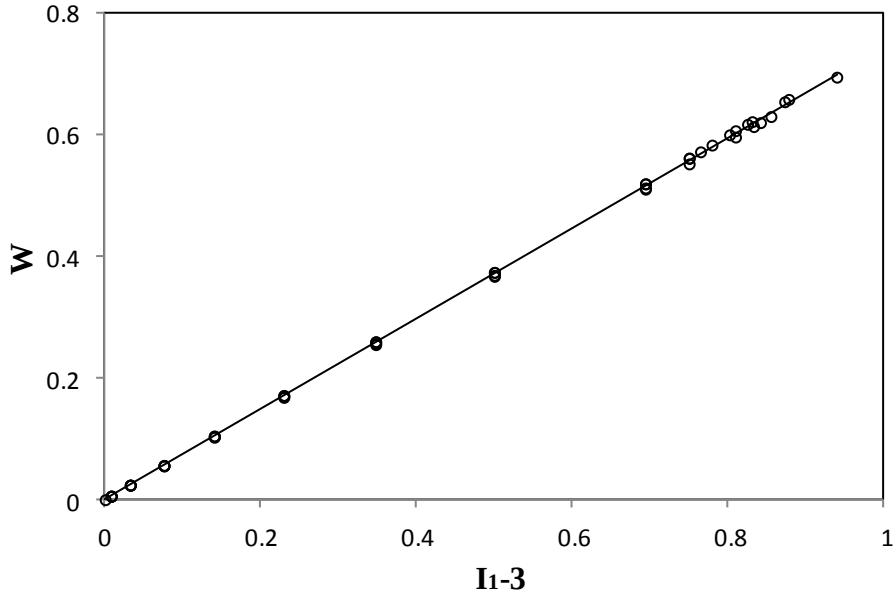

(b) $\overline{W}$ vs. $I_1 - 3$ for uniaxial compression simulations

Figure 3.6 (a) The strain energy results $\overline{W}$ computed from four FEM simulations of an RVE model ($c = 0.2$, $\mu_r = 10$) subjected to uniaxial tensions are plotted against $I_1 - 3$. The data is fitted by $\overline{W} = 0.7441(I_1 - 3)$ (solid line). (b) The strain energy results $\overline{W}$ computed from four FEM simulations of an RVE model ($c = 0.2$, $\mu_r = 10$) subjected to uniaxial compressions are plotted against $I_1 - 3$. The data is fitted by $\overline{W} = 0.7459(I_1 - 3)$ (solid line).

To study the variations between different RVE models, the other three RVE models with $c = 0.2$ are subjected to uniaxial tension along the X_1 and X_2 axial directions, as well as uniaxial compression along the X_3 axial directions and a random direction in FEM simulations ($\mu_r = 10$). In Figure 3.7, all the computed strain energy data $\overline{W}$ from the 20 simulations is plotted against $I_1 - 3$ and they are fitted excellently by a linear relation $\overline{W} = 0.7479(I_1 - 3)$ in MS Excel 2007 ($R^2 = 0.9999$). The effective shear moduli of the 4 RVE model are obtained individually (by fitting the corresponding simulation results on each RVE model) as $\mu_c = 1.4896, 1.4948, 1.505, 1.5064,$ respectively. The relative differences between these effective shear moduli are less than 1.2%. This shows again that the small size RVE models used here are able to obtain exact responses (to a few percent) of the IPRNC.

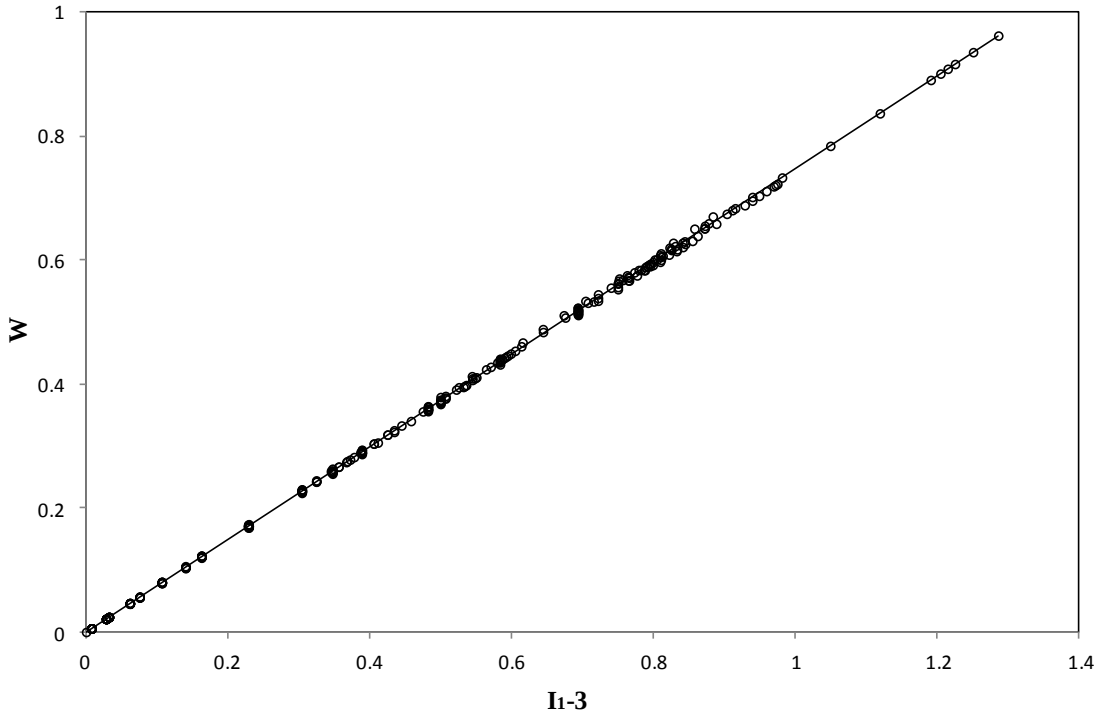

Figure 3.7 Average strain energy $\overline{W}$ vs. $I_1 - 3$ for the 20 uniaxial tension/compression simulations of 4 RVE models ($c = 0.2$, $\mu_r = 10$). The linear fitting curve is plotted in solid line.

3.4.3 Composites embedded with rigid particles

When the particles are rigid (i.e., $\mu_r = \infty$), each particle component (some particles are partitioned into several components by the RVE surface) is defined as a rigid body using the nodes on its matrix-particle surface. Hence there is no need to discretise it into elements (Figure 3.8). If a spherical particle is divided into several components by the RVE surface, the translational and rotational degrees of freedom (d.o.f.s) of those components are constrained properly to make sure the PBC is satisfied on the RVE surface. This can be verified, for example, by the deformed shape of an RVE model with 5 vol% rigid particles under uniaxial tension (Figure 3.8).

Three simple deformations, i.e., uniaxial tension (along the X_1 axial direction and up to $\lambda_1 = 1.85$), uniaxial compression (along the X_3 axial direction and up to $\lambda_3 = 0.60$) and simple shear (in the X_1X_2 plane and up to $k = 0.32$), are simulated for an RVE model with $c = 0.05$. The nominal stress-strain curves are plotted in Figure 3.9. Numerical simulation of a biaxial deformation with nominal strain ratio $\varepsilon_2/\varepsilon_1$ randomly assigned as -0.3432 (because only $\lambda_1 \geq \lambda_2 \geq \lambda_1^{-1/2}$ needs to be considered, a random value between –0.5 and 1 is assigned to $\varepsilon_2/\varepsilon_1 = (\lambda_2 - 1)/(\lambda_1 - 1)$) is performed (up to $\varepsilon_1 = 0.85$) to check the response of the RVE model under general three-dimensional finite deformation. The nominal stress-strain (in the X_1 direction only) curve is plotted in Figure 3.9. The strain energy $\overline{W}$ obtained from the 4 simulations is plotted against $I_1 - 3$ in Figure 3.10 and they are fitted excellently by a linear relation $\overline{W} = 0.5687(I_1 - 3)$ in MS Excel 2007 ($R^2 = 1.0$, and relative error (between the fitted function and the numerical data) well below 0.23%). Therefore the effective shear modulus of the RVE model is predicted as $\mu_c = 1.1374$. The theoretical nominal stress-strain curves from the effective shear modulus are plotted as dotted lines in Figure 3.9, which is almost identical to the numerical results (maximum relative error less than 1.6%.).

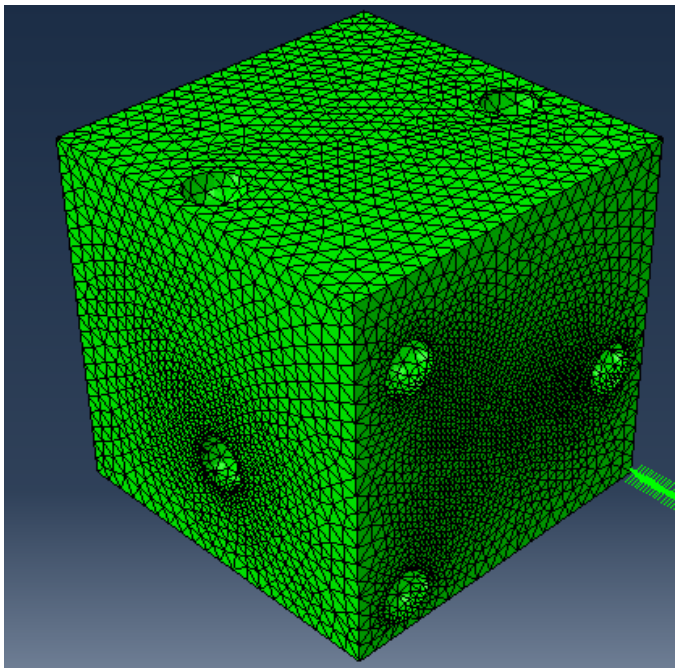

(a)

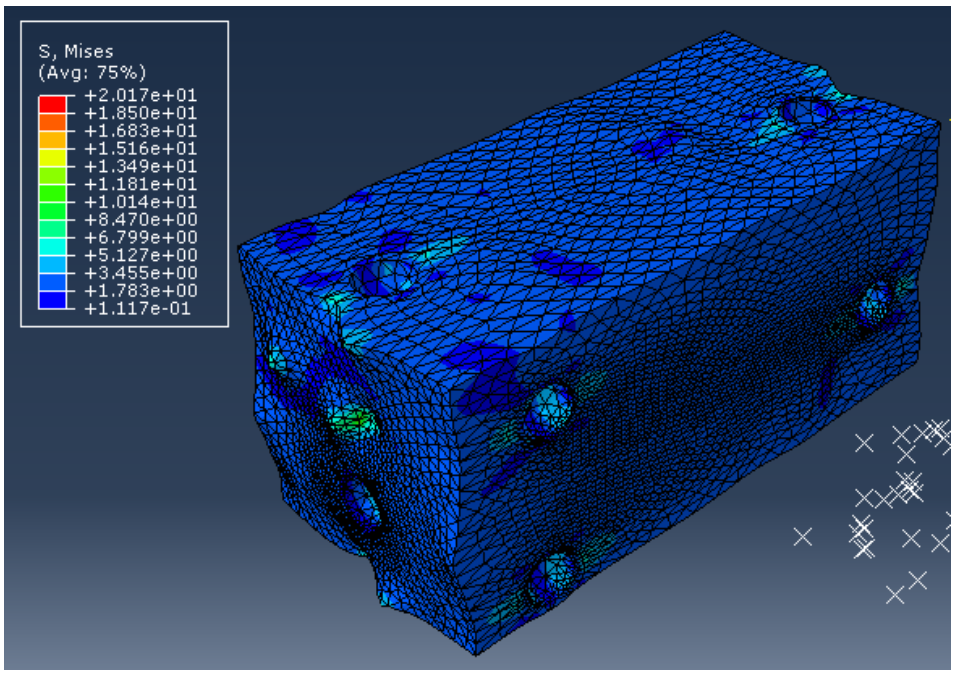

(b)

Figure 3.8 An RVE model with 5 vol% of rigid particles (a) and its deformed shape after uniaxial tension (b).

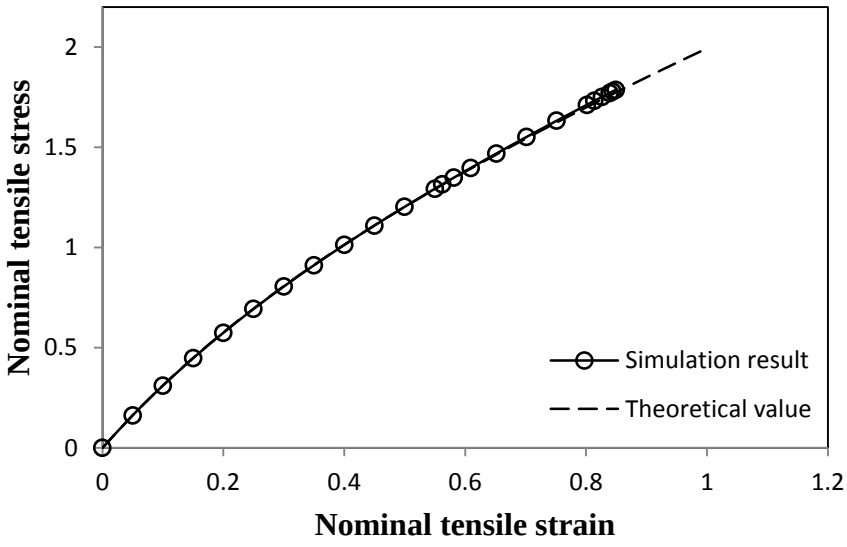

(a) Nominal stress P_{11} vs. nominal strain ε_1 for uniaxial tension simulation along the X_1 axial direction (up to $\lambda_1 = 1.85$)

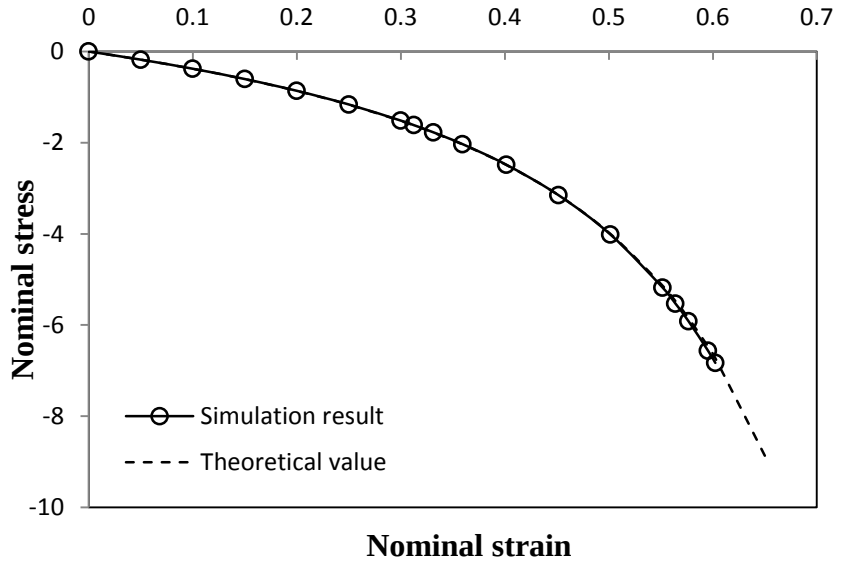

(b) Nominal stress P_{33} vs. nominal strain ε_3 for uniaxial compression simulation along the X_3 axial direction (up to $\lambda_3 = 0.6$)

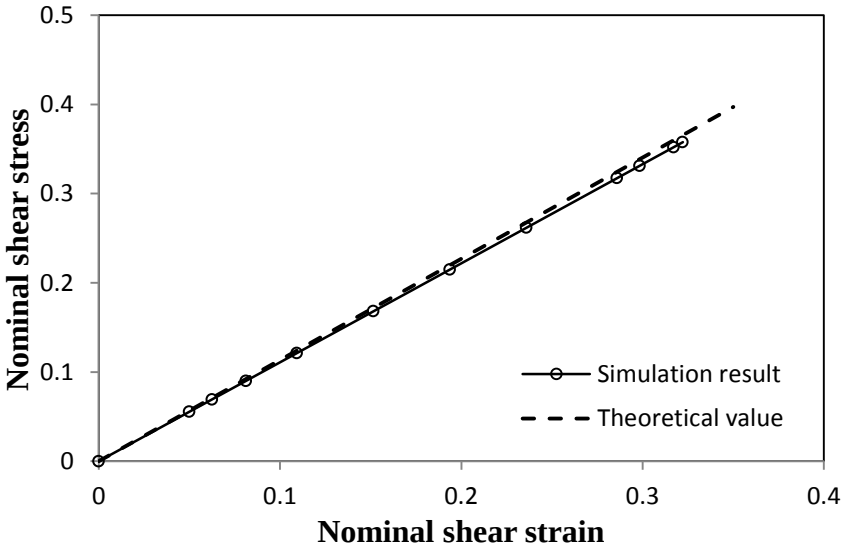

(c) Nominal shear stress P_{12} vs. nominal shear strain F_{12} for simple shear simulation in the X_1X_2 plane (up to $k = F_{12} = 0.32$)

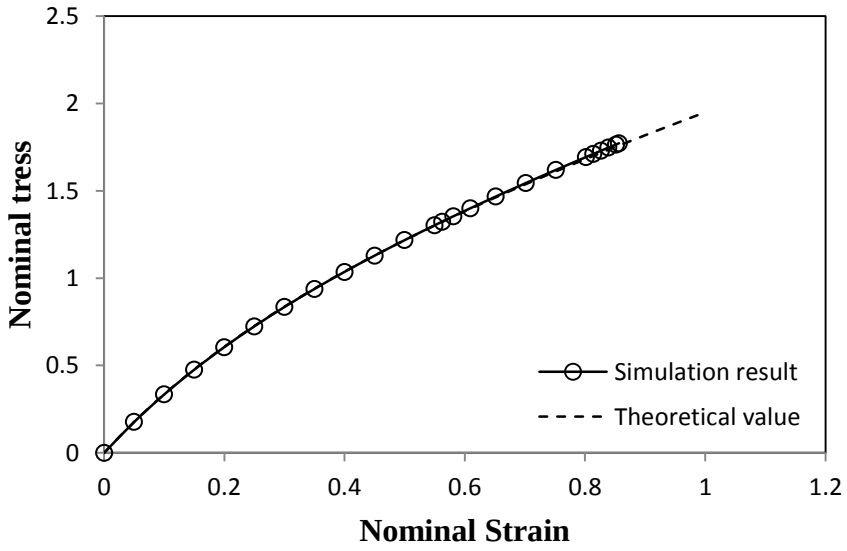

(d) Nominal stress P_{11} vs. nominal strain ε_1 for simulation of a biaxial deformation with nominal strain ratio $\varepsilon_1/\varepsilon_2$ = -0.3424

Figure 3.9 Simulation results of an RVE model with 5 vol% of rigid particles. The theoretical nominal stress-strain curve from the effective shear modulus is plotted as a dotted line in each figure.

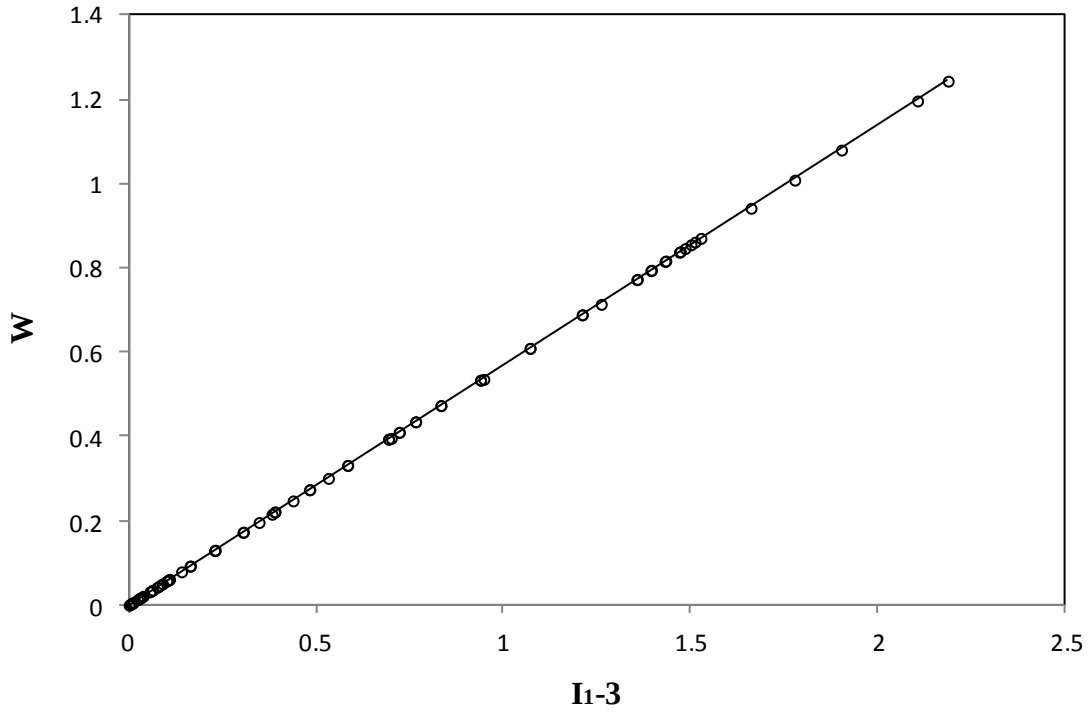

Figure 3.10 Average strain energy $\overline{W}$ vs. $I_1 - 3$ for 4 numerical simulations of an RVE model with 5 vol% of rigid particles. The linear fitting curve is plotted as a solid line.

FE simulations on other three RVE models with $c = 0.05$ are required to obtain an "average" effective shear modulus of the IPRNC with $(c = 0.05, \mu_r = \infty)$. Ideally all the four types of deformations should be examined on every RVE model to compute the effective shear modulus, however, because of the extensive computing time required for the simulations, the following strategy is used: to compute the effective shear modulus for a given (c, μ_r) case, the following three requirements are satisfied: (i) at least 6 FE simulations are performed; (ii) all four types of deformations are simulated; and (iii) all four related RVE models (with the particular volume ratio) are involved. Then the strain energy data from all the FE simulations are collected together to fit the effective shear modulus of the IPRNC. For example, 8 FE simulations are performed on the 4 RVE models for the IPRNC with $(c = 0.05, \mu_r = \infty)$ discussed above, and the effective shear modulus is computed by fitting all the strain energy data from the 6 simulations as $\mu_c = 1.1376$ (Figure 3.10). To investigate the variation between the effective shear moduli of different FE simulations, the effective shear modulus of every simulation is calculated by fitting related strain energy data and the maximum and minimum effective shear moduli are recorded to compare with the average effective shear modulus. For the

IPRNC with $(c = 0.05, \mu_r = \infty)$, the maximum and minimum values of the 6 computed effective shear moduli are $\mu^c_{\max} = 1.1404$ and $\mu^c_{\min} = 1.1350$, and they are represented by the error bars in Figure 3.11.

Similarly, the effective shear modulus of the IPRNC can be computed numerically for $c = 0.1, 0.2, 0.3$ (we note that for RVE models with large rigid particle volume fraction value, ABAQUS standard can only simulate a relatively limited extent of deformation because all deformations are carried by the matrix phase and the mesh in the matrix necking zones between close particles is severely distorted at even the early state of the deformation). The obtained moduli are plotted in Figure 3.11 as a function of the particle volume fraction.

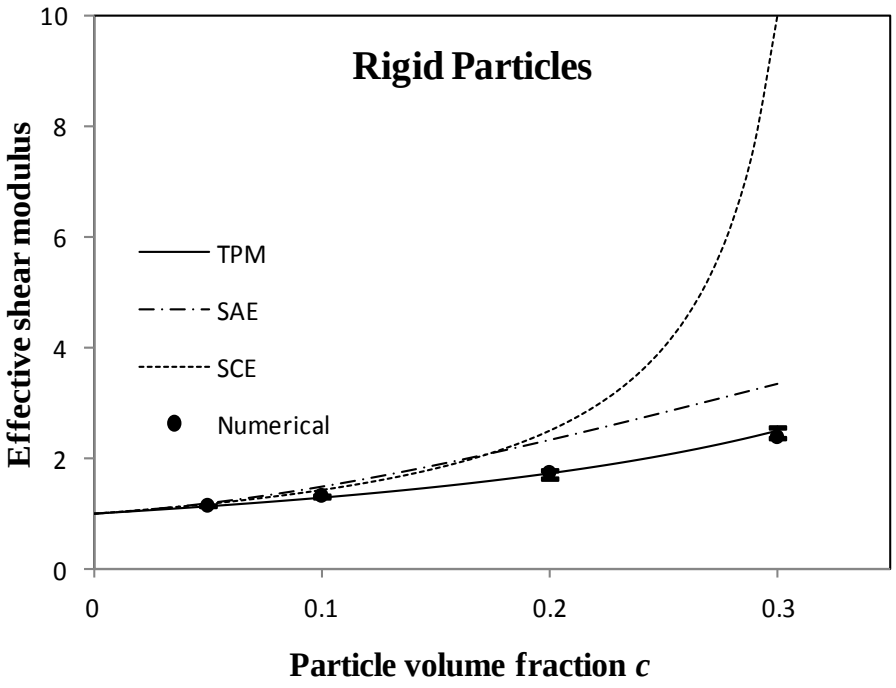

Figure 3.11 The effective shear moduli computed from numerical homogenisation for IPRNC with rigid particles and the SAE (strain amplification estimate), SCE (self-consistent estimate), and TPM (three phase model) predictions.

Based on the concept of strain amplification, Bergstrom and Boyce [62] proposed the following estimate of shear modulus for incompressible neo-Hookean composite embedded with rigid particles:

$$\mu_c = \mu_m (1-c)\left(1+3.5c+30c^2\right). \tag{3.46}$$

Castaneda [53] gave a self-consistent estimate of the effective shear modulus of the IPRNC as follows:

$$\mu_c = \frac{\sqrt{\left[(1-3c)\mu_r + (3c-2)\mu_m\right]^2 + 8\mu_m\mu_r} - \left[(1-3c)\mu_r + (3c-2)\mu_m\right]}{4}. \tag{3.47}$$

When the particles are rigid, it leads to the following result [53]

$$\mu_c = \frac{\mu_m}{1-3c}. \tag{3.48}$$

Obviously it will overestimate μ_c when $c \to 1/3$. The strain amplification estimate, SAE [62], and the self-consistent estimate, SCE [53] are both plotted in Figure 3.11 to be compared with the numerical results. Because the dispersion of the values of the effective shear moduli obtained from different RVE models (maximum and minimum values illustrated by the error bar in Figure 3.11) is remarkably small in all cases (less than 2.1%), the numerical results can be taken as a very close approximation to the "exact" solution. From Figure 3.11, it can be found that both the SCE and the SAE overestimate μ_c when $c > 0.1$. When $c = 0.05$, the prediction of the SCE and the SAE are about 3.42% and 4.39% larger than the numerical result, respectively. The errors increase up to 8.47% and 12.8% when $c = 0.1$. For moderate particle volume fraction $c = 0.2$, 44.3% and 33.9% errors are introduced to the SCE and the SAE predictions, respectively. The SCE result is actually not useable when $c > 0.2$: it will overestimate 3 times the value of μ_c when $c = 0.3$. The SAE prediction overestimate μ_c by 39.8% when $c = 0.3$.

Because the large deformation estimates for PRC cannot well predict the effective modulus of the IPRNC with rigid particles, the classical results for PRC in infinitesimal

deformation regime are examined. Because the formula proposed by Christensen and Lo [18] based on the three phase model (TPM) for the effective shear modulus of the linear elastic PRC agrees very well with the numerical homogenisation results under small strain [31] and is relatively simple, it is chosen to be compared with our numerical results under large deformation (Figure 3.11). Surprisingly, the TPM model originally developed for linear elastic PRC provides a much better prediction than the large deformation formulae. The differences between the predictions of the TPM model and the numerical results are only 0.39%, 2.05%, 0.22%, 5.08% for $c = 0.05$, 0.1, 0.2, and 0.3, respectively. In the case of infinitesimal deformation, Segurado and Llorca's [31] results suggest that the TPM model slightly underestimate the shear modulus of the linear elastic PRC when $c = 0.3$, which is consistent to our observations for neo-Hookean PRC under finite deformation.

3.4.4 Particles 100 times stiffer than matrix

FEM simulations are carried out on the IPRNC with large but finite stiffness contrast between particles and matrix ($\mu_r = 100$). Again the effective shear modulus are obtained by simulations of four types of deformations, i.e., uniaxial tension along the X_1 axial direction (up to $\lambda_1 = 1.50$), uniaxial compression along the X_3 axial direction (up to $\lambda_3 = 0.59$), simple shear in the X_1X_2 plane (up to $k = 0.77$), and general biaxial deformation ($\varepsilon_2/\varepsilon_1$ = 0.8116 up to ε_1 = 0.24) on an RVE with $c = 0.1$. The nominal stress-strain curves are shown in Figure 3.12 (a)-(c) for uniaxial tension, uniaxial compression and simple shear simulations, while the strain energy $\overline{W}$ computed in the four simulations of this RVE is plotted against $I_1 - 3$ in Figure 3.12 (d). The observed linear relation between $\overline{W}$ and $I_1 - 3$ is fitted by $\overline{W} = 0.6457(I_1 - 3)$ (R^2 = 1 in MS Excel 2007). The effective shear moduli computed from numerical homogenisation for the IPRNC with $\mu_r = 100$ are compared with the SCE, TPM predictions in Figure 3.13. The variations represented by the error bars are all below 4.25% (Figure 3.13). The TPM model matches the numerical results very well and the differences for c = 0.05, 0.1, 0.2, 0.3 are only 0.41%, 0.96%, 0.22% and 3.82%, respectively. The SCE result will overestimate the shear modulus significantly when $c > 0.1$, and the relative errors are 3.14%, 8.69%, 36.39% and 123.77% for c = 0.05, 0.1, 0.2, 0.3, respectively.

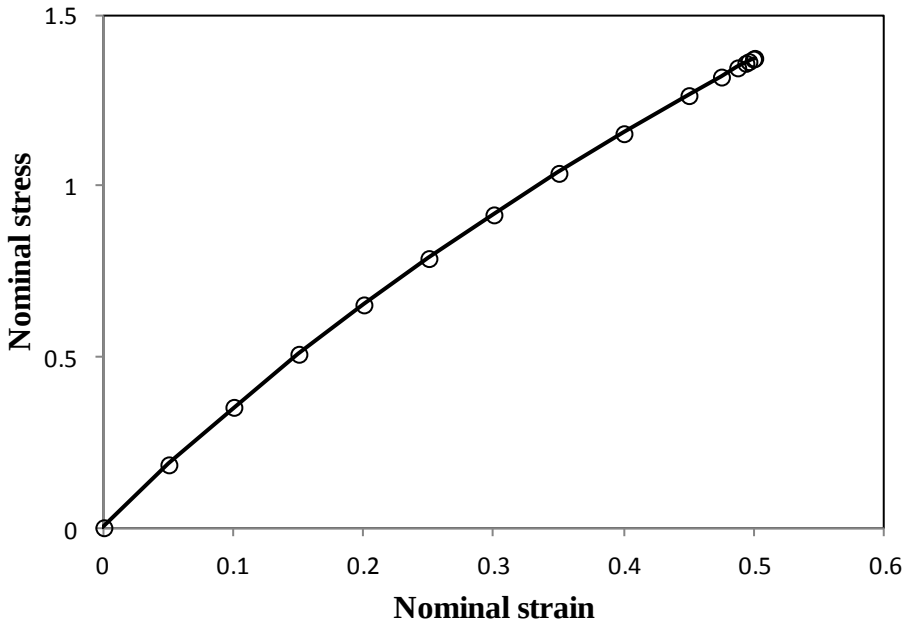

(a) Nominal stress vs. nominal strain for uniaxial tension simulation

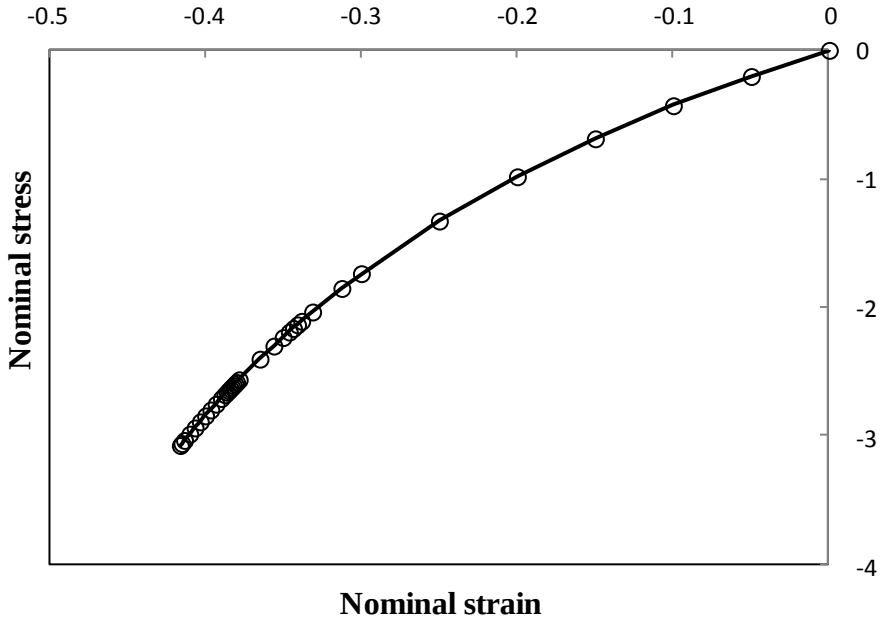

(b) Nominal stress vs. nominal strain for uniaxial compression simulation

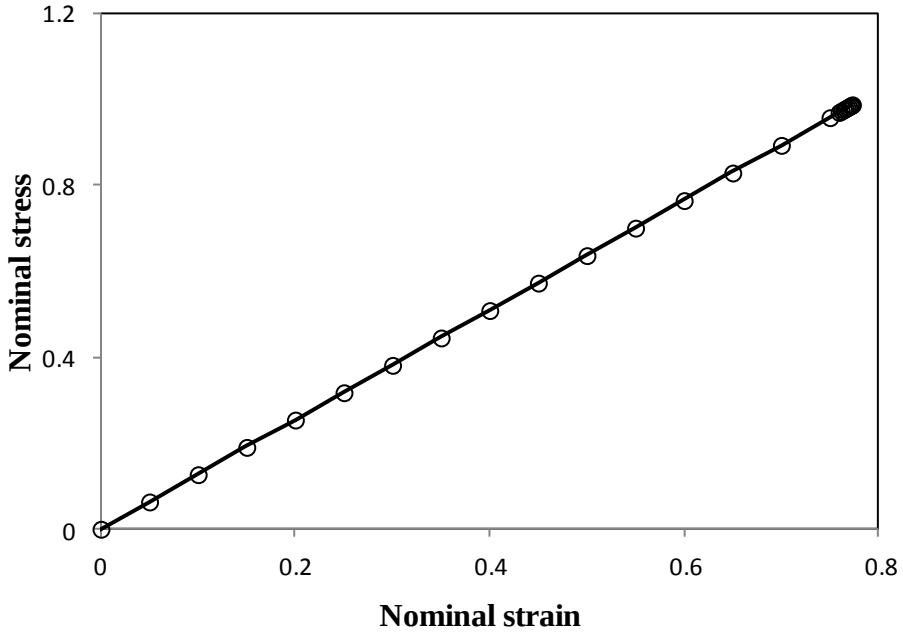

(c) Nominal shear stress vs. nominal shear strain for simple shear simulation

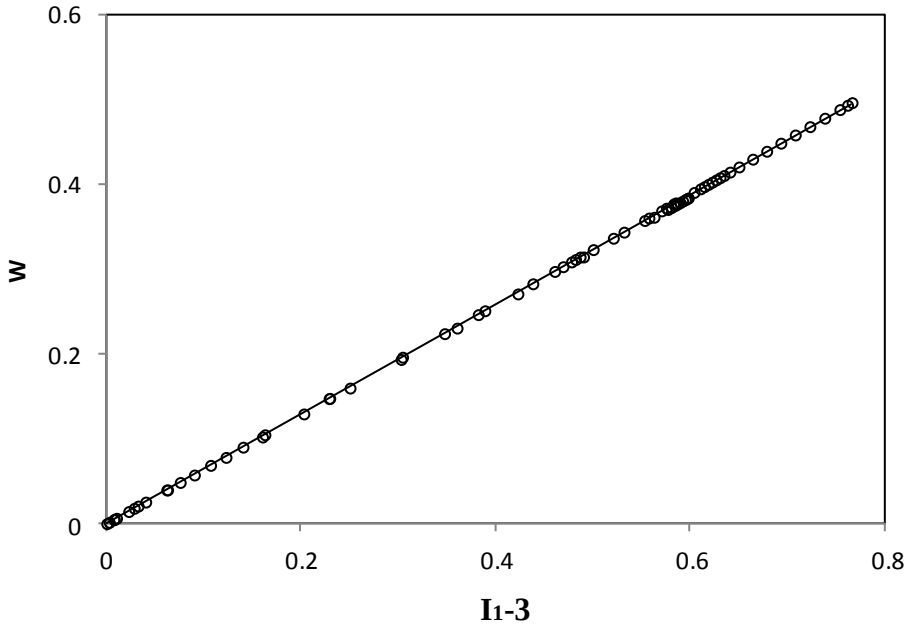

(d) Strain energy $\overline{W}$ vs. $I_1 - 3$

Figure 3.12 The nominal stress-strain curves of an RVE ($c = 0.1, \mu_r = 100$) for uniaxial tension (a), uniaxial compression (b) and simple shear (c) simulations respectively, while the obtained strain energy $\overline{W}$ is plotted against $I_1 - 3$ in (d).

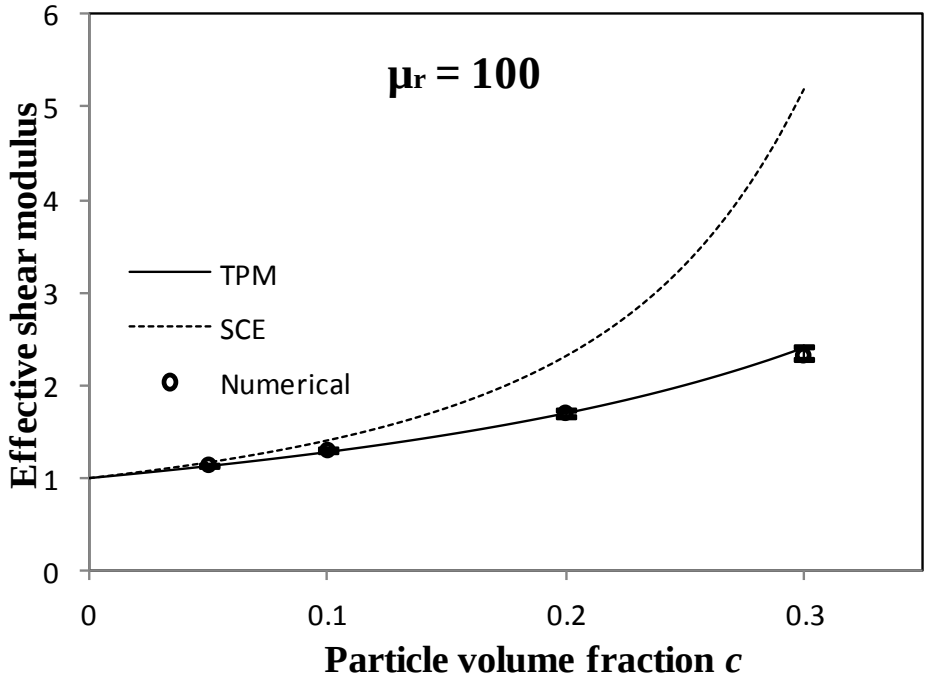

Figure 3.13 The effective shear moduli computed from numerical homogenisation for IPRNC with $\mu_r = 100$ and the SCE (self consistent model), TPM (three phase model) predictions.

3.4.5 Particles 10 times stiffer than matrix

To explore the case that the particle stiffness is comparable to the matrix stiffness, a set of simulations is performed for $\mu_r = 10$ in ABAQUS. Because previously the uniaxial tension and the uniaxial compression deformations have already been investigated extensively to verify the isotropy of the RVE models, only simple shear and general biaxial simulations are required. To validate the neo-Hookean model for the IPRNC, 8 series of biaxial simulations ($\varepsilon_2/\varepsilon_1$ = 1, 0.8, 0.6, 0.4, 0.2, 0, -0.2, -0.4) as well as the simple shear simulation (up to $k = 1.0$) are performed on an RVE model with $c = 0.2$ to cover a significant amount of general deformations. All the $\overline{W}$ vs. $I_1 - 3$ data from 34 FE simulations (9 biaxial, 3 simple shear, 12 uniaxial tension and 10 uniaxial compression simulations) for the IPRNC with $(c = 0.2, \mu_r = 10)$ is fitted by the linear relation $\bar{W} = 0.7480(I_1 - 3)$ (which implies that $\mu = 1.4960$) in Figure 3.14, which is consistent with the effective shear modulus obtained from uniaxial tension simulations

in section 4.2 ($\mu = 1.4958$). The maximum and minimum effective shear moduli from individual simulation are $\mu^c_{\max} = 1.5190$ and $\mu^c_{\min} = 1.4526$, which implies the variations of the effective shear moduli are within 4.5%. This clearly indicates that the IPRNC can be well predicted by a neo-Hookean model.

The numerical results for the effective shear modulus are plotted in Figure 3.15 together with the predictions of the SCE and TPM models, and the reported dispersions in the numerical simulation are less than 4.56%. Again the TPM model represents an excellent approximation the numerical results and the maximum difference for $c =$ 0.3 is only 1.8%. The SCE model still overestimates the shear modulus by 1.65%, 4.41%, 12.36% and 213.22%, respectively, for $c =$ 0.05, 0.1, 0.2, 0.3, though the introduced error for a given volume fraction is smaller than that of the IPRNC with $\mu_r = 100$. This is expected because the difference between the stiffness of the composite and the matrix is smaller due to the reinforcement of less stiff particles.

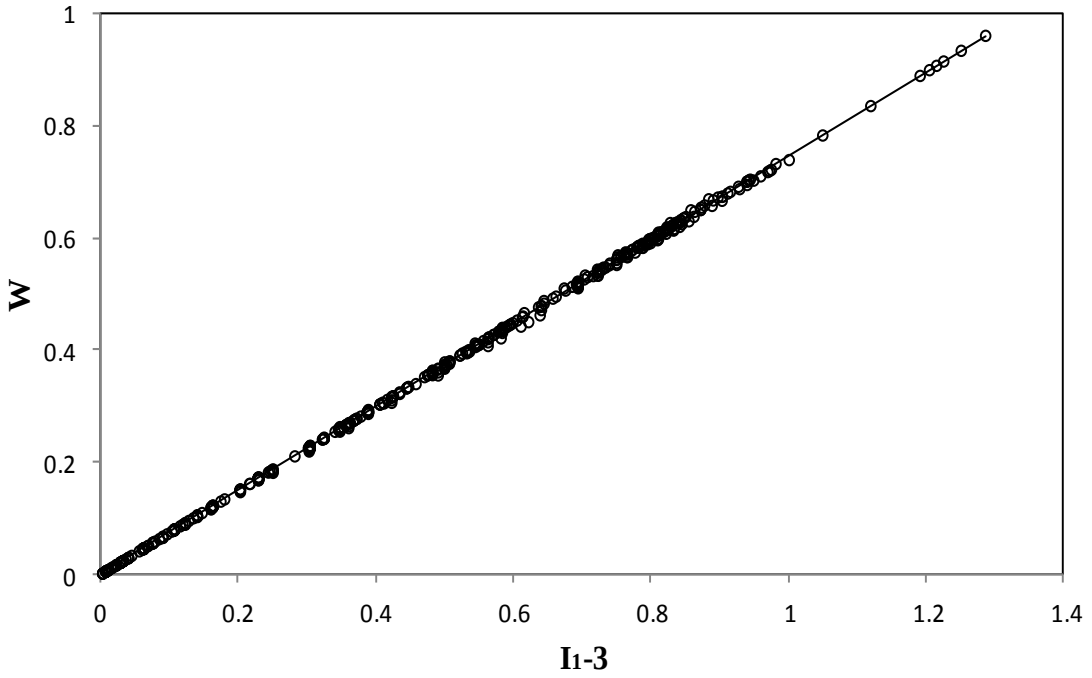

Figure 3.14 All the $\overline{W}$ vs. $I_1 - 3$ data from 34 FE simulations (9 biaxial, 3 simple shear, 12 uniaxial tension and 10 uniaxial compression simulations) for the IPRNC $(c = 0.2, \mu_r = 10)$ are fitted by the linear relation $\bar{W} = 1.496(I_1 - 3)$ ($R^2 = 0.9998$).

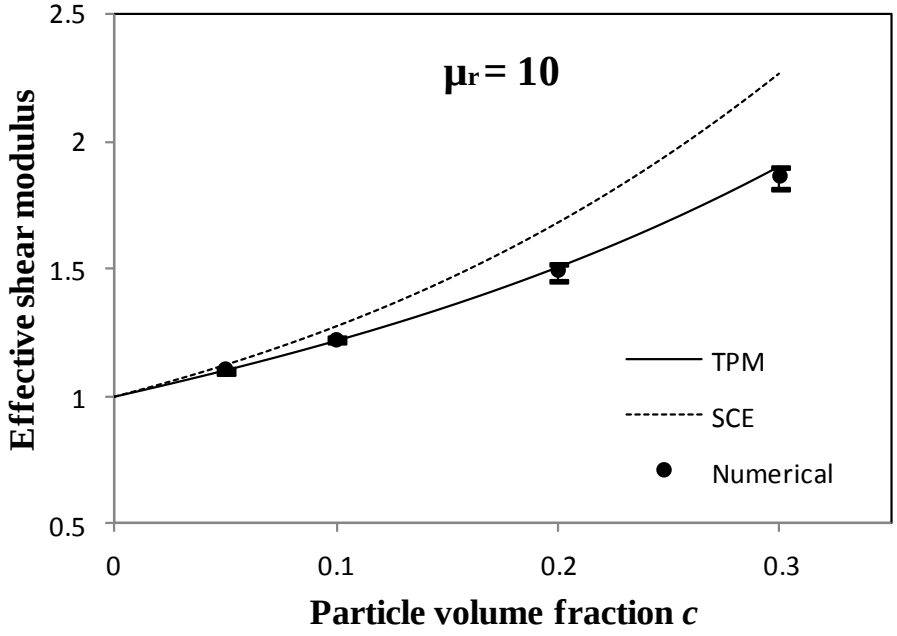

Figure 3.15 The effective shear moduli computed from numerical homogenisation for IPRNC with $\mu_r = 10$ and the SCE(self consistent model) and TPM (three phase model) predictions.

3.4.6 Matrix twice stiffer than particles

In previous simulations, the particles are always stiffer than the matrix. The opposite case (i.e., the matrix is stiffer than the particles) is considered here to fully examine the effect of stiffness contrast between particles and matrix. A small stiffness contrast ($\mu_m/\mu_r = 2$, or $\mu_r = 0.5$) is used to make relatively large deformation possible in the numerical simulation (the convergence problem usually occurs at relatively moderate deformation in previous simulations, which partly comes from the large stiffness contrast, i.e., $\mu_r/\mu_m \geq 10$). The FE simulations of uniaxial tension (up to $\lambda_1 = 2.0$), uniaxial compression (up to $\lambda_3 = 0.17$), simple shear (up to $k = 2.40$), and general biaxial ($\varepsilon_2/\varepsilon_1$ = -0.4025 up to ε_1 = 1.0) deformation are performed on an RVE with $c =$ 0.3. The strain energy data $\bar{W}$ from all the 4 simulations are fitted in Figure 3.16 (a) and the obtained effective shear modulus $\mu_c = 0.8296$. The nominal stress-strain curve is plotted Figure 16 (b), which is almost identical to the theoretical result based on the computed effective shear modulus. This suggests that the IPRNC's response at significant stretch still follows the neo-Hookean model's prediction.

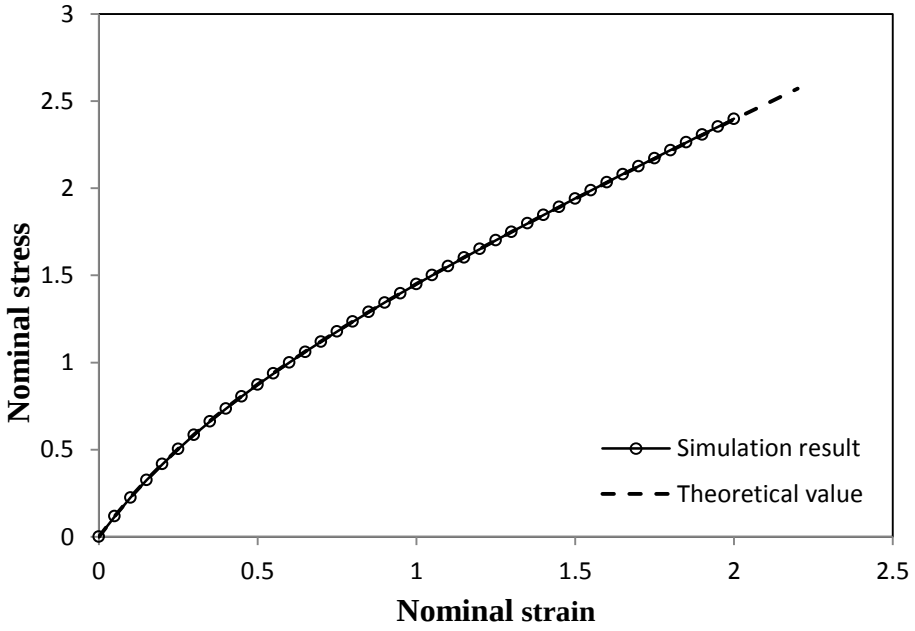

(a) Nominal stress vs. nominal strain for uniaxial tension simulation

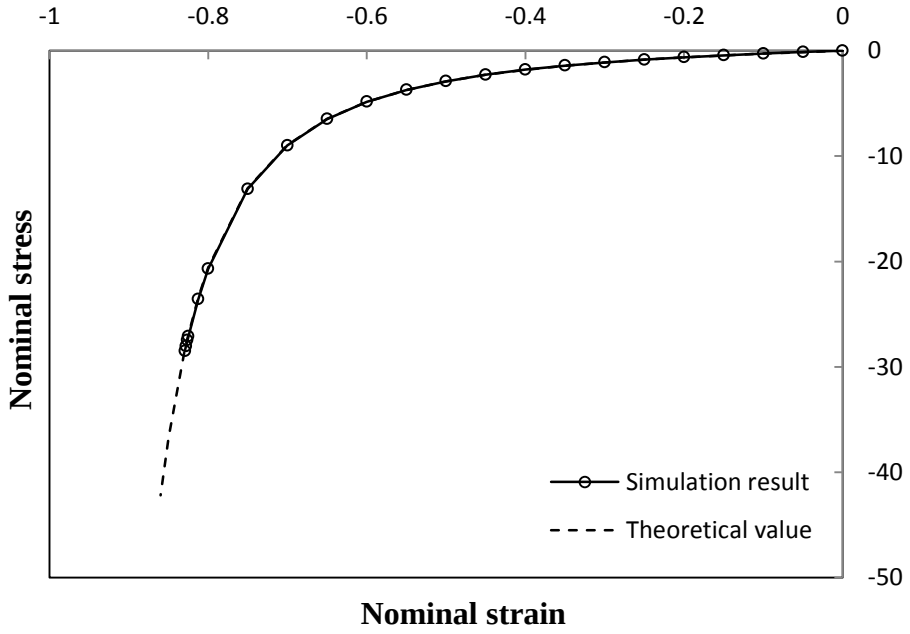

(b) Nominal stress vs. nominal strain for uniaxial compression simulation

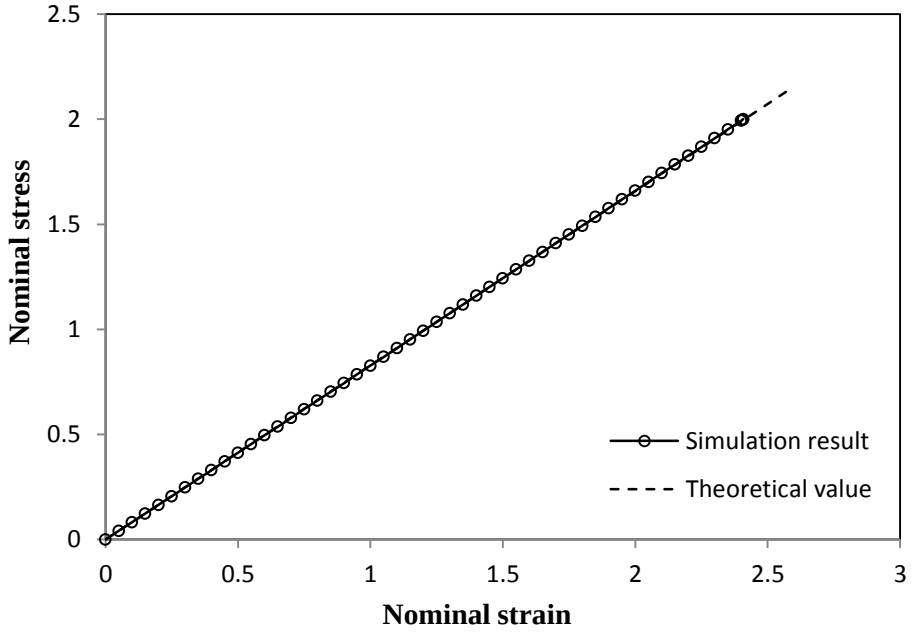

(c) Nominal shear stress vs. nominal shear strain for simple shear simulation

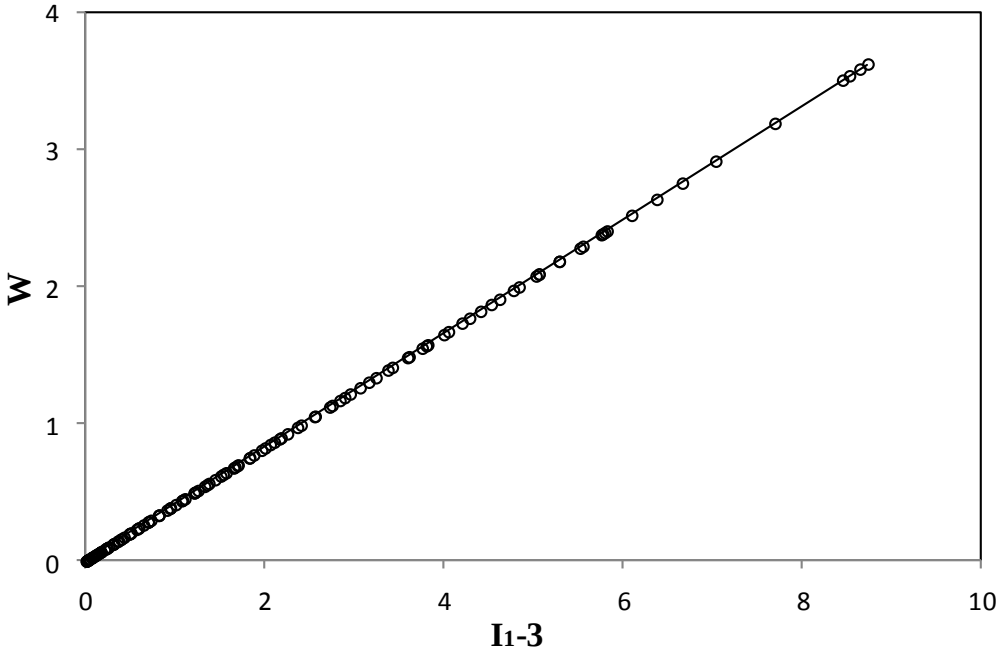

(d) Strain energy $\overline{W}$ vs. $I_1 - 3$

Figure 3.16 The nominal stress-strain curves are shown in (a), (b) and (c) for uniaxial tension, uniaxial compression and simple shear simulations respectively, while the obtained strain energy $\overline{W}$ is plotted against $I_1 - 3$ for an RVE ($c = 0.3$, $\mu_r = 0.5$) in (d).

The effective shear moduli derived from the FE simulation results are shown in Figure 3.17 with maximum dispersions represented by error bars (all less than 0.7%). The numerical results are also compared with the theoretical approximations of the SCE and TPM models. Because the stiffness contrast between the particles and the matrix is small, the effective shear moduli of the IPRNC are close to the shear modulus of the matrix. It is then not surprising that both the SCE and TPM models agree well with the numerical results. The maximum errors for $c = 0.3$ are only 0.36% and 0.76% for the SCE and TPM models, respectively.

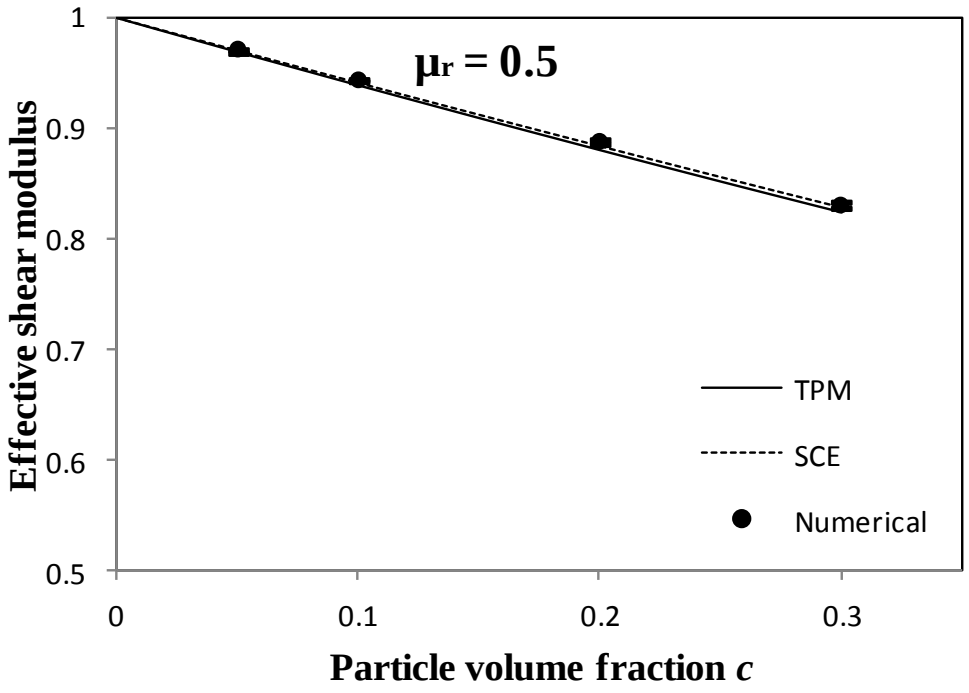

Figure 3.17 The effective shear moduli computed from numerical homogenisation for IPRNC with $\mu_r = 0.5$ are compared with the SCE (self consistent model) and TPM (three phase model) predictions.

3.4.7 Deformation ranges of the FE simulations

Altogether 152 FE simulations have been performed on the 16 RVE models. The strain energy $\bar{W}$ computed from each FE simulation shows a clear linear proportional relation with $I_1 - 3$, which suggests a neo-Hookean type response and the corresponding effective shear modulus can be obtained by data fitting for each FE simulation. The dispersions of fitted effective shear moduli are within 7.5% as shown in Figures 3.11, 3.13, 3.15 and 3.17.

It should be noted that convergence is a big issue in our numerical simulation even for RVE models with very refined mesh (e.g., with more than 200,000 elements), particularly when the stiffness contrast between the particles and the matrix is large (e.g. $\mu_r = \infty$, 100). Because we can only claim the neo-Hookean type response of the IPRNC with the deformations simulated by our FE simulations, it is worthy to report the deformation ranges of the FE simulations for various IPRNC in Table 3.2, in which the deformation range is represented by the maximum I_1 reached by the FE simulations, as well as the principal stretches for uniaxial tension/compression, or nominal shear strain for simple shear deformation.

For IPRNCs with particular volume fraction of particles, the larger the stiffness contrast between the particles and the matrix, the smaller deformation range the FE simulations can reach. For IPRNCs with particular μ_r/μ_m , the larger the volume fraction of particles, the more limited the FE simulations. The reason is that larger volume fraction of particles usually means more severe mesh distortion at the necking area between particles due to the deformation localisation.

c \ μ_r/μ_m	0.5	10	100	∞
0.05	17.55 (λ = 4.13) 13.71 (λ = 0.14) 13.68 (k = 3.26) 5.03	4.96 (λ = 1.98) 6.31 (λ = 0.32) 4 (k = 1) * 5.66	3.87 (λ = 1.62) 3.74 (λ = 0.58) 4 (k = 1) * 3.41	4.5 (λ = 1.84) 5.19 (λ = 0.39) 3.21 (k = 0.45) 4.53
0.1	17.16 (λ = 4.08) 17.79 (λ = 0.11) 10.42 (k = 2.72) 8.17	4.4 (λ = 1.81) 5.02 (λ = 0.41) 4 (k = 1) * 4.49	3.58 (λ = 1.49) 3.77 (λ = 0.58) 3.60 (k = 0.77) 3.47	3.31 (λ = 1.35) 3.66 (λ = 0.60) 3.08 (k = 0.28) 3.3
0.2	14.36 (λ = 3.71) 19.63 (λ = 0.10) 11.96 (k = 2.99) 7.81	4.22 (λ = 1.75) 4.29 (λ = 0.49) 4 (k = 1) * 3.9	3.35 (λ = 1.37) 3.41 (λ = 0.67) 3.6 (k = 0.77) 3.43	3.05 (λ = 1.13) 3.17 (λ = 0.78) 3.06 (k = 0.24) 3.25
0.3	13.77 (λ = 3.63) 11.74 (λ = 0.17) 8.80 (k = 2.40) 5.06	3.51 (λ = 1.46) 3.92 (λ = 0.55) 3.53 (k = 0.72) 3.43	3.08 (λ = 1.17) 3.14 (λ = 0.8) 3.07 (k = 0.27) 3.15	3.06 (λ = 1.14) 3.003 (λ = 0.96) 3.03 (k = 0.17) 3.006

* The simulations finished without convergence problems.

Table 3.2 Deformation range represented by I_1 for all the FE simulations.

3.4.8 One particle unit cell model

The simple "one particle in the centre" unit cell model (Figure 3.18) is sometimes used in the literature to simulate PRC (e.g., Boyce). This type of unit cell represents composites embedded with cubic arrays of spheres [94], which is macroscopically orthotropic. To examine the mechanical responses of the IPRNC with this particular type of microstructure under finite deformation, FEM simulations of the unit cell model are performed in ABAQUS for uniaxial tension/compression and simple shear. The particle volume fraction $c = 0.2$ and there are around 20,000 tetrahedral elements and 30,000 nodes in the FEM model. Both the matrix and the particles are modelled as incompressible neo-Hookean materials with $\mu_m = 1$ and $\mu_r = 10$, respectively. In all simulations, PBC is applied to get a good estimate of the real response of the composite and a deformed unit cell is shown in Figure 3.18.

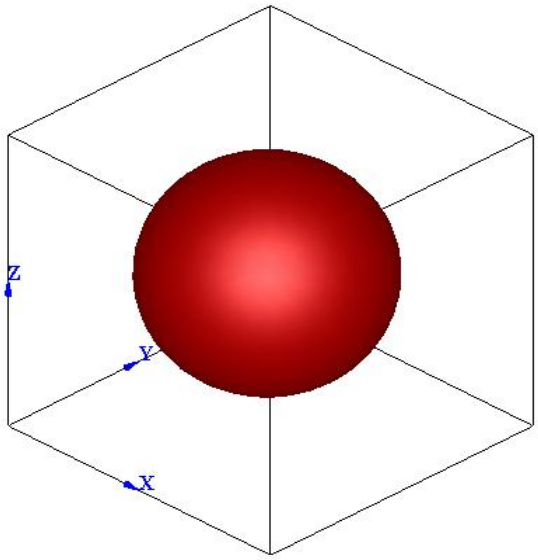

Figure 3.18 Simple "one particle in the centre" unit cell model.

The average strain energy $\overline{W}$ vs. $I_1 - 3$ curves are plotted for three loading cases (Figure 3.19). For each loading case, a clear proportional relation between $\overline{W}$ and $I_1 - 3$ can be observed and the effective shear moduli predicted from uniaxial tension/compression and simple shear simulations are $\mu_c = 1.6698$ ($R^2 = 0.9999$, uniaxial tension), 1.8596 ($R^2 = 0.9989$, uniaxial compression) and 1.4150 ($R^2 = 1.0$, simple shear), respectively, and the relative difference is about 27.2%. While for the multi-particle RVE models with $(c = 0.2, \mu_r = 10)$ used in the study, the maximum relative difference between effective shear moduli predicted by different loading cases is well below 1.2%. The effective modulus predicted by the multi-particle RVE models ($c = 0.2$, $\mu_r = 10$) is $\mu_c = 1.4946$. The comparisons between results from one-particle unit cell model and multi-particle RVE models suggest that, although the effective modulus predicted by the one-particle unit cell model is close to the one predicted by multi-particle RVE models (relative error about 20%), the behaviour of the one-particle unit cell model is anisotropic under finite deformation, as determined by its orthotropic microstructure. Furthermore, a one-particle unit cell model cannot capture the characteristics of the stress/strain field in the matrix necking zone, which is critical to the strength investigation of the IPRNC. Hence multi-particle RVE models should be used to obtain realistic response of IPRNC under finite deformation.

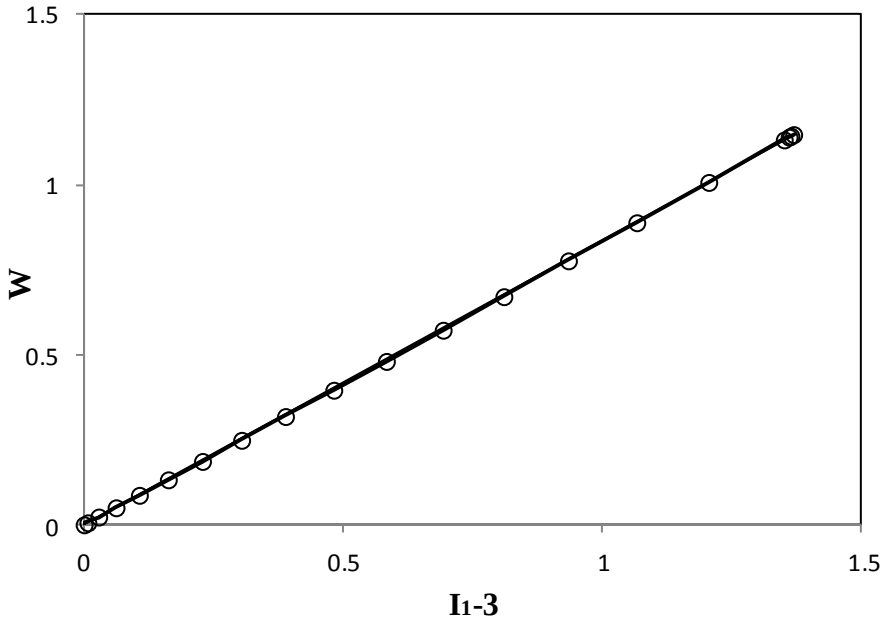

(a) Strain energy $\overline{W}$ vs. $I_1 - 3$ for uniaxial tension simulation

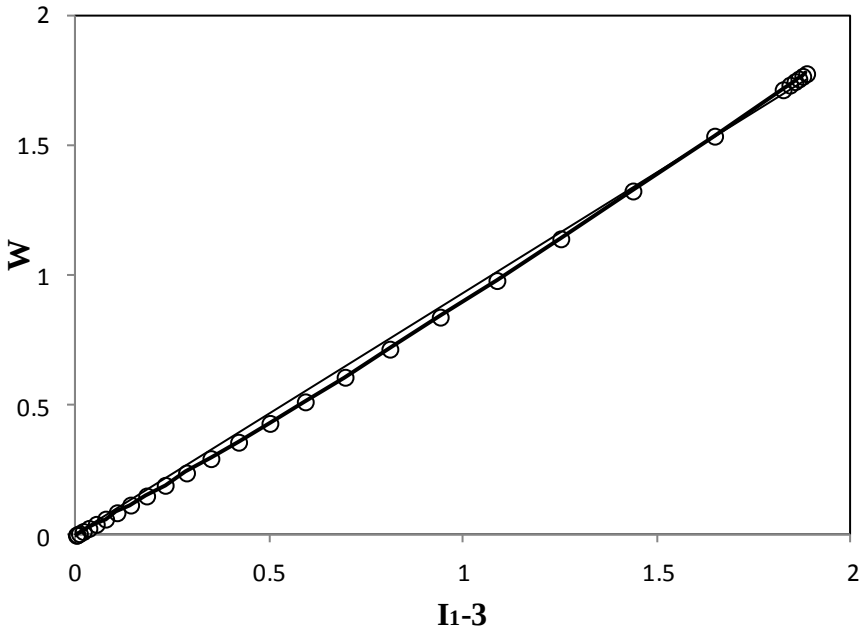

(b) Strain energy $\overline{W}$ vs. $I_1 - 3$ for uniaxial compression simulation

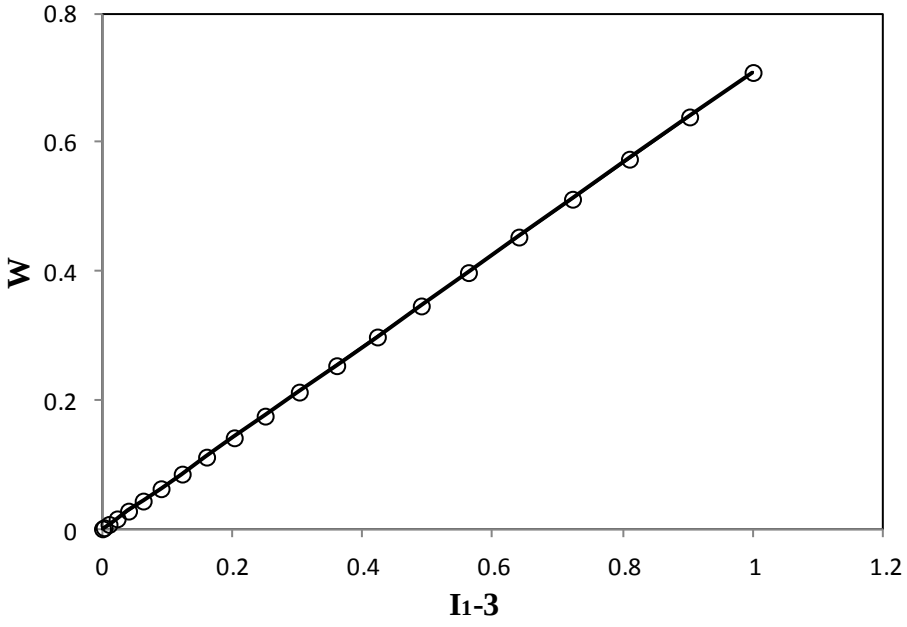

(c) Strain energy $\overline{W}$ vs. $I_1 - 3$ for simple shear simulation

Figure 3.19 The average strain energy $\overline{W}$ vs. $I_1 - 3$ curves are plotted for three loading cases

3.5 Concluding Remarks

Three-dimensional RVE models are employed to investigate the mechanical behaviour of the IPRNC, in which both the matrix and the particle reinforcement are incompressible neo-Hookean materials. To consider different particle volume fractions (i.e., $c = 0.05, 0.1, 0.2, 0.3$), 16 RVE samples (4 for each volume fraction value) with periodic microstructures are created. In each RVE, 27 non-overlapping identical spheres are randomly distributed in a cubic unit. The isotropy of the random distributions of particles in the 16 RVE models is then examined, and the RVE models are meshed for finite element computation. Periodic meshes are generated so that the periodic boundary conditions can be applied during the FE simulations. The mesh convergence study shows that a standard mesh with about 80,000 elements can obtain accurate result, which means the errors between both results (standard mesh and refined mesh) are well below 2%.

To double check the isotropy of the RVE models' mechanical responses, uniaxial tension and compression along different directions are simulated for the RVE models and the isotropy of the RVE models is verified directly. The simulation results of the uniaxial tension and compression are consistent, which implies that the small-size RVE models used are sufficient to obtain accurate responses of the IPRNC. The computed strain energy data suggests that the mechanical response of the IPRNC can be well predicted by an incompressible neo-Hookean model.

Four different particle/matrix stiffness ratios are studied in the FE simulations: $\mu_r/\mu_m = \infty$ (i.e., rigid particles), 100, 10, 0.5, to investigate the effect of stiffness ratio between the particle and the matrix. The following four types of finite deformations are simulated: uniaxial tension and compression along coordinate axial directions and random directions, simple shear, and general biaxial deformation. All the simulation results (i.e., RVE with any particle volume fraction, any particle/matrix stiffness ratio and any loading case) show that the average strain energy $\bar{W}$ is proportional to $I_1 - 3$, which suggests that the overall behaviour of the IPRNC can be modelled by an incompressible neo-Hookean model. The effective shear moduli μ_c of the IPRNCs are obtained by fitting the strain energy data from the numerical simulation results. Because

the dispersion in the values of the obtained moduli is remarkably small in all cases, the numerical results can be considered as a very close approximation to the "exact" effective shear moduli of the IPRNC. They are compared with three theoretical models: the self-consistent estimate, SCE [53], the strain amplification estimate for composites with rigid particles, SAE [62], and the classical linear elastic three phase model, TPM [18]. It is found that the TPM provide very accurate approximation to the numerical results (maximum relative difference less than 5.1%) though it is developed for linear elastic PRC. Even though the SCE and the SAE are proposed for neo-Hookean composites, they overestimate the effective shear modulus of the IPRNC when the particle volume fraction $c > 0.1$.

We note that mesh of the matrix necking zone between close particles is very challenging and severe deformation localisation may happen when the stiffness contrast between the particle and the matrix is large. Hence convergence is a big issue in our numerical simulation even for RVE models with very refined mesh (e.g., with more than 200,000 elements). For example, it is only possible to reach moderate deformation state for some cases (e.g., $I_1 = 3.06$, or 14% tension for the IPRNC with $(\mu_r = \infty, c = 0.3)$. For much less critical case like the IPRNC with $(\mu_r = 0.5, c = 0.3)$, huge deformation can be reached (i.e, 313% tension or 86% compression). The numerical results show clearly that up to the deformations the FE simulations can reach (that is, until there is a convergence problem), all the numerical results of $\bar{W}$ and $I_1 - 3$ can be fitted almost exactly using the linear relation suggested by the incompressible neo-Hookean model. Therefore it is safe to conclude that the mechanical behaviour of the IPRNC studied here can be well modelled by another incompressible neo-Hookean model within the limit of current FE software ABAQUS.

Chapter 4 Fibre-Matrix Interaction in Fibre-Reinforced Composites under Finite Deformation

Objective

- To investigate the strain energy contribution from the ground matrix of the human annulus fibrosus (HAF) with collagen fibres under contraction by fitting the experimental data of the uniaxial tension along the axial direction of the HAF available in the literature;
- To investigate the strain energy contribution from the ground matrix of the HAF with collagen fibres under different stretch ratios by fitting the corresponding uniaxial and biaxial testing results available in the literature;
- To identify the fibre-matrix interaction from the fibre stretch dependent behaviour of the ground matrix, which cannot be explained by the classical uncoupled constitutive models for soft tissue;
- To analyse the significance of the identified fibre-matrix interaction by comparing the finite element simulations of the uniaxial test of the HAF along the circumferential direction with the experimental data in the literature;
- To discuss the potential physical mechanisms related to the identified fibre-matrix interaction and various constitutive models considering fibre-matrix interaction.

Summary

Although the mechanical behaviour of the human annulus fibrosus (HAF) has been extensively studied, the interaction between the collagen fibres and the ground matrix has not been well understood and is therefore ignored by most constitutive models. The objective of this study is to identify the significance of the fibre-matrix interaction in the HAF by careful investigation of the experimental data, the theoretical constitutive models, and the numerical simulation results in the literature. Based on the experimental

results from biaxial and uniaxial tests, it is shown that the mechanical behaviour of the matrix can be well simulated by an incompressible neo-Hookean type model, but the effective stiffness of the matrix depends on fibre stretch ratio, which can only be explained by fibre-matrix interaction. Furthermore, it is found that this interaction takes place anisotropically between the matrix and the fibres distributed in different proportions in different directions. The dependence of the tangent stiffness of the matrix on the first invariant of the deformation tensor can also be explained by this fibre orientation dispersion.

4.1 Introduction

It is reported that about 85% of the population in the Western countries are likely to experience lower back pain (LBP) during their lives. The most important etiologic factor for LBP is the degeneration of intervertebral disc (human annulus fibrosus, HAF), which usually stems from fibre disorganisation in the disc, due to excessive physical activities or an extreme lack of physical activity that causes degeneration of the collagen fibres. In the latter case, a simple improper posture, can cause the HAF to deform excessively or even to rupture as the stresses experienced by the degenerated HAF are well above the level the tissue can accommodate [105]. Many other spine-related diseases and injury (i.e. Degenerative Disc Disease or vehicle injury) are also related to the degeneration or mechanical damage of the HAF. An accurate understanding of the mechanical properties of the HAF is very important for (i) understanding of the intrinsic sources of related diseases; (ii) assessing optimised surgical options for patients; and (iii) optimal design of the implants. Because of these reasons, the mechanical behaviour of the HAF has been extensively studied [106-108].

The simplest model for the HAF treats the matrix as an isotropic solid while collagen fibres are modelled as separate nonlinear springs or rebars [108] (i.e., the HAF is not modelled as one single composite material). Obviously a much better approach is to model the HAF as a hyperelastic fibre-reinforced composite material. One approach of the hyperelastic modelling is to use the strain components directly, e.g., the classical "Fung-type" model [78, 109], which is widely used in the literature [81]. Normally the parameters involved in this kind of model do not have clear physical meaning and this approach usually has the convexity problem [79, 110]. It will most likely violate the traction free boundary conditions [81]. Another approach is to model soft tissue as a

hyperelastic material using the invariants of the deformation tensor and fibre directions [83, 106, 111, 112]. However, it was recently found out that none of these models are able to predict a general multiaxial behaviour of the HAF: Bass et al. [81] found that none of the available constitutive models can adequately reproduce the experimental results as evidenced by both uniaxial and biaxial tests of the HAF simultaneously. Hence the reliability of general numerical simulations based on current models remains questionable. This is probably because the precise nature of the mechanism of the interaction between the fibres and the ground matrix is still elusive.

Adams and Green [93] found that the strength of the HAF soft tissue depends on the specimen size. This size dependence stems from the fibre-matrix shear interaction, as well as the boundary effect. However, currently most hyperelastic models ignore the interaction between the fibre and the matrix. These models decouple the strain energy function only into contributions from the fibres and the matrix [83, 84], and they are denominated as "classical decoupled models" thereafter. Recently Peng et al. [7] found that the angle change observed in the uniaxial test of the HAF along the circumferential direction cannot be predicted by the classical decoupled models, and the fibre-matrix shear interaction has to be counted. In the popular invariant set proposed by Spencer [87], no invariant can fully characterise the fibre-matrix interaction. Wu and Yao [106] tried to predict the fibre-matrix interaction based on curve fitting of uniaxial test of the HAF along the circumferential direction, but their model cannot be applied to other loading situations (e.g., uniaxial test of the HAF along the axial direction). To overcome this problem, Criscione et al. [82] developed a physically based strain invariant set for transversely isotropic material. Based on this strain invariant set, Blemker et al. [86] proposed a muscle model with a interaction term while the matrix term is ignored. In their model, the effective along-fibre shear modulus and cross-fibre (transverse) shear modulus are both assumed to be constant. Peng et al. [7] used the relative shear angle between the fibre and the matrix plane originally perpendicular to the fibre direction to describe the fibre-matrix shear interaction. The same relative shear angle is used in the finite deformation version of the microplane model [113, 114]. A phenomenological model was then developed to predict the fibre-matrix shear interaction [7]. In this model, the along fibre shear stiffness depends on the fibre stretch, which is consistent with the experimental study [115]. Guo et al. [6] found that the phenomenological shear interaction term can be explained by composite theory. This so-called "composites-based" (shear) interaction comes from the inhomogeneous deformation due to the

different mechanical properties of the fibres and the matrix. deBotton et al. [90] found similar fibre-matrix interaction for incompressible neo-Hookean composites. The mechanism of the composites-based interaction was later verified theoretically [116, 117] and numerically [90, 91, 97]. Caner et al. (2007) used the microplane model to simulate the collagen fibre orientation dispersion in the HAF and concluded that although some of the experimental data can be simulated by taking into account the directional distribution of the collagen fibres only, in reality there must also be some fibre-matrix interaction in the HAF.

However, the fibre-matrix interaction in soft tissue has not been characterised from experimental results directly. For anisotropic materials, biaxial experiments are usually required to characterise the mechanical properties of the materials [118]. The objective of this study is to identify the significance of the fibre-matrix interaction in the HAF by careful investigation of the experimental data, the theoretical constitutive models, and the numerical simulation results in the literature.

First the uniaxial and biaxial experimental data [81] is used to reveal the fibre-stretch dependence of the effective matrix stiffness of the HAF, which can only be explained by fibre-matrix interaction. The finite element (FE) results are also employed to show that the classical uncoupled models fail to capture the deformation characteristics of the soft tissues due to the absence of the fibre-matrix interaction in the models. Several typical constitutive models of soft tissues with fibre-matrix interaction are then investigated and the associated physical interpretations are discussed in detail. The quantitative analysis suggests that a combination of the composite effect and the fibre orientation dispersion is required to explain the fibre-matrix interaction in the HAF.

The structure of this chapter is as follows. In section 4.2, the framework of classical uncoupled constitutive models of soft tissue is introduced. The assumptions involved are briefly discussed. In section 4.3, the uniaxial experimental result [81] of HAF along the axial direction is first used to investigate the strain energy of the ground matrix with collagen fibres under contraction. It is found that the incompressible neo-Hookean model is sufficient to approximate the strain energy of the ground matrix. Then the biaxial experimental data [81] is analysed to obtain the strain energy of the ground matrix with the collagen fibres under different stretch ratios. The result shows that the effective matrix stiffness depends on the collagen fibre stretch ratio, which cannot be

explained by the classical uncoupled models. In section 4.4, it is shown that the FE simulations based on the classical uncoupled models predict incorrect deformation of the HAF for uniaxial tensile test along the circumferential direction because the fibre stretch dependence of the effective matrix stiffness is not modelled. In section 4.5, several typical constitutive models of soft tissues with fibre-matrix interaction are studied and the associated physical interpretations are investigated in details. After several issues are discussed briefly in section 4.6, some concluding remarks are given in section 4.7.

4.2 Classical uncoupled constitutive models of soft tissue

Soft tissue is usually treated as pseudo-elastic material and modelled as hyperelastic fibre reinforced composite in order to study its mechanical behaviours under finite deformation [78]. The mechanical behaviour of a hyperelastic material can be fully characterised by the strain energy density function *W*, which is a scalar function of the right Cauchy-Green deformation tensor $\mathbf{C}$. If the hyperelastic material is isotropic, *W* can be written as a function of the three principle invariants of $\mathbf{C}$, i.e., $W(\mathbf{C}) = W(I_1, I_2, I_3)$. Because the soft tissues are reinforced by collagen fibre, and most of them are not isotropic. Some well-organized soft tissues, such as ligaments, tendons, and lamellae in the HAF, are reinforced with unidirectional collagen fibres, so they are treated as transversely isotropic materials in mechanical analysis. For these unidirectional fibre-reinforced composites, the fibre direction (also the preferred direction of the material, or the axis of isotropy), which is represented by a unit vector $\mathbf{a}_0$, needs to be introduced to the strain energy function, i.e., $W = W(\mathbf{C}, \mathbf{a}_0)$. The strain energy can now be represented as a function of five invariants [87]:

$$W(\mathbf{C}, \mathbf{a}_0) = W(I_1, I_2, I_3, I_4, I_5), \tag{4.1}$$

where all the five invariants have been defined in chapter 2. The stretch ratio along the preferred direction of the material can be expressed by $\lambda_F = \|\mathbf{F}\mathbf{a}_0\|$. The physical meaning of I_5 is related to the fibre-matrix shear interaction: $I_5 - I_4^2$ defines the extent of along fibre shear deformation [6, 97, 117, 119]. Because the energy contribution from the fibre-matrix interaction has not been well-understood yet, it is usually ignored in many hyperelastic models for soft tissues in the literature, such as models for the

ligaments [120], the HAF [121], and the arterial walls [83]. These models use the following classical uncoupled framework:

$$W\left(\mathbf{C},\mathbf{a}_0\right)=W_{matrix}\left(I_1,I_2,I_3\right)+W_{fibre}\left(I_4\right), \tag{4.2}$$

where the energy contribution from the matrix $W_{matrix}\left(I_1,I_2,I_3\right)$ is only a function of the right Cauchy-Green deformation tensor but not related to fibre direction $\mathbf{a}_0$; while the contribution from the fibre family $W_{fibre}\left(I_4\right)$ only depends on the fibre stretch ($\lambda_F=\sqrt{I_4}$). This equation based on the following assumptions: (i) the deformation in the matrix phase is homogeneous and the composite shows identical "overall" deformation as the matrix phase; (ii) the fibres are treated as non-linear springs embedded in the ground matrix and their shear deformation, as well as the interaction between the fibres and the matrix, is not considered; and (iii) fibre-fibre interaction is ignored.

To identify and illustrate the significance of the fibre-matrix interaction, experimental data in the literature and the finite element (FE) simulation results of the uncoupled models will be employed to show that the uncoupled models cannot predict the mechanical responses of the HAF correctly. For soft tissue like the arterial wall and the multi-lamellae HAF (Figure 4.1), there are two families of reinforced collagen fibres, whose original directions can be denoted as $\mathbf{a}_0$ and $\mathbf{b}_0$. When the mechanical properties of these two fibre families are identical (which is usually assumed for many soft tissues, such as the HAF and the arterial wall), the uncoupled framework can be extended to include these two fibre families as follows:

$$W\left(\mathbf{C},\mathbf{a}_0,\mathbf{b}_0\right)=W_{matrix}\left(I_1,I_2,I_3\right)+W_{fibre}\left(I_4\right)+W_{fibre}\left(I_6\right), \tag{4.3}$$

where $I_6=\mathbf{b}_0\cdot\mathbf{C}\cdot\mathbf{b}_0$ is similar to I_4. Then I_4 and I_6 could be expressed as $I_4=\lambda_{Fa}^2$ and $I_6=\lambda_{Fb}^2$, where λ_{Fa} and λ_{Fb} represent the stretch ratios of fibre family *a* and *b*, respectively. The potential fibre-fibre interaction between the two fibre families is ignored in the strain energy equation. The choice of the strain energy function $W_{fibre}\left(I_4\right)$ usually depends on the experimental data which the constitutive models

attempt to fit. For example, Holzapfel et al. [83] adopted an exponential function for arterial wall, and Peng et. al. [7] chose a polynomial equation to model HAF, while a piecewise formula was employed by Quapp and Weiss [84] to simulate ligament's mechanical responses. Although these models employed different functions to describe $W_{fibre}(I_4)$, they adopted a common assumption, which assumes that the contribution of the fibres can be ignored when the fibres are under contraction ($\lambda_F < 1$), i.e.,

$$W_{fibre}(I_4) = 0 \qquad \text{when } I_4 < 1. \tag{4.4}$$

This assumption comes from the wavy nature of the collagen fibres from physiological point of view, which is observed in most soft tissues [122]. On the other hand, most hyperelastic models for soft tissues chose the simplest hyperelastic model, the incompressible neo-Hookean model, to simulate the mechanical behaviour of the matrix [6, 83, 84]:

$$W_{matrix}(I_1, I_2, I_3) = \frac{1}{2}\mu_m (I_1 - 3), \tag{4.5}$$

where only one parameter μ_m, the shear modulus of the material, and one invariant I_1 are employed.

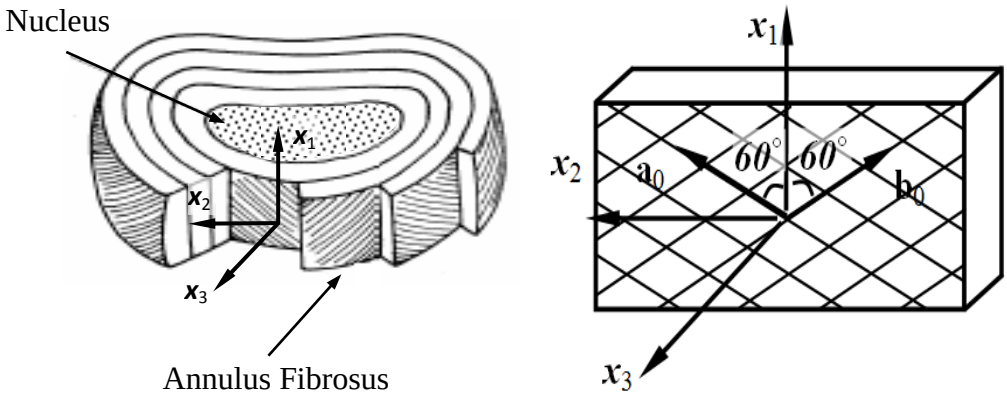

(a) Laminated structure of HAF [7] (b) Coordinate system

Figure 4.1 Schematic of the intervertebral disk.

4.3 Strain energy based analysis of uniaxial and biaxial testing results

4.3.1 Strain energy of the matrix with collagen fibres under contraction

To identify the strain energy contribution of the potential fibre-matrix interaction, we need first to verify whether the incompressible neo-Hookean model is sufficient to simulate the mechanical behaviour of the matrix. It is predicted that both collagen fibre families in HAF are under contraction during the starting stage of the uniaxial tension along the axial direction [6] (This is also verified later in this section by the careful analysis of the experimental data in Bass et al. [81]), and the strain energy contribution from the collagen fibres under contraction is assumed to be negligible (or, in other words, Eq. (4.4) is still valid). Therefore the uniaxial tensile test along the axial direction can be applied to investigate the strain energy contribution from the matrix. The laminated structure of HAF is illustrated in Figure 4.1. For the sake of consistency, the coordinate system used in Bass et al. [81] is adopted. The axial direction is defined as the $\mathbf{x}_1$ axis, while the circumferential direction is used as the $\mathbf{x}_2$ axis. Therefore the third axis can be determined by $\mathbf{x}_3 = \mathbf{x}_1 \times \mathbf{x}_2$, which coincides with the radial direction (Figure 4.1). In the undeformed configuration, the angle between each fibre direction and the x_1 axis is $\theta_0 = 60^o$ (Figure 4.1). Two fibre directions can be expressed as:

$$\mathbf{a}_0 = \mathbf{x}_1 \cos 60^o + \mathbf{x}_2 \sin 60^o, \quad \mathbf{b}_0 = \mathbf{x}_1 \cos 60^o - \mathbf{x}_2 \sin 60^o. \tag{4.6}$$

It is assumed that the mechanical properties of these two fibre families are identical. The overall HAF is therefore orthotropic and the $\mathbf{x}_1$, $\mathbf{x}_2$, and $\mathbf{x}_3$ axes coincide with the symmetric axes of the composite. The experimental results reported in Bass et al. [81] (i.e., the 2nd Piola-Kirchhoff (PK2) stress component vs. the Lagrangian strain component curves) are digitalized and fitted by cubic polynomials (Table 4.1).

Type	$\bar{x}$ (strain)	$\bar{y}$ (MPa)	x_0 (strain)	y_0 (MPa)	Fitting ($x=\bar{x}-x_0$, $y=\bar{y}-y_0$)
Uniaxial (1-dir)	E11 E22	S11 S11	0 0	0 0	$y=0.4695x-2.553x^2+9.607x^3$ $y=-0.5882x-4.588x^2-27.96x^3$
Uniaxial (2-dir)	E22 E11	S22 S22	0 0	0 0	$y=1.943x+6.182x^2+765.0x^3$ $y=-1.643x-12.60x^2-165.7x^3$
Biaxial +0.0375	E11 E11	S11 S22	–0.0749 –0.0749	0 0.1219	$y=1.923x-7.374x^2+190.6x^3$ $y=1.419x+21.39x^2+93.94x^3$
Biaxial +0.025	E11 E11	S11 S22	–0.0456 –0.0456	0 0.0644	$y=1.400x+7.420x^2+156.6x^3$ $y=2.144x+23.03x^2+109.4x^3$
Biaxial +0.0125	E11 E11	S11 S22	–0.0182 –0.0182	0 0.0267	$y=2.305x+5.487x^2+177.8x^3$ $y=5.674x-22.67x^2+338.4x^3$
Biaxial 0.0	E11 E11	S11 S22	0 0	0 0	$y=2.990x+1.739x^2+193.0x^3$ $y=7.881x-51.69x^2+475.6x^3$
Biaxial –0.0125	E11 E11	S11 S22	0.0155 0.0155	0.0067 0	$y=2.262x+26.49x^2+36.54x^3$ $y=8.441x-59.22x^2+520.2x^3$
Biaxial –0.025	E11 E11	S11 S22	0.0307 0.0307	0.0123 0	$y=2.597x+30.11x^2+24.98x^3$ $y=10.22x-99.18x^2+788.3x^3$

Table 4.1 Cubic polynomial curve fitting results of the uniaxial and the biaxial experiments in Bass et al. [81]

For the uniaxial tensile test along the axial direction (the $\mathbf{x}_1$ axis), the relation between the PK2 stress component S_{11} and the Lagrangian strain component E_{11} can be best fitted by (Figure 4.2(a))

$$S_{11} = 0.4695E_{11} - 2.553E_{11}^2 + 9.607E_{11}^3 \text{ (MPa)}. \tag{4.7}$$

Here the HAF at the original (undeformed) configuration is assumed to be stress free, which means $S_{11} = S_{22} = 0$ when $E_{11} = E_{22} = 0$. This is therefore enforced in the curve fitting. The Lagrangian strain tensor is defined as $\mathbf{E} = (\mathbf{C} - \mathbf{I})/2$, where $\mathbf{I}$ is the unit 2nd order tensor. The PK2 stress tensor $\mathbf{S}$ is work-conjugate to $\mathbf{E}$, i.e., $\mathbf{S} = \partial W/\partial \mathbf{E}$. The optimal cubic polynomial for the relation between S_{11} and E_{22} reads (Figure 4.2(b))

$$S_{11} = -0.5882E_{22} - 4.588E_{22}^2 - 27.96E_{22}^3 \text{ (MPa)}. \tag{4.8}$$

For any given Lagrangian strain E_{11}, PK2 stress S_{11} can be computed from (4.7). Substitute it into (4.8), E_{22} can be obtained numerically (only one root in the range $(-0.5, 0)$). With the incompressibility assumption, the corresponding stretches in the principal directions are then given by

$$\lambda_1 = \sqrt{2E_{11} + 1},\ \lambda_2 = \sqrt{2E_{22} + 1},\ \lambda_3 = 1/\lambda_1\lambda_2 . \tag{4.9}$$

Because the geometries of the specimen and deformation are symmetric, the fibre stretch ratios can be computed as

$$\lambda_{Fa} = \lambda_{Fb} = \lambda_F = \sqrt{I_4} = \sqrt{\lambda_1^2 \cos^2 60^\circ + \lambda_2^2 \sin^2 60^\circ} = \frac{1}{2}\sqrt{\lambda_1^2 + 3\lambda_2^2}, \tag{4.10}$$

which means the stretch ratios of the two fibre families are identical. We note that this is true for both the uniaxial and biaixial experiments discussed in this chapter [81]. The stretches λ_2, λ_3 and λ_F are plotted against the stretch in the loading direction λ_1 in Figure 4.2(c-e). It is clear that the fibres are under contraction ($\lambda_F < 1$) during the experiment. The deformation observed here is consistent with the results observed in

other experiments [119, 123]. Then the strain energy W is derived directly from the S_{11} vs. E_{11} curve as:

$$W\left(E_{11}\right)=\int_0^{E_{11}} S_{11}dE_{11}. \tag{4.11}$$

The strain energy W is plotted against I_1-3 (here $I_1=\lambda_1^2+\lambda_2^2+\lambda_3^2$) in Figure 4.2(f) and the data points computed from the fitted cubic polynomials can be well fitted by a linear equation, $W=0.0628\left(I_1-3\right)$ (unit: MPa, here $R^2=0.991$ implies a very good fitting). This means that the incompressible neo-Hookean model is adequate to simulate the mechanical behaviour of the matrix when the fibres are under contraction. The shear modulus of the matrix can be obtained from the fitting result as $\mu_m=0.1256$ MPa.

The linear relation between W and I_1-3 does not depend on the choice of the fitting functions. For example, if the experimental results are fitted by quadratic polynomials, the relation between W and I_1-3 can still be well fitted by a linear equation ($R^2=0.974$) and the corresponding shear modulus is $\mu_m=0.1212$ MPa, which is consistent with the value obtained from the cubic polynomial fitting functions (the difference is less than 4%). The reason is that the energy result is usually less sensitive compared to the stress-strain results. Because of the measurement noise, the measured strain and stress values at the initial stage of the uniaxial tension are less reliable. However, the effect of the measurement noise is reduced significantly when an integration procedure (e.g. Eq. (4.11)) is adopted to compute the strain energy W.

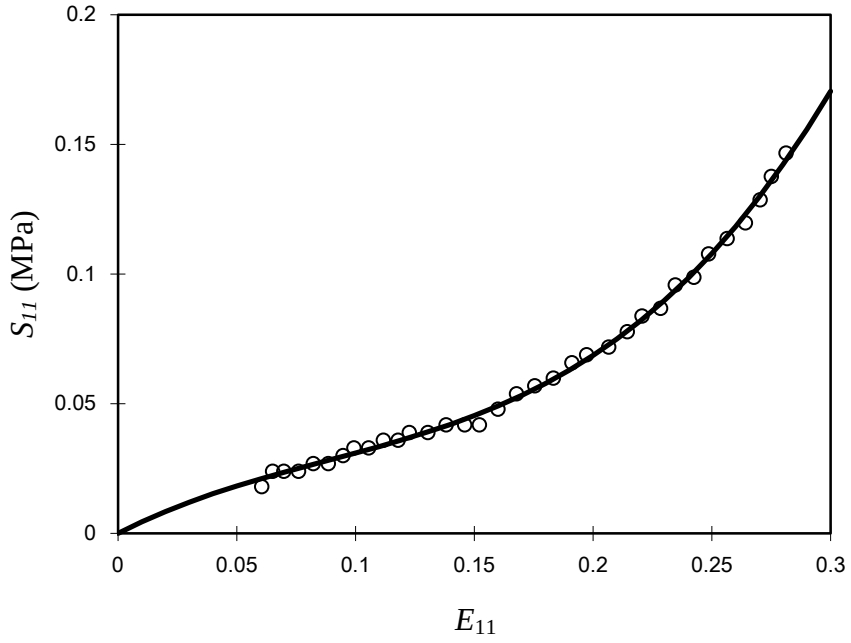

(a) Axial (PK2) stress S_{11} vs. Lagrangian strain E_{11}, experimental data (o) and the fitted cubic polynomial curve.

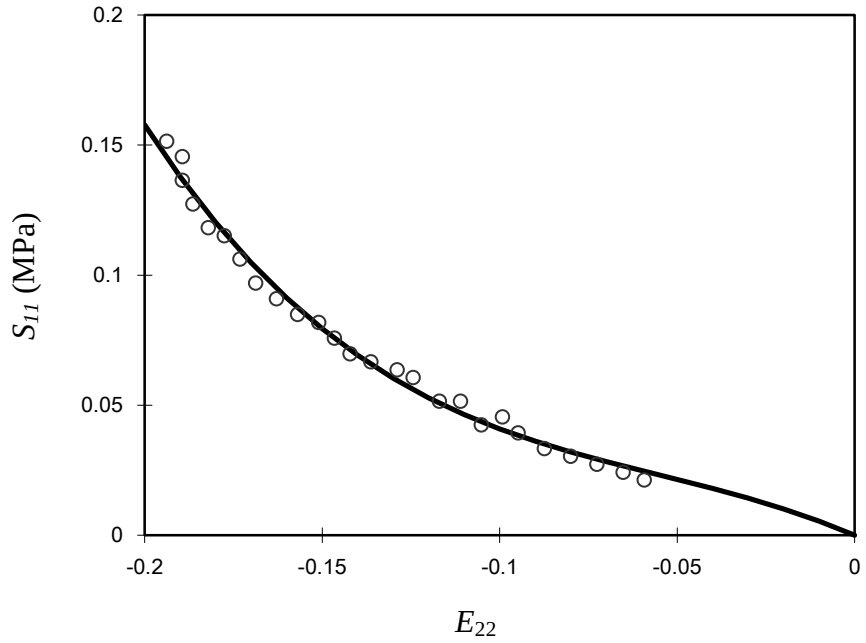

(b) Axial (PK2) stress S_{11} vs. Lagrangian strain E_{22}, experimental data (o) and the fitted cubic polynomial curve.

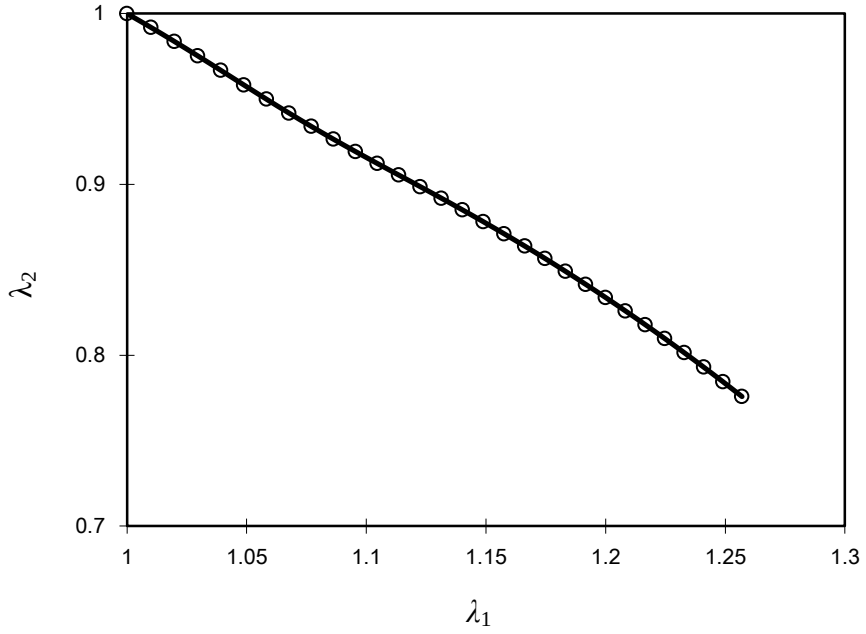

(c) Circumferential stretch λ_2 vs. axial stretch λ_1, computed from the fitted polynomial functions.

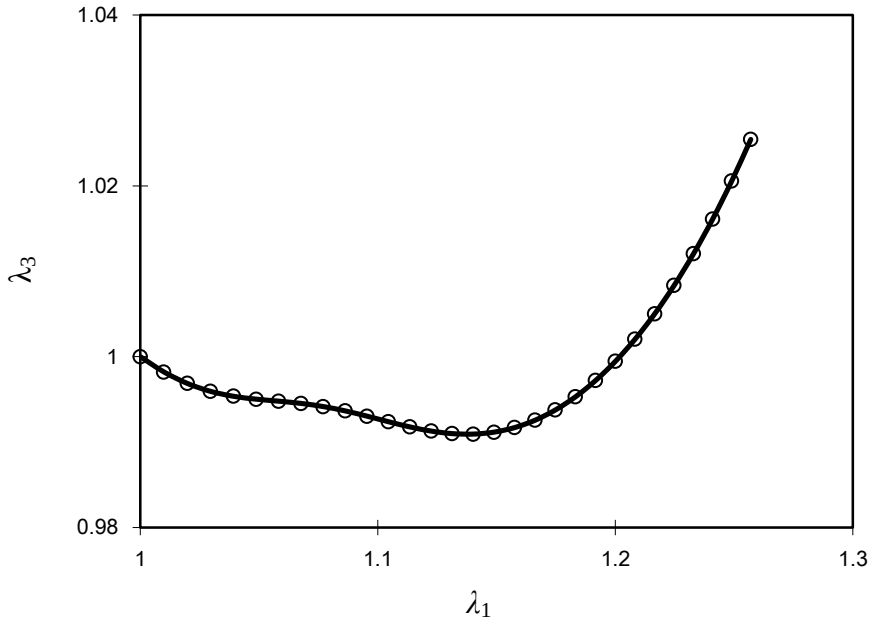

(d) Radial stretch λ_3 vs. axial stretch λ_1, computed from the fitted polynomial functions.

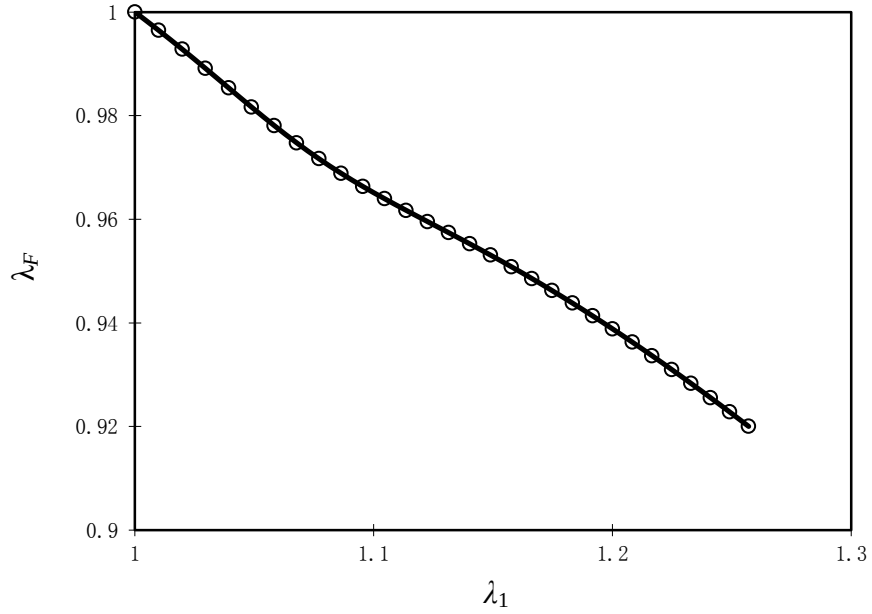

(e) Fibre stretch λ_F vs. axial stretch λ_1, computed from the fitted polynomial functions

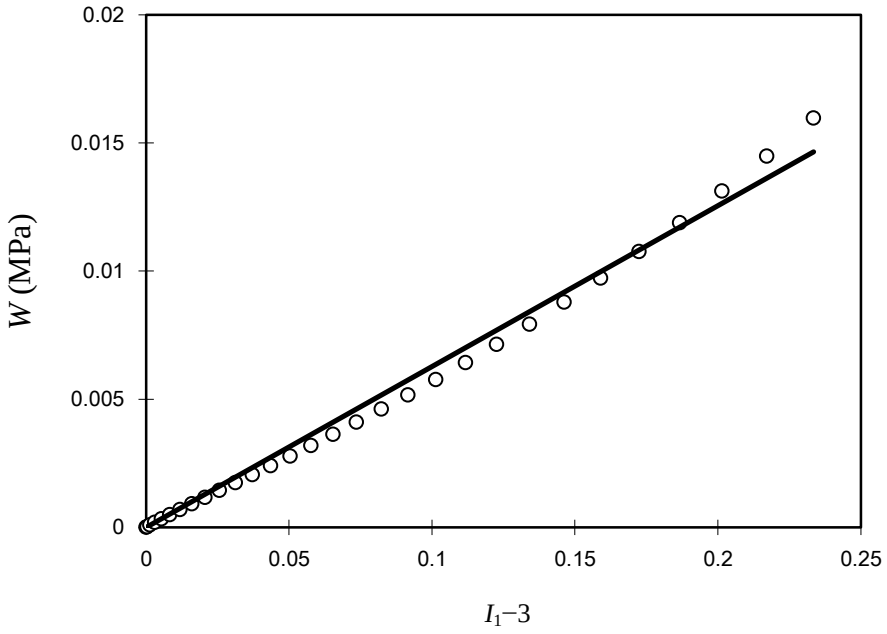

(f) Strain energy W vs. I_1-3, data points (o) computed from the fitted polynomial function. The relation between W and I_1-3 is fitted by a linear function (the solid line).

Figure 4.2 Curve fitting results of the experimental data of the uniaxial tensile test of HAF along the axial direction reported in Bass et al. [81]

4.3.2 Fibre-stretch dependent stiffness of the matrix

To investigate fibre-matrix interaction, we need to study the strain energy of the HAF with collagen fibres under different stretch ratios. It can be done by examining the strain energies of the biaxial experimental results in Bass et al. [81]. In a biaxial test, the normal strain in the circumferential axis E_{22} is constrained to be constant (E_{22} = 0.0, $\pm$ 0.0125, $\pm$ 0.025, +0.0375, respectively), and the tensile load is applied along the axial direction. The corresponding stretch ratio in the circumferential direction $\lambda_2^{(i)}$ is computed based on Eq. (4.9) and listed in Table 4.2. Because the geometry is symmetric, and the $\mathbf{x}_1, \mathbf{x}_2$ and $\mathbf{x}_3$ axes are still the principal directions of the deformation (here we still assume that the mechanical properties of these two fibre families are identical), Eq. (4.10) holds in the biaxial experiments.

$E_2^{(i)}$	$\lambda_2^{(i)}$	Max λ_1	Min λ_1	Max I_4	Min I_4
0.0375	1.0368	1.0592	0.9421	1.0868	1.0198
0.025	1.0247	1.0863	0.9664	1.0825	1.021
0.0125	1.0124	1.1045	0.9899	1.0738	1.0138
0.0	1.0	1.118	1.0	1.0625	1.0
–0.0125	0.9874	1.1314	1.0392	1.0513	1.0013
–0.025	0.9746	1.1384	1.077	1.0365	1.0025

Table 4.2 Ranges of I_4 in biaxial experiments in Bass et al. [81]

Since the stretch ratio in the $\mathbf{x}_3$ axis direction can be calculated based on the incompressibility assumption, the deformation state in the biaxial test can be represented as $\left(\lambda_1, \lambda_2^{(i)}\right)$, and the corresponding strain energy can be written as $W\left(\lambda_1, \lambda_2^{(i)}\right)$. The HAF at the original (undeformed) configuration is assumed to be stress free, therefore the strain energy $W\left(\lambda_1, \lambda_2^{(i)}\right)$ can be determined from the stress-strain curves of the biaxial and uniaxial tests.

If $\lambda_2^{(i)} = 1$, the stretch along the circumferential direction is fixed as 1.0 from the beginning and then the load is applied along the axial direction. The strain energy can be computed directly from the S_{11} vs. E_{11} curve (Figure 4.3(c)) of the biaxial tests using Eq. (4.11). If $\lambda_2^{(i)} > 1$, a uniaxial tensile load is first applied along the circumferential direction until the stretch in this direction reaches $\lambda_2^{(i)}$. The associated strain energy can be obtained from the S_{22} vs. E_{22} curve of the corresponding uniaxial test (Figure 4.3(a)). After that, the circumferential stretch is fixed as $\lambda_2^{(i)}$ and the tensile load is applied along the axial direction. The associated strain energy of this part can be computed from the S_{11} vs. E_{11} curve of the biaxial tests (Figure 4.3(c)).

Similarly, if $\lambda_2^{(i)} < 1$, a uniaxial tensile load has to be applied along the axial direction until the compression ratio in the circumferential direction reaches $\lambda_2^{(i)}$. The strain energy needed can be computed from the S_{11} vs. E_{11} curve of the corresponding uniaxial test (Figure 4.2(a)). After that, the stretch in the circumferential direction is fixed as $\lambda_2^{(i)}$, and the tensile load in the axial direction is increased. The strain energy required can be obtained from the S_{11} vs. E_{11} curve of the biaxial tests (Figure 4.3(c)).

From above, it is clear that the biaxial testing results must be consistent with the uniaxial testing results. Take $\lambda_2^{(1)} = 1.0368$ (i.e., $E_{22}^{(1)} = 0.0375$) for example. From the curve fitting results of the uniaxial test along the circumferential direction, the uniaxial stress deformation state is observed as $E_{11} = -0.0749$, $E_{22} = 0.0375$, $S_{22} = 0.1219$, and $S_{11} = S_{33} = 0$. This deformation state is the starting point of the biaxial test, hence we enforce that the fitted cubic curve passes through this point. The corresponding fitting results of the biaxial series of $E_{22} = 0.0375$ listed in Table 4.1 are interpreted as follows:

$$\begin{aligned} S_{11} &= 1.923\left(E_{11}+0.0749\right) - 7.374\left(E_{11}+0.0749\right)^2 + 190.6\left(E_{11}+0.0749\right)^3 \\ S_{22} - 0.1219 &= 1.419\left(E_{11}+0.0749\right) + 21.39\left(E_{11}+0.0749\right)^2 \\ &\quad + 93.94\left(E_{11}+0.0749\right)^3 \end{aligned} \tag{4.12}$$

The unit for stress here is MPa. It is obvious that the curves above are compatible with the calculated uniaxial stress deformation. Other series of biaxial tests are fitted in a similar way so that they are consistent with the fitting results of the two uniaxial tests. The fitting curves are all shown in Figure 4.3. We note that in Bass et al. [81] the original experimental data points in biaxial tests are compatible with those of uniaxial tests.

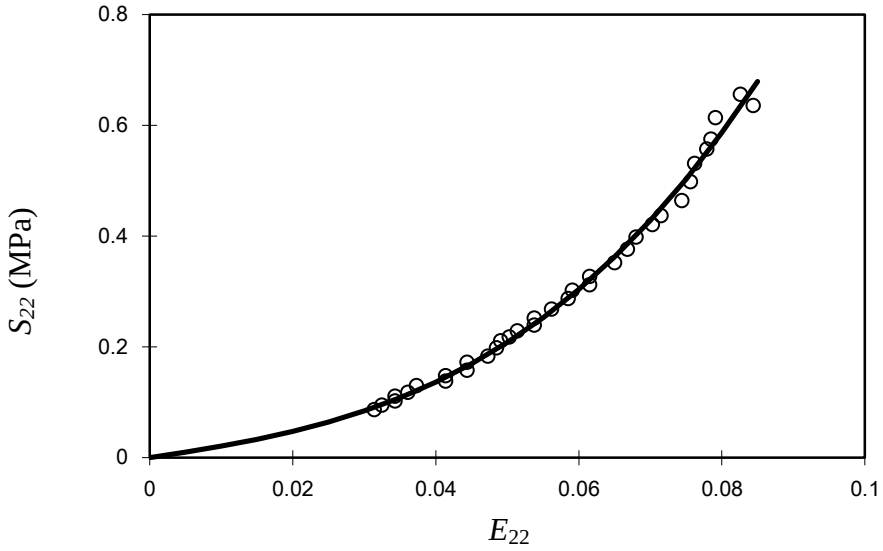

(a) The axial (PK2) stress S_{22} vs. the Lagrangian strain E_{22}, experimental data (o) and the fitted cubic polynomial curve for the uniaxial tensile testing along the circumferential direction.

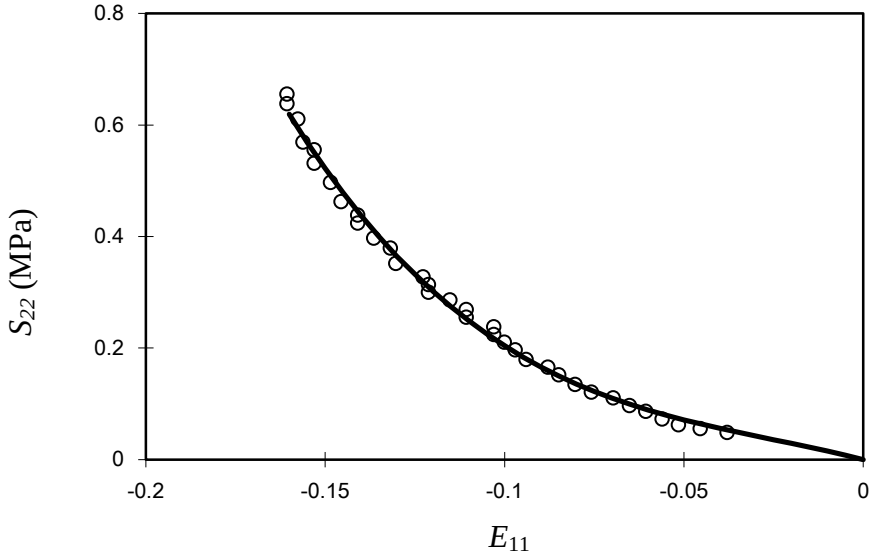

(b) the axial (PK2) stress S_{22} vs. the Lagrangian strain E_{11}, experimental data (o) and the fitted cubic polynomial curve for the uniaxial tensile testing along the circumferential direction.

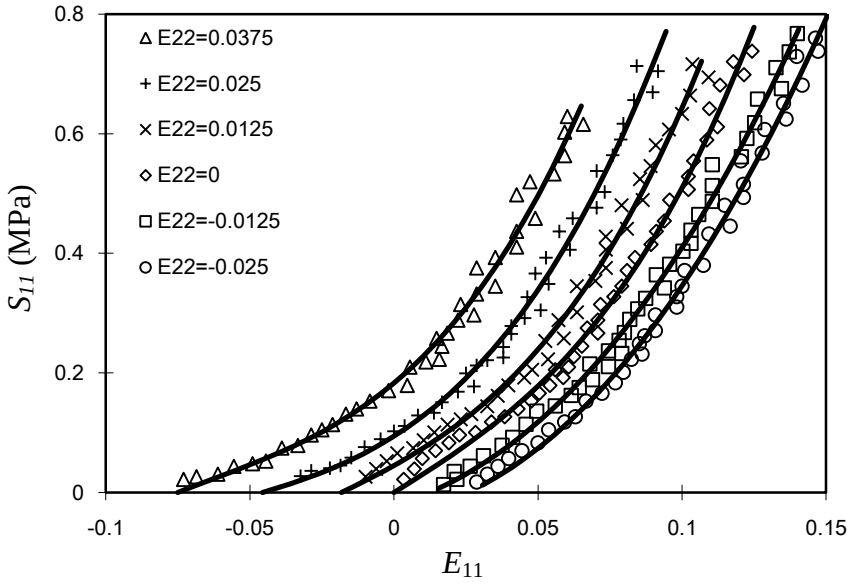

(c) The axial (PK2) stress S_{11} vs. the Lagrangian strain E_{11}, experimental data and the fitted cubic polynomial curves for the biaxial testing.

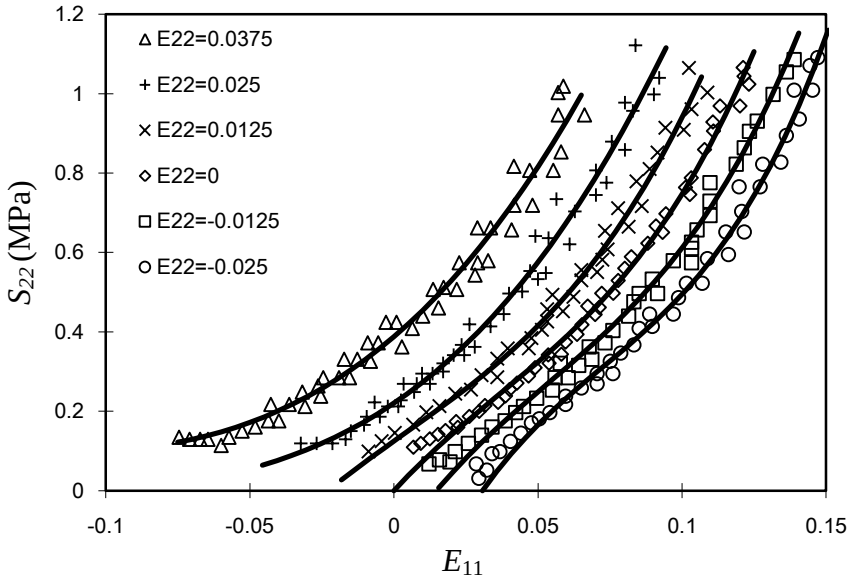

(d) the axial (PK2) stress S_{22} vs. the Lagrangian strain E_{11}, experimental data and the fitted cubic polynomial curves for the biaxial testing.

Figure 4.3 Curve fitting results of the experimental data of the uniaxial tensile test of HAF along the circumferential direction and the biaxial test reported in Bass et al. [81]. For (c) and (d), there are six series of biaxial testing data with different E_{22}: E_{22} = 0.0375 (Δ), 0.025 (+), 0.0125 (x), 0.0 (◊), -0.0125 (□) and -0.025 (○).

Based on Eq. (4.10), the ranges of I_4 (square of the fibre stretch ratio) can be calculated for each series of biaxial tests (Table 4.2). For the first series of biaxial test ($\lambda_2^{(1)} = 1.0368$), when $I_4 = 1.03$, the corresponding stretch in the axial direction (λ_1) is determined by Eq. (4.10). The associated strain energy and $I_1 - 3$ are then obtained. Similarly, for other series of biaxial tests, the deformation states with $I_4 = 1.03$ are determined and the corresponding strain energies are computed in Table 4.3. The strain energy W vs. $I_1 - 3$ is plotted in Figure 4.4(a) and can be well fitted by a linear function. Based on Eq. (4.3), Eq. (4.5) and the experimental result, the fitting result is interpreted as (note we have $I_6 = I_4$ here)

$$W = W(I_1, I_4) = \frac{1}{2}\mu_m^e (I_1 - 3) + 2W_{fibre}(I_4). \tag{4.13}$$

Here μ_m^e is the effective shear modulus of the matrix, which is still treated as a neo-Hookean material. When $I_4 = 1.03$, the fitting result shows that μ_m^e = 1.0022 MPa. In the previous section, when the fibres are under contraction (i.e., $I_4 < 1.0$), the shear modulus of the matrix is only $\mu_m = 0.1256$ MPa. The effective matrix stiffness increases significantly (about 8 times larger) when the fibres are stretched to $\lambda_F = \sqrt{I_4} = 1.0149$.

Follow the same procedure, we can obtain the effective matrix stiffness when I_4 = 1.04, 1.05, 1.06, and 1.07, respectively (Table 4.4). The fitting results show that the matrix can be well described by the incompressible neo-Hookean model (Figure 4.4), and the effective matrix stiffness depends on the fibre stretch (ratio). From Table 4.4, it can be observed that the larger the fibre stretch ratio, the larger the effective stiffness of the matrix (with the only exception of I_4 = 1.06, in which the effective stiffness of the matrix is slightly smaller than that with I_4 = 1.05. This exception may come from the measurement noise). However, based on Eq. (4.3), the uncoupled models assume the effective matrix stiffness as a constant, and the observed fibre stretch dependence of the effective matrix stiffness cannot be explained by the classical uncoupled models.

$\lambda_2^{(i)}$	λ_1	W (MPa)	I_1-3
1.0368	1.0592	0.00232	0.00937
1.0247	1.0863	0.00110	0.00184
1.0124	1.1045	0.00186	0.00360
1.0	1.118	0.00554	0.01286
0.9874	1.1314	0.01340	0.02828
0.9746	1.1384	0.02411	0.04884

Table 4.3 Strain energies in the biaxial experiments in Bass et al. [81] when $I_4=1.03$.

I_4	μ_m^e (MPa)	Data fitting results (Unit: MPa)
<1.0	0.1256	$W = 0.0628(I_1-3)$
1.03	1.0022	$W = 0.5011(I_1-3)-0.0007$
1.04	1.155	$W = 0.5775(I_1-3)-0.0004$
1.05	1.2208	$W = 0.6104(I_1-3)+0.0012$
1.06	1.19	$W = 0.595(I_1-3)+0.0034$
1.07	1.398	$W = 0.699(I_1-3)+0.0039$

Table 4.4 Effective shear modulus of the matrix μ_m^e in the biaxial experiments in Bass et al. [81] and the W vs. I_1-3 curve fitting results.

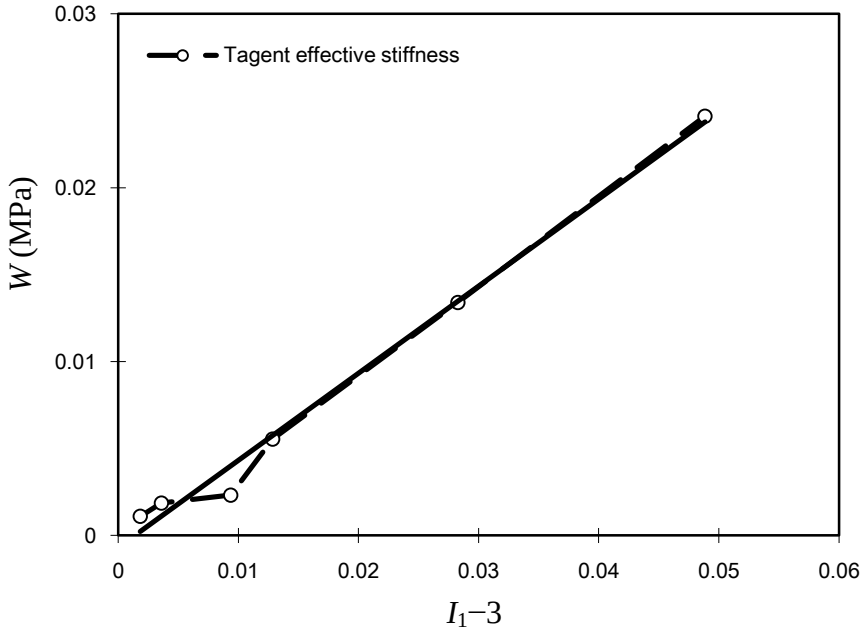

(a) $I_4 = 1.03$

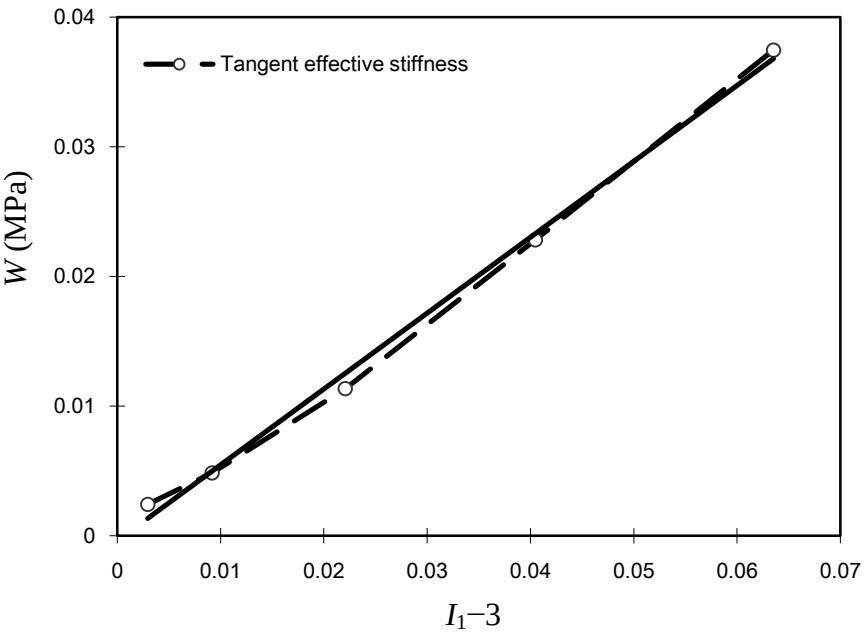

(b) $I_4 = 1.04$

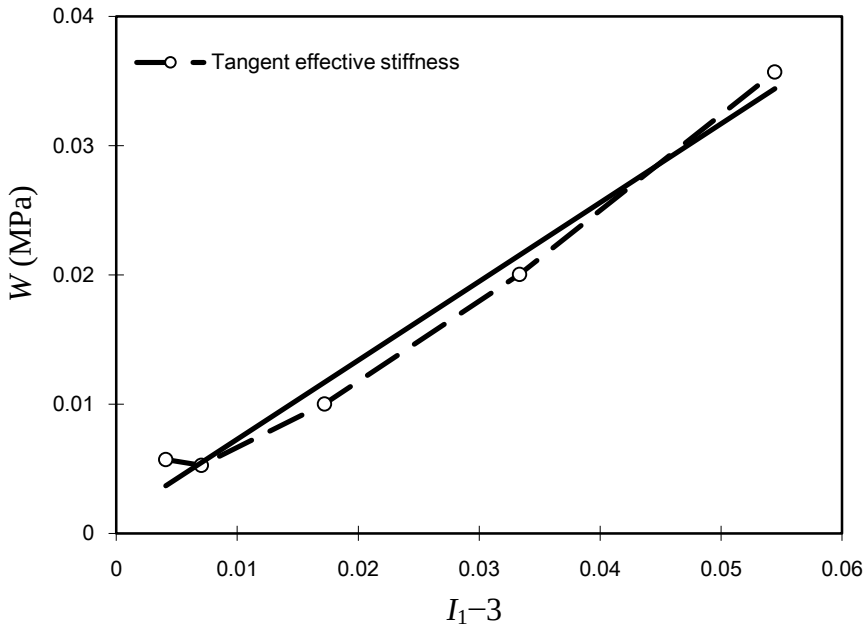

(c) $I_4 = 1.05$

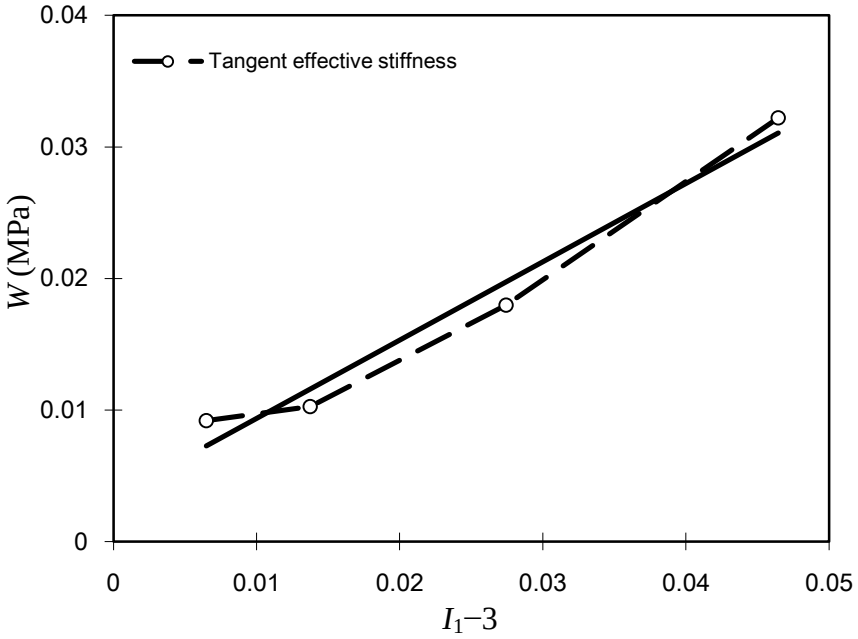

(d) $I_4 = 1.06$

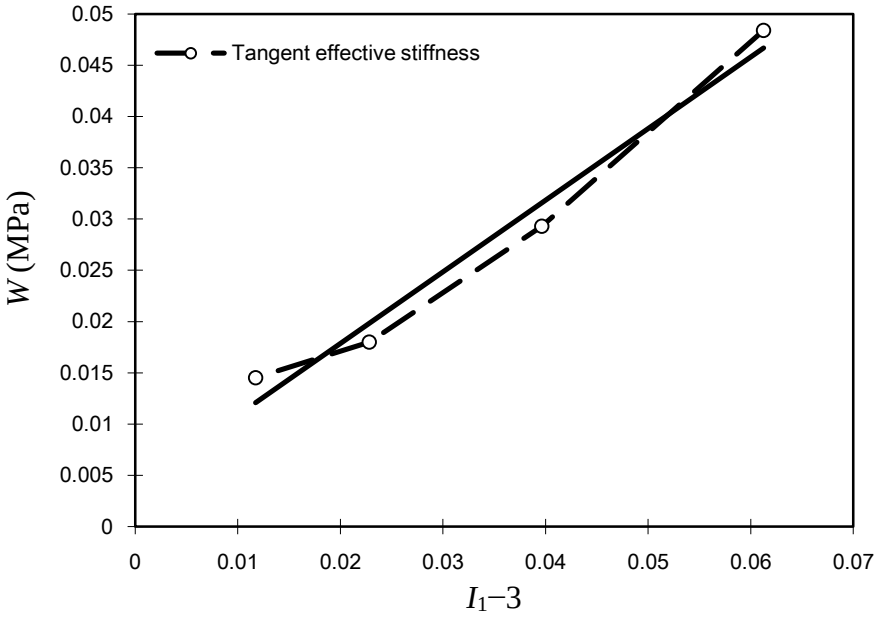

(e) $I_4 = 1.07$

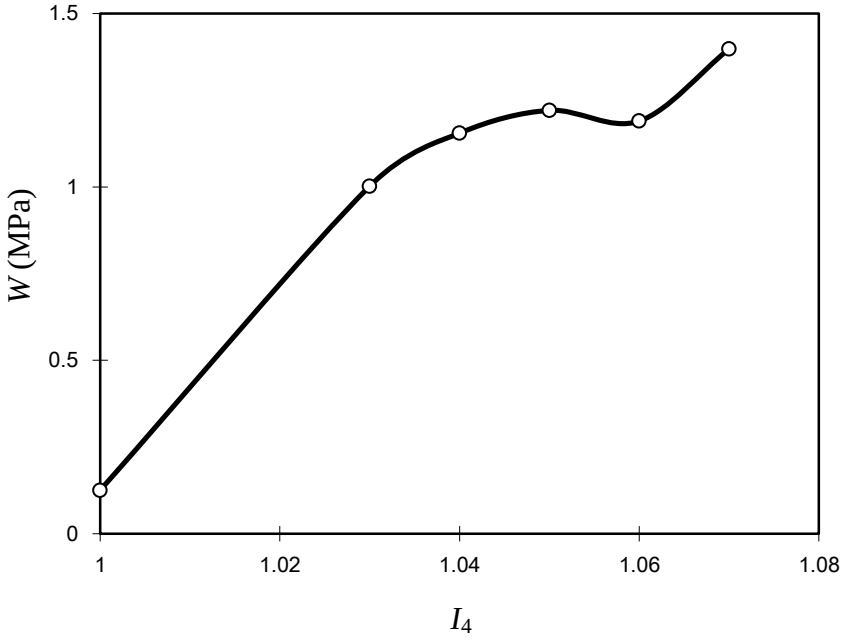

(f) The effective matrix shear modulus μ_m^e vs. I_4

Figure 4.4 The strain energy W vs. $(I_1 - 3)$ for the biaxial testing in Bass et al. [81] at certain fibre stretch values and the effective matrix shear moduli. The data points (o) are computed from the fitted polynomial function, and they are fitted by linear functions (the solid lines), and the dashed segments between the data points in (a)-(e) show roughly the tangent effective stiffness of the matrix.

4.4 Deformation predicted by FE simulation of uncoupled models

In the previous section, it is shown that the strain energy obtained from uniaxial and biaxial experimental results cannot be explained by the classical uncoupled models. In this section, the FE simulation results of typical uncoupled models will be employed to show that the uncoupled models cannot capture the deformation characteristics of the HAF correctly when it is under simple uniaxial tension along the circumferential direction. When the uncoupled models are adopted to model the mechanical behaviour of the HAF, the stress-strain result of the uniaxial tensile test along the axial direction is first used to obtain the shear modulus of the matrix, which is similar to the procedure in the previous section. The stress-strain curve of the uniaxial test along the circumferential direction is then employed to estimate the parameters in the function $W_{fibre}(I_4)$, which is the strain energy contribution from the fibre. Although the uncoupled model can fit the stress-strain curves of both uniaxial tensile tests, one important aspect, the deformation in the transverse directions, is usually ignored (it is noted that the transverse deformation is not recorded in most HAF uniaxial tensile experiments available in the literature due to either limitations in the facilities or being ignored by experimentalists). In the HAF uniaxial tensile test, the deformation in the transverse direction is directly associated with the relative angle change between the two fibre families. For example, for the uniaxial tensile test along the circumferential direction, the angle between the two fibre families (named as "fibre-fibre angle") φ is $\varphi_0 = 180^\circ - 2\theta_0 = 60^\circ$ in the undeformed configuration, θ_0 is the fibre angle. In the deformed configuration, we have

$$\varphi = 2\arctan\left[\frac{\lambda_2}{\lambda_1}\tan\frac{\varphi_0}{2}\right]. \tag{4.14}$$

For an uncoupled model with a polynomial format $W_{fibre}(I_4)$, when the nominal tensile strain reaches 20% in the uniaxial tensile test along the circumferential direction, the FE simulation result shows that the fibre-fibre angle φ will decrease from 60^o to 27^o (Figure 5 in [7]), while the experiments only record a change of about 42^o [106, 124]. According to Eq. (4.14), this excessive fibre-fibre angle change implies unrealistic large transverse deformation in the axial direction. Similar excessive transverse deformation

is also observed when an uncoupled model with an exponential format $W_{fibre}(I_4)$ is applied to simulate the uniaxial tension of the arterial tissue (see Figure 9 in [85]. It is noted that arterial tissue has a similar microstructure with two fibre families and the fibre-fibre angle is also 60^o in the undeformed configuration).

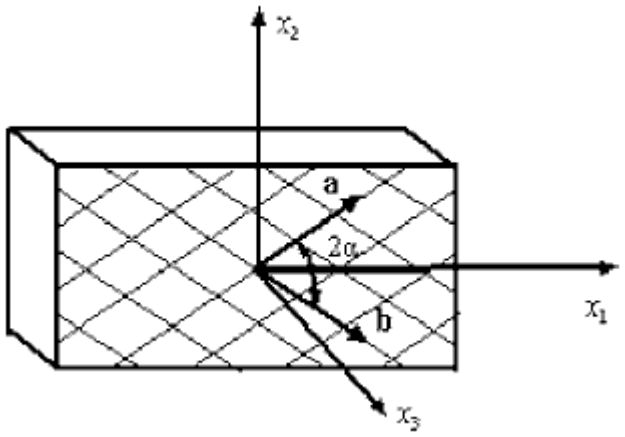

Figure 4.5 Angle between two fibre families (Figure 5 from [7])

The source of this type of incorrect deformation prediction is that uncoupled models assume constant effective matrix stiffness and fail to model the increase of the effective matrix stiffness when the fibres are under stretch, as illustrated in the previous section. With a less stiff matrix, the fibres can rotate more easily in the matrix ground substance and their directions are closer to the loading direction to carry the load. Therefore this excess rotation leads to the prediction of larger fibre-fibre angle change, larger transverse deformation and lower fibre stretch.

4.5 Constitutive models with fibre-matrix interaction and physical interpretation

In classical uncoupled models, as suggested by Eq. (4.2) and Eq. (4.3), the fibres are actually treated as nonlinear springs and they only contribute to the stiffness along the fibre directions, while the deformation in the matrix phase is homogeneous and identical to the "overall" deformation of the composite. Because of the wavy nature of the collagen fibres in soft tissues, when the fibre stretch increases, the stiffness of the fibre increases, which means that the stiffness of the soft tissue along the fibre direction increases. In the uncoupled models, the effective matrix stiffness μ_m^e will not change when the fibre stretch changes, as stated in Eq. (4.3). However, the strain energy based analysis of the biaxial testing results shows clearly that the effective matrix stiffness

also increases when the fibre stretch increases. As illustrated in the previous section, the constant effective matrix stiffness assumption will also lead to incorrect deformation prediction in the FE simulations. Hence the fibre stretch dependence of the effective matrix stiffness (i.e., the fibre-matrix interaction) has to be modelled for the HAF. In this section, several typical constitutive models of soft tissues with fibre-matrix interaction are investigated and the associated physical interpretations are discussed in detail.

4.5.1 Constitutive models with phenomenological fibre-matrix interaction strain energy

Physically, the fibres are not just nonlinear springs, and they should be modelled as a separate solid phase, especially if the collagen fibre network in the tissue is sufficiently dense. If the fibres are treated as a solid phase, based on composite theory, the deformation distribution in the composite is no longer homogeneous and the strain energy stored in the composite is always larger than the estimation given by Eq. (4.2), which is based on the assumption of homogeneous deformation [14]. In some phenomenological constitutive models of soft tissues, the difference between the real strain energy and the estimation based on the homogeneous deformation distribution assumption is termed as "fibre-matrix interaction strain energy" [7, 106, 119].

It is noted that physically all strain energy is stored either in the matrix phase or the fibre phase. The fibre-matrix interaction strain energy is an artificial concept and it mathematically represents the difference between the real strain energy and the estimation based on the homogeneous deformation distribution assumption. However, the real deformation distribution in the composite is complex and it is generally impossible to derive the real strain energy analytically. Hence, in a phenomenological model with fibre-matrix interaction, the fibre-matrix interaction energy term is usually constructed based on experimental data, the observations of the strain energy of the composite under simple deformation states, and some estimations based on the micromechanics of the composites. For example, when the composite with unidirectional fibre reinforcement is stretched along the fibre direction, the deformation distribution in the composite is homogeneous [6] and the fibre-matrix interaction energy should be zero. This phenomenon implies that the fibre-matrix interaction energy is

related to the fibre-matrix shear interaction and sometimes it is named as “fibre-matrix shear interaction energy”.

A proper fibre-matrix interaction energy term will usually increase the energy required to rotate the fibres in the matrix ground substance, that is, it makes the fibres more difficult to rotate in the matrix ground substance. Therefore the incorrect deformation prediction by the uncoupled model can be prevented [7]. The advantage of this phenomenological approach is that it allows the flexibility to choose different formula for the fibre-matrix interaction. However, the main disadvantage is that the fibre-matrix interaction energy functions used in these models are usually based on data fitting and they do not carry strict physical interpretations. The fibre-matrix interaction strain energy fitted from one type of experimental data may lead to incorrect results in other types of experiments. For example, the fibre-matrix interaction strain energy function proposed in Wu and Yao [106] fitted from the HAF uniaxial tensile test along the circumferential direction leads to negative interaction energy when the HAF is under uniaxial tensile test along the axial direction.

4.5.2 Composites-based constitutive model for soft tissues

To correctly predict the effect of fibre-matrix interaction in a general deformation state, the constitutive model should use micromechanics of the composite based on the composite’s microstructure to estimate the strain energy of the composite. In classical linear elastic composite theories, the effective moduli of a composite with unidirectional fibre reinforcement have been studied extensively and various formulae were proposed to predict the overall behaviour of the composite. Among them, the semi-analytical Halpin-Tsai equations fit experimental results very well [28]. The Halpin-Tsai equations have recently been extended to the finite deformation regime [6] and it is consistent with micromechanics based models [90, 97]. In Guo et al. [6]’s composites-based soft tissue model, the matrix is still treated as an incompressible neo-Hookean matrix described by Eq. (4.5) (but I_1 here should be interpreted as I_1^m, the first invariant of the deformation tensor $\mathbf{C}_m$ in the matrix, because the inhomogeneous distribution of the deformation in the composite is considered in this model). Collagen fibres are modelled by a generalised neo-Hookean material with the following strain energy function:

$$W^F = W^F\left(I_1^f, I_4\right) = \frac{1}{2}\mu_m f\left(I_4\right)\left(I_1^f - 3\right), \tag{4.15}$$

where $f\left(I_4\right)$ is the stiffness ratio between the fibres and the matrix (which implies that the stiffness of the fibres depends on the stretch ratio). Here $I_1^f = \mathrm{tr}\mathbf{C}_f$, where $\mathbf{C}_f$ is the deformation tensor in the fibres. Note that in general the deformation distribution in the composite is not homogeneous, i.e., $\mathbf{C}_f \neq \mathbf{C}_m \neq \mathbf{C}$ (here $\mathbf{C}$ represents the homogenised deformation tensor of the composite). In Guo et al. [6], a simple exponential equation is proposed for $f\left(I_4\right)$:

$$f\left(I_4\right) = a_1 + a_2 \exp\left[a_3\left(I_4 - 1\right)\right], \tag{4.16}$$

where a_1, a_2 and a_3 are all material parameters. Assuming the volume fraction of the fibre is v_f (the fibres are considered as solid here), based on micromechanics, the strain energy function of the soft tissue can be estimated as:

$$W = \frac{1}{2}\mu_m g\left[f\left(I_4\right)\right]\left(I_1 - 3\right) + \frac{1}{2}\mu_m\left\{\mathrm{v}_m + f\left(I_4\right)\mathrm{v}_f - g\left[f\left(I_4\right)\right]\right\}\left(I_4 + 2I_4^{-1/2} - 3\right) \tag{4.17}$$

where the volume fraction of the matrix $\mathrm{v}_m = 1 - \mathrm{v}_f$; $g\left[f\left(I_4\right)\right]$ is associated with the effective transverse shear stiffness of the composite μ_c as follows [6]:

$$g\left[f\left(I_4\right)\right] = \frac{\mu_c}{\mu_m} = \frac{\left(1+\mathrm{v}_f\right)f\left(I_4\right) + \left(1-\mathrm{v}_f\right)}{\left(1-\mathrm{v}_f\right)f\left(I_4\right) + \left(1+\mathrm{v}_f\right)}. \tag{4.18}$$

Comparing Eq. (4.17) with Eq. (4.13), the composites-based model predicts the effective matrix stiffness of the HAF as

$$\mu_m^e = \mu_c = \mu_m g\left[f\left(I_4\right)\right], \tag{4.19}$$

which is fibre stretch dependent. This means that the composites-based model can model the fibre stretch dependent effective matrix stiffness. The biaxial test simulation

results of the composites-based model follow the same trends as the experimental results of Bass et al. [81]. Eq. (4.19) and Eq. (4.18) indicate that the effective matrix stiffness depends on the volume fraction of the fibres. Recent experimental results show that the HAF has approximately 60% collagen per dry weight [125]. Considering other factors such as the swelling of collagen fibres (which leads to larger volume), the density of the fibre and the matrix ground substance, the estimated volume fraction of the fibres in the HAF is in the range of 50%-70%. When the fibre is under stretch, the fibre/matrix stiffness ratio $f(I_4)$ is usually very large and the relative increase of the effective matrix stiffness is estimated as

$$g\left[f(I_4)\right] \approx \frac{1+\mathrm{v}_f}{1-\mathrm{v}_f} = 3\square 6, \tag{4.20}$$

which is less than the increase suggested in Table 4.4 (for example, when I_4 = 1.07, we have $g\left[f(I_4)\right] = \mu_m^e/\mu_m$ =1.398/0.1212 = 11.53, which implies that the volume fraction of the collagen fibres $\mathrm{v}_f \approx 0.84$). The reasons for this mismatch include: (i) the effective matrix stiffness obtained by data fitting in Table 4.4 is higher than the reality because it predicts a too small (or even negative) contribution of the strain energy from the fibres; and (ii) there might be other factor(s) which contribute to the fibre stretch dependence of the effective matrix stiffness (e.g., the fibre orientation dispersion discussed below). Nevertheless, based on our investigation, the composite effect can explain a major part of the observed increase of the effective matrix stiffness when the fibres are under stretch.

4.5.3 Constitutive models of soft tissues considering fibre orientation dispersion

Up to now, the collagen fibres are assumed to be unidirectional aligned in the soft tissues. This is an ideal assumption because there is always some dispersion of the fibre orientations in many soft tissues. Gasser et al. [85] proposed a hyperelastic model to consider the distributed collagen fibre orientations in arterial layers, in which the strain energy function *W* is written as:

$$W = \frac{1}{2}\mu_m(I_1-3) + \frac{k_1}{2k_2}\left[\exp\left\{k_2\left[\kappa I_1 + (1-3\kappa)I_4 - 1\right]^2\right\} - 1\right], \tag{4.21}$$

where μ_m is the shear modulus of the ground matrix. The material parameters k_1 and k_2 are to be determined from the mechanical behaviour of the collagen fibres. Parameter $\kappa \in [0,1/3]$ characterises the distribution of the collagen fibres. When κ = 0, the collagen fibres are aligned. If κ = 1/3, the fibres are evenly distributed and the composite is isotropic. This is an extension of the soft tissue model with aligned collagen fibres [83] by replacing I_4 with $\hat{I}_4 = \kappa I_1 + (1-3\kappa) I_4$ to take into account the fibre orientation dispersion. If Eq. (4.21) is compared with Eq.(4.13), the first impression is that Eq. (4.21) also implies a constant effective transverse shear stiffness of the composite. However, a more careful observation shows that the second term on the right hand side of Eq. (4.21) depends on I_1 and I_4; while in Eq.(4.13), W_{fibre} is only a function of I_4. Using a Taylor series expansion, based on a particular value of $I_1^{(0)}$, the strain energy function W in Eq. (4.21) can be approximated as follows:

$$\begin{aligned} W \approx & \left[\frac{1}{2}\mu_m + k_1\kappa\left[\hat{I}_4^{(0)} - 1\right]\exp\left\{k_2\left[\hat{I}_4^{(0)} - 1\right]^2\right\}\right](I_1 - 3) \\ & + \left\{\left[k_1\kappa\left(\hat{I}_4^{(0)} - 1\right)\left(3 - I_1^{(0)}\right) + \frac{k_1}{2k_2}\right]\exp\left[k_2\left(\hat{I}_4^{(0)} - 1\right)^2\right] - \frac{k_1}{2k_2}\right\}, \end{aligned} \tag{4.22}$$

where $\hat{I}_4^{(0)} = \kappa I_1^{(0)} + (1-3\kappa) I_4$ is a function of I_4 only (that is, it is independent of I_1). Now the second term on the right hand side of Eq. (4.22) can be written as a function of I_4 only, and the effective transverse shear stiffness of the composite is

$$\mu_m^e = \frac{1}{2}\mu_m + k_1\kappa\left[\hat{I}_4^{(0)} - 1\right]\exp\left\{k_2\left[\hat{I}_4^{(0)} - 1\right]^2\right\}. \tag{4.23}$$

The behaviour of μ_m^e depends on the value of κ. When κ = 0 (perfectly aligned), μ_m^e is a constant and the model itself is reduced to a classical uncoupled model. If κ = 1/3 (isotropic composite), μ_m^e is also a constant because $\hat{I}_4^{(0)} = I_1^{(0)}/3$ is reduced to a constant. When 0 < κ < 1/3, μ_m^e depends on I_4, and the larger I_4 is, the larger μ_m^e will be. Hence we know that the collagen fibre orientation distribution can also contribute to the fibre stretch dependence of the effective matrix stiffness of the soft tissue. The

approximation in Eq. (4.22) only works when I_1 is close enough to $I_1^{(0)}$, therefore Eq. (4.23) can be regarded as the tangent stiffness of the composite at $I_1 = I_1^{(0)}$. We can then find that the tangent stiffness μ_m^e also depends on the value of I_1. The larger I_1, the larger μ_m^e. If we connect the data points in the W vs. $(I_1 - 3)$ plots in Figure 4.4 with dashed lines, the segments between the data points show roughly the tangent effective stiffness of the soft tissue. In Figure 4.4, it is shown that the tangent stiffness of the composite increases when I_1 increases, which agrees well with Eq. (4.23). Although the model (i.e., Eq. (4.21)) is an extension of a phenomenological uncoupled model, the inclusion of the fibre orientation dispersion is based on the micromechanics analysis. The fibre-matrix interaction effect from this model can capture the deformation characteristics of soft tissues and a uniaxial tension example is shown in Figure 10 in [85].

Recently, Caner et al. [89] used the microplane model to simulate the collagen fibre orientation dispersion in the HAF by means of numerical integration. Although there is no explicit strain energy function defined in this model, similar dependence of the tangent effective stiffness of the composite on I_1 and I_4 can be derived based on the integration scheme. The FE simulation results show that this microplane model can predict the fibre-fibre angle change of the HAF in the uniaxial test along the circumferential direction (see Figure 7 in [89]). Because the real distribution of the fibre orientation dispersion in the HAF is not measured, the real proportion of its contribution to the fibre-matrix interaction is unknown. However, in Caner et al. [89], when a small fibre orientation dispersion is assumed, the FE simulation results show that the fibre orientation dispersion effect alone (that is, without the composite effect) can explain the fibre-matrix interaction effect in the uniaxial tensile tests. This suggests that the fibre orientation dispersion effect can claim the extra increase of the effective matrix stiffness which is beyond the composite effect as identified previously.

4.6 Discussion

4.6.1 Physical interpretation of the fibre-matrix interaction

The constitutive models analysed above show that both the composite effect and the potential fibre orientation dispersion contribute to the fibre stretch dependence of the effective matrix stiffness. Other microstructural characters, however, are not well modelled and their effects on this issue are unclear. For example, the shape of the zig-zag waviness of the collagen fibres is not modelled in detail. Only a rough assumption is made that the strain energy contribution of the collagen fibres can be ignored when they are under contraction. The potential fibre-fibre interaction is ignored as well in all the constitutive models discussed in the previous section because it is not well understood.

The quantitative analysis above shows that the combination of the composite effect and the fibre orientation dispersion effect is sufficient to explain the fibre-matrix interaction effect identified in the experiments. This implies that probably it is fine to ignore other microstructural character. Therefore, a more comprehensive and micromechanics based model, which considers both the composite effect and the fibre orientation dispersion, is required to predict the fibre-matrix interaction observed here.

4.6.2 Value of fibre-matrix interaction energy

Comparing the models considering fibre-matrix interaction with the classical uncoupled models, the strain energy contribution from the "fibre-matrix interaction" can be expressed as $\left(\mu_m^e - \mu_m\right)\left(I_1 - 3\right)/2$. If the total strain energy of the soft tissue is decomposed into three parts (like in the phenomenological models): the energy contributions from the matrix, the fibres, and the fibre-matrix interaction, respectively [7], in general deformation state, the value of the strain energy associated with the fibre-matrix interaction is much smaller than the contribution from the fibres because the fibres are much stiffer than the matrix. Based on this argument, the fibre-matrix interaction is ignored in many constitutive models.

However, as discussed in section 4.4, the mechanical consequence of the fibre-matrix interaction strain energy is significant because it increases the effective matrix stiffness considerably and prevents the excessive rotation of the fibres in the matrix ground substance. The strain energy based analysis of the experimental data shows that the fibre-matrix interaction energy $\left(\mu_m^e - \mu_m\right)\left(I_1 - 3\right)/2$ is comparable to the strain energy contribution from the matrix. Therefore the strain energy associated with the fibre-matrix interaction may considerably affect the mechanical responses of the soft tissue and it should not be ignored even though the value of the associated strain energy may be much smaller than the strain energy contribution from the fibres.

4.6.3 Data fitting based approach for HAF modelling

Humphrey et al. [126] proposed a phenomenological method to determine the strain energy function W directly from the combined finite extension and torsion test for transversely isotropic papillary muscle with the assumption that $W = W\left(I_1, I_4\right)$ (that is, W is independent of I_2 and I_5). The uniaxial and biaxial tests in Bass et al. [81], however, are not sufficient to fully determine the general strain energy function of the orthotropic HAF soft tissue. For orthotropic HAF, it is not difficult to construct a strain energy function to fit all the uniaxial and biaxial testing results, but it is difficult to have such a function valid for other general deformation states. For example, we may define W as $W\left(E_{11}, E_{22}\right)$. From the uniaxial and biaxial experimental results, each deformation state $\left(E_{11}, E_{22}\right)$ links to $\partial W/\partial E_{11}$ $\left(= S_{11}\right)$, $\partial W/\partial E_{22}$ $\left(= S_{22}\right)$ and the value of W can be computed. Hence the strain energy function W can be constructed by piecewise (quadratic) interpolation. Obviously this function can reproduce the uniaxial and biaxial results exactly. But its ability to predict the mechanical response of the HAF under other deformation state (e.g., shear deformation) is questionable because it is solely based on data fitting without any physical interpretation. Hence in a good constitutive model for soft tissues, the strain energy function should be constructed using micromechanics analysis rather than direct data fitting.

4.7 Concluding remarks

(1) The experimental data of the uniaxial and biaxial tests of the HAF in Bass et al. [81]

is carefully fitted by polynomial curves so that the fitted results are consistent and can be used to compute the strain energy of any uniaxial or biaxial deformation state which occurred in the experiments. In the uniaxial test of the HAF along the axial direction, the collagen fibres are all under contraction and their contribution to the strain energy is assumed negligible. The strain energy computed from the fitted polynomial curves can then be employed to investigate the mechanical behaviour of the ground matrix. The obtained result shows that the matrix can be simulated well by an incompressible neo-Hookean model when the fibres are under contraction.

(2) The classical uncoupled models treat the collagen fibres as nonlinear springs, and the potential fibre-matrix interaction is ignored. These models predict that the mechanical behaviour of the matrix is independent of the fibre stretch.

(3) Using the experimental data of a series of biaxial tests, we find that when the fibres are stretched, the response of the ground matrix can still be described by the incompressible neo-Hookean model, but the effective stiffness of the matrix depends on the fibre stretch ratio. This stiffness can be more than 10 times larger than the one obtained with collagen fibres under contraction. This phenomenon can only be explained by the fibre-matrix interaction.

(4) It is found that the inhomogeneous distribution of the deformation (which comes naturally from the inhomogeneity of the composites) can explain part of the fibre-stretch dependence. The potential fibre orientation dispersion also contributes to the fibre-stretch dependence.

(5) The simulation results of the uniaxial test of the HAF along the circumferential direction shows that the fibre-matrix interaction strain energy can affect significantly the mechanical behaviour of the soft tissue. Hence it should not be ignored in constitutive models.

(6) The uniaxial and biaxial tests are not sufficient to fully determine the strain energy function of the orthotropic HAF. A comprehensive micromechanics-based model which considers both the composite effect and the fibre orientation dispersion is required to predict the fibre-matrix interaction found in this chapter.

Chapter 5 Conclusions

To model the mechanical behaviours of the incompressible particle-reinforced neo-Hookean composite (IPRNC), in which both the matrix and the particle reinforcement are incompressible neo-Hookean materials, under finite deformation, three-dimensional RVE models are created for FE simulations. Four different particle volume fractions (i.e., $c = 0.05, 0.1, 0.2, 0.3$) are investigated, and for each sphere volume fraction, four different RVE samples with periodic microstructures are generated. There are 27 non-overlapping identical spheres randomly distributed in each cubic unit RVE. After the isotropy of the random distributions of particles in the 16 RVE models is examined, periodic meshes are generated for the RVE models so that the periodic boundary conditions can be applied during the FE simulations. The mesh convergence study shows that a standard mesh with about 80,000 elements is sufficient obtain accurate result.

Simulations of uniaxial tension and compression along different directions are performed for every RVE model to double check the isotropy of the RVE models's mechanical responses directly. The simulation results of the uniaxial tension and compression are consistent, which implies that the small-size RVE models used are sufficient to obtain accurate responses of the IPRNC. A clear proportional relation between the computed strain energy data and $I_1 - 3$ is observed, which suggests that the mechanical response of the IPRNC can be well predicted by an incompressible neo-Hookean model.

To investigate the effect of the stiffness ratio between the particle and the matrix, four different particle/matrix stiffness ratios are studied in the FE simulations: $\mu_r/\mu_m = \infty$ (i.e., rigid particles), 100, 10, 0.5. Four types of finite deformations (i.e., uniaxial tension and compression along coordinate axial directions and random directions, simple shear, and general biaxial deformation) are simulated. All the simulation results (i.e., RVE with any particle volume fraction, any particle/matrix stiffness ratio and any

loading case) show that the average strain energy $\bar{W}$ is proportional to $I_1 - 3$, which suggests that the overall behaviour of the IPRNC can be modelled by an incompressible neo-Hookean model. The effective shear moduli μ_c of the IPRNCs are obtained by fitting the strain energy data from the numerical simulation results. Because the dispersion in the values of the obtained moduli is remarkably small in all cases, the numerical results can be considered as a very close approximation to the "exact" effective shear moduli of the IPRNC. They are compared with three theoretical models: the self-consistent estimate, SCE [53], the strain amplification estimate for composites with rigid particles, SAE [62], and the classical linear elastic three phase model, TPM [18]. It is found that the TPM provide very accurate approximation to the numerical results (maximum relative difference less than 5.1%) though it is developed for linear elastic PRC. Even though the SCE and the SAE are proposed for neo-Hookean composites, they overestimate the effective shear modulus of the IPRNC when the particle volume fraction $c > 0.1$.

We note that mesh of the matrix necking zone between close particles is very challenging and severe deformation localisation may happen when the stiffness contrast between the particle and the matrix is large. Hence convergence is a big issue in our numerical simulation even for RVE models with very refined meshes (e.g., with more than 200,000 elements). For example, it is only possible to reach moderate deformation state for some cases (e.g., $I_1 = 3.06$, or 14% tension for the IPRNC with $(\mu_r = \infty, c = 0.3)$. For much less critical case like the IPRNC with $(\mu_r = 0.5, c = 0.3)$, large deformation can be reached (i.e, 313% tension or 86% compression) compared to other conditions discussed in the previous sections. The numerical results show clearly that up to the deformations the FE simulations can reach (that is, until there is a convergence problem), all the numerical results of $\bar{W}$ and $I_1 - 3$ can be fitted almost exactly using the linear relation suggested by the incompressible neo-Hookean model. Therefore it is safe to conclude that the mechanical behaviour of the IPRNC studied here can be well modelled by another incompressible neo-Hookean model within the limit of current FE software ABAQUS.

In chapter 4, the significance of fibre-matrix interaction in fibre-reinforced composite under finite deformation is investigated. The experimental data from Bass [81] provided the uniaxial and biaxial data of Human Annulus Fibrosus (HAF), which can be fitted

and applied to work out the strain energy of the corresponding deformation states. The collagen fibres are under contraction in the uniaxial tests along the axial direction, so the contribution to the strain energy from fibres could be ignored. The strain energy calculated from the fitted polynomial curves was then adopted to analyse the mechanical performance of the ground matrix. The results indicated that the incompressible neo-Hookean model was capable of simulating the ground matrix when the collagen fibres were under contraction.

The potential fibre-matrix interaction is neglected in the classical uncoupled models because the collagen fibres are treated as nonlinear springs. According to their prediction, there is no relation between the mechanical behaviours of the matrix and the fibre stretch ratio. By investigating series of biaxial experimental data, it is found that the ground matrix can be described by the incompressible neo-Hookean model, but the effective stiffness of the matrix depends on the fibre stretch ratio. This obtained stiffness could be more than 10 times larger than the one with collagen fibres under contraction. This phenomenon can only be explained by the fibre-matrix interaction.

Part of the fibre stretch dependence is due to the inhomogeneous distribution of the deformation and the inhomogeneity of the composites. The potential fibre orientation dispersion also contributes to the fibre-stretch dependence. The experimental data of the uniaxial tests of the HAF long the circumferential direction illustrated that the strain energy contributed by fibre-matrix interaction can affect significantly the mechanical properties of the soft tissue. Hence it should not be ignored in constitutive models.

Uniaxial and biaxial tests are insufficient to well determine the strain energy function of the heterogeneous HAF, so a comprehensive micromechanics-based model considering both composite effect and fibre orientation dispersion is demanded to predict the fibre-matrix interaction analysed in this paper.

Chapter 6 Future Work

In chapter 3, three-dimensional RVE models are developed to simulate the mechanical behaviour of incompressible particle-reinforced neo-Hookean composites (IPRNC). The potential extensions of this research work include:

1. Theoretical analysis and modelling of the mechanical behaviour of IPRNC: Based on the observation of the stress/strain field in the IPRNC models in the FE simulation, it might be possible to propose some approximation format of the elasticity field in IPRNC. Christensen and Lo's [18] three phase model can be extended to finite deformation regime and we may learn from Imam et al.'s [54] result to derive an approximate format of the elasticity field, based on which the effective shear modulus of the IPRNC can be obtained by an averaging procedure.

2. Effects of size distribution and shape of particles: In the current RVE, the particles are identical spheres. Non-spherical particles of various sizes can be embedded in the unit cube to investigate the effects of size distribution and shape of particles in IPRNC. In that case, it is important to study the RVE size required to obtain accurate results of the composite.

3. Composites consisting of other material phases: In this research work, we only considered a neo-Hookean matrix in which neo-Hookean (or rigid) particles were embedded. Actually similar RVE models can be employed to simulate the mechanical behaviours of composites with constituents of other materials. For example, for composite consisting Mooney-Rivlin matrix embedded with rigid particles, the mechanical behaviour of the composite can be fitted by an Ogden model (or even another Mooney-Rivlin model). The RVE models can be used to study the relations between the Odgen model's parameters and the properties of the matrix, as well as the particle volume fraction.

4. Strength, fracture, damage of IPRNC: Because the stress/strain field is obtained in the FE simulations, the numerical result can be adopted to study the strength, fracture and damage properties of the IPRNC. Usually the critical points with maximum stress measure are first identified, and related criteria can be established to analyse the strength of the composite. Simulation of the fracture and damage process of the composite is also possible if the fracture or damage can be modelled properly in the FE program.

5. Porous neo-Hookean media: The same RVE models can be used to simulate the mechanical behaviour of porous neo-Hookean media by setting the particles as voids. Now the material becomes compressible because of the existence of the voids. Hydrostatic loading and general triaxial deformation simulations are required to obtain the mechanical behaviours of the porous material under general deformation.

6. Composites with compressible phases: After the porous neo-Hookean media is investigated, general PRC with compressible phases can be studied by numerical homogenisation based on the RVE models developed in this research work. Similarly, hydrostatic loading and general triaxial deformation simulations will be performed to investigate the composite's mechanical behaviours.

7. Composites with other microstructures: Although the RVE models developed in the thesis only represents PRC with a particular microstructure (i.e., with identical randomly distributed spherical particles), composite with other microstructure can be modelled in a similar way. For example, the mechanical responses of FRC can also be investigated by corresponding RVE models with proper microstructure.

In chapter 4, the significance of the fibre-matrix interaction in HAF is identified and discussed. The potential physical sources of the interaction are investigated in detail. It is found that both the fibre-matrix shear interaction and the fibre orientation distribution contribute to the fibre-matrix interaction. However, there is no constitutive model in the literature which considers both effects. Therefore, the following research directions are possible for us to extend current study here:

1. Development a constitutive model considering both the fibre-matrix shear interaction and fibre orientation distribution. This can be performed in two approaches. In the first

approach, the fibre orientation distribution can be introduced into the current models with fibre-matrix shear interaction considered (e.g., Guo et al.'s [6] composites-based model). A simple integration scheme can be employed to consider the fibre orientation distribution. In the second approach, the fibre-matrix shear interaction mechanism can be introduced into the current models with fibre orientation distribution considered (e.g., Caner et al.'s [89] microplane model). This can be done by using a coupled model with fibre-matrix shear interaction in each microplane's constitutive relation. The models developed can then be used to re-produce the uniaxial and biaxial experimental results in [81].

2. Numerical approach to model zig-zag (curved) fibres: In all FRC models discussed in this study for soft tissue, the fibres are assumed as straight. However, in the real soft tissue, the collagen fibres are usually in a zig-zag shape [122]. To model the soft tissue embedded with zig-zag shape collagen fibres accurately, precise RVE models can be developed to simulate the mechanical behaviours of soft tissue under general finite deformation. The challenges here include how to construct RVE models with periodic microstructure and how to define periodic boundary conditions.

3. Theoretical approximations for soft tissue with zig-zag fibres: The numerical results obtained from the numerical approach can be used to construct some theoretical closed-form approximation for the soft tissue. The model can be further validated by experimental data available in the literature. It should be noted that the material may not be transversely isotropic anymore if the fibres are not straight. This will potentially make the model very complex. In that case, the strain components in the principal coordinate system of HAF (i.e., the axial circumferential and radial directions as the axes of the coordinate system) can be used to describe the strain energy function. The model will look like a Fung's type model, but the terms can carry clear physical meanings.

4. Effect of fibre-fibre interaction: Because of the complexity of the fibre-fibre interaction, almost all models in the literature ignore the effect of fibre-fibre interaction. The potential approach to study the fibre-fibre interaction is probably through numerical simulation. RVE models with a number of fibres can be developed and the FE simulations may suggest some mechanisms of the fibre-fibre interaction.

Appendix A: Geometries of 16 RVE models

The geometry of every RVE model is presented in Appendix A, and there are 16 models in total. In the table below each model, the centres of spheres is listed.

- Volume ratio (V): c = 0.05
- Diameter: d = 0.1524

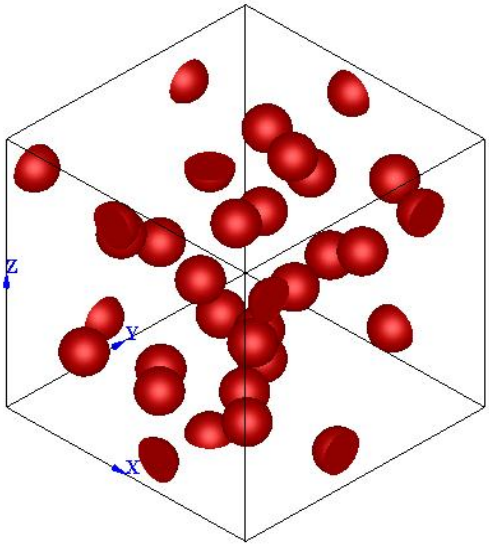

Inclusions	X	Y	Z	Inclusions	X	Y	Z
1.1	-0.0146	0.4002	0.1303	15.1	-0.0183	0.7561	0.8366
1.2	0.9854	0.4002	0.1303	15.2	0.9817	0.7561	0.8366
2.1	0.5484	0.5096	0.3082	16.1	1.0109	0.1064	0.8450
3.1	0.2957	0.5154	0.3648	16.2	0.0109	0.1064	0.8450
4.1	0.5580	0.6386	0.8932	17.1	0.3441	0.6161	0.5493
5.1	0.7916	0.2378	0.5169	18.1	0.6496	0.3458	0.2093
6.1	0.3596	0.2858	0.1812	19.1	0.4419	0.0059	0.8930
7.1	0.2673	0.8218	0.7623	19.2	0.4419	1.0059	0.8930
8.1	0.2304	0.4118	0.5250	20.1	0.1349	0.1900	0.1793
9.1	0.4484	0.9060	0.3381	21.1	0.8540	0.1520	0.2960
10.1	0.4638	0.6048	0.1107	22.1	0.6253	-0.0115	0.1151
11.1	0.5261	0.3234	0.9946	22.2	0.6253	0.9885	0.1151
11.2	0.5261	0.3234	-0.0054	23.1	0.7407	0.8820	0.7805
12.1	0.5216	0.1181	0.2626	24.1	0.6767	0.5261	0.5232
13.1	0.5148	0.7563	0.7529	25.1	0.7598	0.7281	0.5968
14.1	0.3115	0.1688	0.7166	26.1	0.1981	0.6988	0.0984
				27.1	0.2112	0.8587	0.4061

V0.05Model1

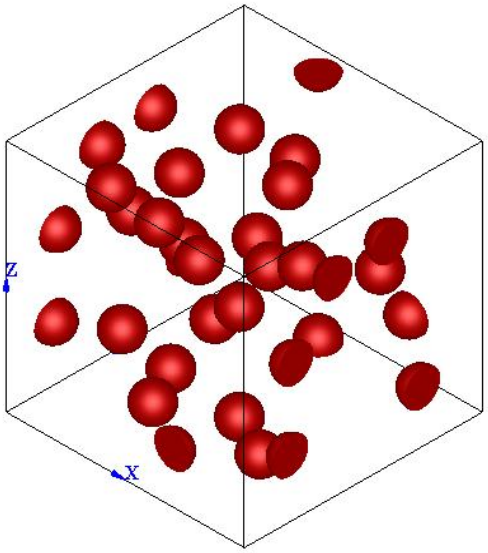

Inclusions	X	Y	Z	Inclusions	X	Y	Z
1.1	0.2506	0.2755	0.7300	14.1	0.3559	0.8568	0.6820
2.1	0.3626	0.1240	0.4255	15.1	0.4871	0.1285	0.2167
3.1	0.6532	0.5281	0.8988	16.1	0.4010	0.9088	1.0186
4.1	0.5206	0.2898	0.6761	16.2	0.4010	0.9088	0.0186
5.1	0.5264	0.1168	0.9028	17.1	0.6252	0.3542	0.1179
6.1	0.8477	0.1302	0.7460	18.1	0.7670	0.4779	0.6836
7.1	1.0046	0.1927	0.2421	19.1	0.4260	0.4491	0.3320
7.2	0.0045	0.1927	0.2421	20.1	0.3126	0.3788	0.1271
8.1	0.9945	0.7470	0.2158	21.1	0.1778	0.5692	0.4284
8.2	-0.0055	0.7470	0.2158	22.1	0.2918	0.1487	0.8989
9.1	0.4849	0.6195	0.4702	23.1	0.8137	0.2514	0.1258
10.1	0.1633	0.8172	0.7161	24.1	-0.0033	0.6140	0.8174
11.1	0.6971	0.9934	0.2113	24.2	0.9967	0.6140	0.8174
11.2	0.6971	-0.0066	0.2113	25.1	-0.0030	0.2140	0.5701
12.1	0.1698	0.5569	0.6886	25.2	0.9970	0.2140	0.5701
13.1	1.0133	0.3804	0.8016	26.1	0.2077	0.8460	0.3247
13.2	0.0133	0.3804	0.8016	27.1	0.6798	0.8896	0.4199

V0.05Model2

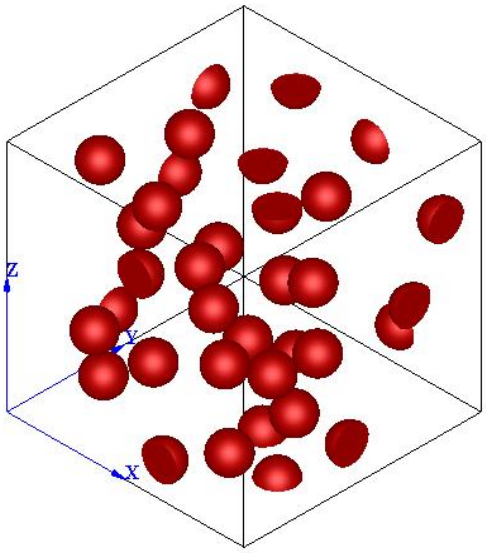

Inclusions	X	Y	Z	Inclusions	X	Y	Z
1.1	0.7947	0.1437	0.1744	15.1	0.6178	0.4609	0.0120
2.1	0.2014	0.1684	0.3174	15.2	0.6178	0.4609	1.0120
3.1	0.6887	0.2293	0.4049	16.1	0.9969	0.4498	0.1540
4.1	0.3019	0.2686	0.7080	16.2	-0.0031	0.4498	0.1540
5.1	0.3188	0.8516	0.2202	17.1	0.8865	0.2332	0.4656
6.1	0.1735	0.2332	0.1050	18.1	1.0035	0.7107	0.5339
7.1	0.2560	0.5138	0.8978	18.2	0.0035	0.7107	0.5339
8.1	0.8114	0.3290	-0.0085	19.1	0.8046	0.5052	0.3657
8.2	0.8114	0.3290	0.9915	20.1	0.5079	0.1100	0.3824
9.1	0.8226	0.3885	0.2120	21.1	0.4110	0.8070	0.0129
10.1	0.7055	0.1656	0.6524	21.2	0.4110	0.8070	1.0129
11.1	0.5182	0.4970	0.2769	22.1	0.9002	0.3903	0.7320
12.1	0.9835	0.8521	0.7758	23.1	0.1676	0.2252	0.9022
12.2	-0.0165	0.8521	0.7758	24.1	0.2340	0.5794	0.3630
13.1	0.5384	0.0189	0.7688	25.1	0.6918	0.6552	0.8141
13.2	0.5384	1.0190	0.7688	26.1	0.1172	0.7751	0.2797
14.1	0.4360	0.1966	0.8799	27.1	0.6433	0.0152	0.1357
				27.2	0.6433	1.0152	0.1357

V0.05Model3

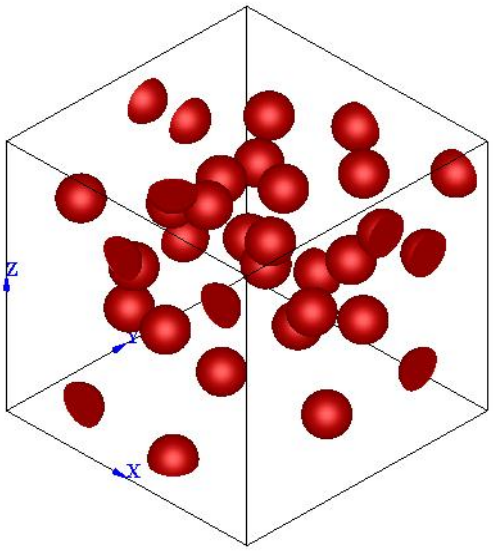

Inclusions	X	Y	Z	Inclusions	X	Y	Z
1.1	0.5406	0.6704	0.2520	16.1	0.5999	0.4784	0.6049
2.1	0.5125	0.3244	0.8562	17.1	0.9918	0.7528	0.7016
3.1	0.3802	0.5127	0.7907	17.2	-0.0082	0.7528	0.7016
4.1	0.4330	0.5734	0.5704	18.1	-0.0146	0.5781	0.8609
5.1	0.6371	0.8459	0.2326	18.2	0.9854	0.5781	0.8609
6.1	0.8826	-0.0134	0.8302	19.1	0.2504	0.8414	0.7993
6.2	0.8826	0.9866	0.8302	20.1	0.7253	0.7069	0.5684
7.1	0.5219	0.1394	0.4918	21.1	0.1090	0.4025	0.2353
8.1	0.6604	0.8245	0.7977	22.1	0.6022	0.5499	0.8502
9.1	0.2196	0.8300	0.6136	23.1	0.4777	0.9797	0.8032
10.1	0.1709	0.1385	0.8046	23.2	0.4777	-0.0203	0.8032
11.1	0.0206	0.7155	0.2962	24.1	0.3115	0.9890	0.1770
11.2	1.0206	0.7155	0.2962	24.2	0.3115	-0.0110	0.1770
12.1	0.7993	0.4706	0.5311	25.1	0.4512	0.4432	0.1489
13.1	0.8191	0.2780	0.8985	26.1	0.8565	0.4755	0.1775
14.1	0.3719	0.1580	0.6426	27.1	0.5375	0.1555	1.0131
15.1	0.1211	0.5655	0.5466	27.2	0.5375	0.1555	0.0131

V0.05Model4

- Volume ratio (V): c = 0.1
- Diameter: d = 0.1920

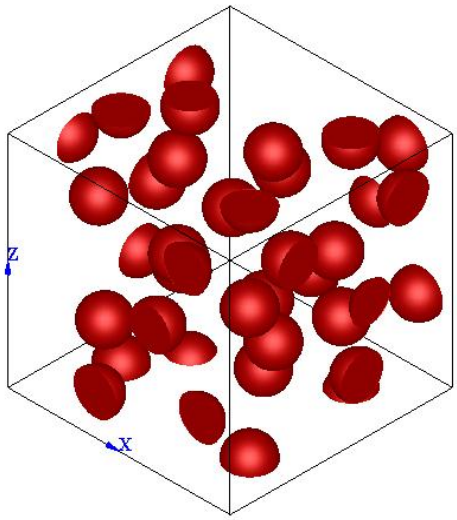

Inclusions	X	Y	Z	Inclusions	X	Y	Z
1.1	0.6389	1.0303	0.5508	15.1	0.3915	0.0058	0.1737
1.2	0.6389	0.0303	0.5508	15.2	0.3915	1.0058	0.1737
2.1	0.5955	0.5582	0.3644	16.1	-0.0136	0.5936	0.2439
3.1	0.1893	0.8184	0.3936	16.2	0.9864	0.5936	0.2439
4.1	0.8198	0.2680	0.5901	17.1	0.7956	-0.0128	0.8629
5.1	0.1629	0.3460	1.0053	17.2	0.7956	0.9872	0.8629
5.2	0.1629	0.3460	0.0053	18.1	0.2829	0.4966	0.3821
6.1	0.1931	0.5695	0.7129	19.1	1.0382	0.6310	0.5207
7.1	0.8630	0.9835	0.3118	19.2	0.0382	0.6310	0.5207
7.2	0.8630	-0.0165	0.3118	20.1	0.4383	0.7922	0.6866
8.1	0.2625	0.5569	-0.0408	21.1	0.7217	0.7489	0.5247
8.2	0.2625	0.5569	0.9592	22.1	0.4208	0.3431	0.5647
9.1	0.6212	0.5293	0.1252	23.1	0.1968	0.2396	0.2459
10.1	0.8296	0.2579	1.0106	24.1	0.9646	0.3077	0.8295
10.2	0.8296	0.2579	0.0106	24.2	-0.0354	0.3077	0.8295
11.1	0.7834	0.4117	0.3675	25.1	0.7694	0.7314	0.2985
12.1	0.2135	0.1952	0.7622	26.1	0.5514	0.6426	0.8809
13.1	0.9952	0.7985	0.8418	27.1	0.7698	0.7738	-0.0275
13.2	-0.0048	0.7985	0.8418	27.2	0.7698	0.7738	0.9725
14.1	0.5521	0.8121	0.3428				

V0.1Model1

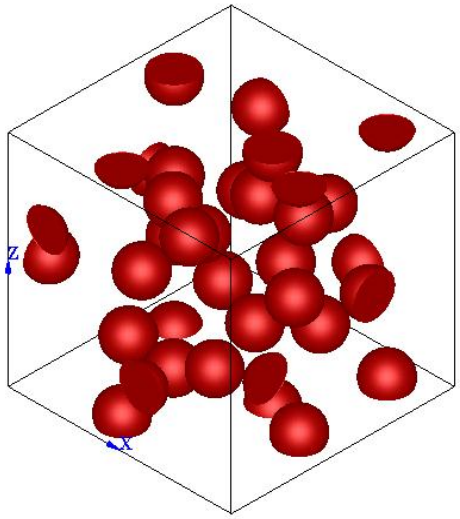

Inclusions	X	Y	Z	Inclusions	X	Y	Z
1.1	0.1223	0.6212	0.9706	16.1	0.5927	-0.0079	0.2922
1.2	0.1223	0.6212	-0.0294	16.2	0.5927	0.9921	0.2922
2.1	0.1867	0.8811	0.4251	17.1	0.2538	0.2848	0.1875
3.1	0.6821	0.2421	0.2909	18.1	0.1405	0.6086	0.3578
4.1	0.2318	0.7299	0.1695	19.1	0.8657	0.4377	0.0365
5.1	0.7982	0.5257	0.8064	19.2	0.8657	0.4377	1.0365
6.1	0.4009	0.7289	0.5891	20.1	0.7006	0.7321	0.7041
7.1	0.1842	0.5620	0.6410	21.1	0.4914	0.7526	0.3602
8.1	0.3817	0.4848	0.5495	22.1	0.6517	0.5332	0.9795
9.1	0.6853	0.1267	0.8680	22.2	0.6517	0.5332	-0.0205
10.1	0.7145	0.5692	0.4224	23.1	0.3953	0.1157	1.0334
11.1	1.0267	0.1588	0.4518	23.2	0.3953	0.1157	0.0334
11.2	0.0267	0.1588	0.4518	24.1	0.4538	0.6520	0.1520
12.1	0.4370	0.3016	0.7994	25.1	0.1721	0.9626	0.7023
13.1	0.6898	0.7073	0.2374	25.2	0.1721	-0.0374	0.7023
14.1	0.4098	0.1887	0.5666	26.1	0.4779	0.2614	0.1814
15.1	0.8399	0.8572	0.0307	27.1	0.9802	0.6401	0.5358
15.2	0.8399	0.8572	1.0307	27.2	-0.0198	0.6401	0.5358

V0.1Model2

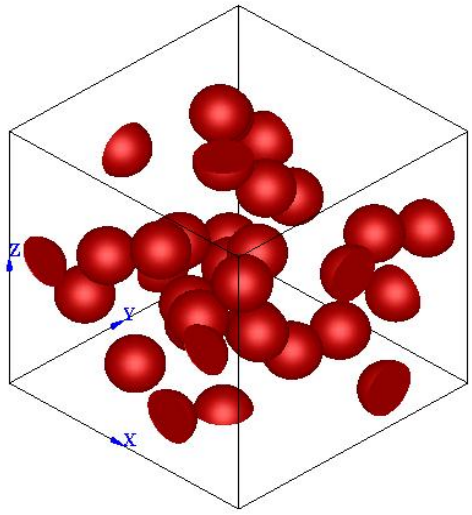

Inclusions	X	Y	Z	Inclusions	X	Y	Z
1.1	0.8509	0.3821	0.3649	15.1	0.6981	-0.0135	0.2152
2.1	0.2739	0.4680	0.4664	15.2	0.6981	0.9865	0.2152
3.1	0.6346	0.1908	0.4781	16.1	0.8557	0.1598	0.7453
4.1	0.5679	0.3653	-0.0200	17.1	0.7878	0.6540	0.2766
4.2	0.5679	0.3653	0.9800	18.1	0.2691	0.6493	0.8806
5.1	0.3162	0.4938	0.1508	19.1	0.3470	0.2019	0.1505
6.1	0.3909	0.8447	0.5136	20.1	0.8495	0.7424	0.6474
7.1	0.4741	0.1853	0.6735	21.1	0.4514	0.3353	0.3705
8.1	0.9895	0.4997	0.6788	22.1	0.1497	0.9656	0.5586
8.2	-0.0105	0.4997	0.6788	22.2	0.1497	-0.0344	0.5586
9.1	0.2881	0.6815	0.2696	23.1	0.9966	0.6542	0.1482
10.1	0.1223	0.8367	0.2038	23.2	-0.0034	0.6542	0.1482
11.1	0.8699	0.2153	0.5276	24.1	0.2502	0.1764	0.5438
12.1	0.5267	0.5426	0.2107	25.1	0.1208	0.8117	0.7150
13.1	0.5507	0.5676	0.7659	26.1	0.8499	0.9696	0.5566
14.1	0.1153	0.2132	0.3051	26.2	0.8499	-0.0304	0.5566
				27.1	0.4598	0.6209	0.4369

V0.1Model3

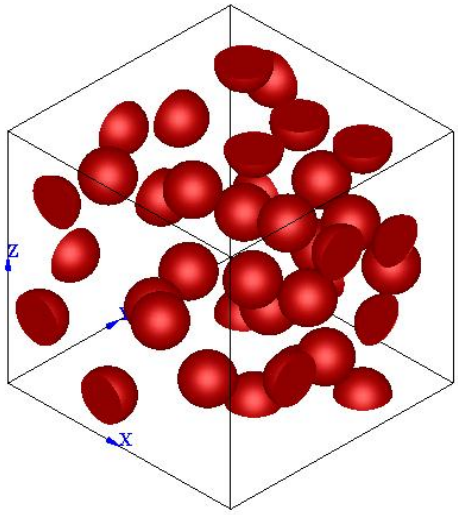

Inclusions	X	Y	Z	Inclusions	X	Y	Z
1.1	0.3019	0.3545	0.2770	13.1	0.5286	0.8726	0.3644
2.1	0.8232	0.6028	0.2145	14.1	0.6215	0.4825	1.0010
3.1	0.7910	0.7479	0.6542	14.2	0.6215	0.4825	0.0009
4.1	0.5438	0.1400	0.4498	15.1	0.1749	0.6356	0.2130
5.1	0.9899	0.2882	0.3663	16.1	0.2307	0.2178	0.8287
5.2	-0.0102	0.2882	0.3663	17.1	0.8313	0.8902	0.4377
6.1	1.0223	0.7465	0.6894	18.1	0.8895	0.2093	0.7507
6.2	0.0223	0.7465	0.6894	19.1	0.8379	0.7545	-0.0113
7.1	0.5936	0.7152	0.9753	19.2	0.8379	0.7545	0.9887
7.2	0.5936	0.7152	-0.0247	20.1	0.4963	0.3329	0.8494
8.1	0.4407	0.6207	0.5885	21.1	0.7235	0.5309	0.7310
9.1	1.0262	0.6628	0.4200	22.1	0.2065	0.9859	0.8189
9.2	0.0261	0.6628	0.4200	22.2	0.2065	-0.0141	0.8189
10.1	0.4193	0.0291	0.1473	23.1	0.8397	0.5062	0.5058
10.2	0.4193	1.0291	0.1473	24.1	0.6544	0.2420	0.2235
11.1	0.1290	0.0117	0.3168	25.1	0.5237	0.8847	0.6267
11.2	0.1290	1.0117	0.3168	26.1	0.2564	0.8027	0.9956
12.1	-0.0054	0.5017	0.7631	26.2	0.2564	0.8027	-0.0044
12.2	0.9946	0.5017	0.7631	27.1	0.5174	0.6567	0.2362

V0.1Model4

- Volume ratio (V): c = 0.2
- Diameter: d = 0.2418

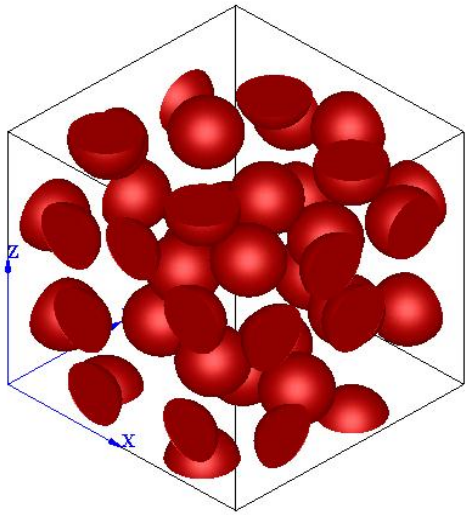

Inclusions	X	Y	Z	Inclusions	X	Y	Z
1.1	0.3401	0.6266	0.5142	14.1	0.1276	0.7130	0.2340
2.1	0.6094	0.5218	0.7802	15.1	0.0376	0.2103	0.1907
3.1	0.7995	0.6845	0.3503	15.2	1.0376	0.2103	0.1907
4.1	0.5239	0.2475	0.5966	16.1	0.2343	0.6342	0.7993
5.1	-0.0430	0.7781	0.7315	17.1	0.3745	-0.0434	0.1490
5.2	0.9570	0.7781	0.7315	17.2	0.3745	0.9566	0.1490
6.1	0.4422	0.7254	0.0141	18.1	0.0158	0.5303	0.4952
6.2	0.4422	0.7254	1.0141	18.2	1.0158	0.5303	0.4952
7.1	0.8665	0.6409	0.9662	19.1	0.2636	0.9759	0.7178
7.2	0.8665	0.6409	-0.0338	19.2	0.2636	-0.0241	0.7178
8.1	0.3176	-0.0321	0.4120	20.1	0.7398	0.1600	0.3858
8.2	0.3176	0.9679	0.4120	21.1	0.5789	0.4519	0.1249
9.1	0.2194	0.2102	0.9747	22.1	0.0179	0.4296	0.7499
9.2	0.2194	0.2102	-0.0253	22.2	1.0179	0.4296	0.7499
10.1	0.0230	0.1696	0.5993	23.1	0.8496	0.4176	0.1979
10.2	1.0230	0.1696	0.5993	24.1	0.5750	0.8176	0.4558
11.1	0.8027	-0.0121	0.6548	25.1	0.5416	0.9564	0.8073
11.2	0.8027	0.9879	0.6548	25.2	0.5416	-0.0436	0.8073
12.1	0.3512	0.3198	0.2723	26.1	0.7800	0.2758	0.7442
13.1	0.7164	0.1351	-0.0169	27.1	0.7940	-0.0420	0.2154
13.2	0.7164	0.1351	0.9831	27.2	0.7940	0.9580	0.2154

V0.2Model1

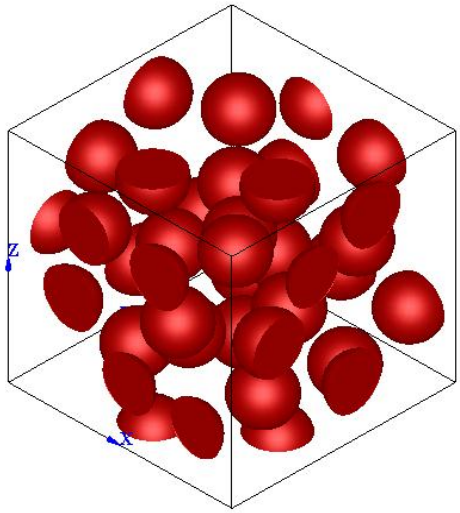

Inclusions	X	Y	Z	Inclusions	X	Y	Z
1.1	0.4807	0.3235	0.2830	15.1	1.0441	0.3663	0.7356
2.1	0.4756	0.1706	-0.0367	15.2	0.0441	0.3663	0.7356
2.2	0.4756	0.1706	0.9633	16.1	0.6613	0.9780	0.7461
3.1	0.7948	0.4090	0.9721	16.2	0.6613	-0.0220	0.7461
3.2	0.7948	0.4090	-0.0279	17.1	0.3534	0.3830	0.5318
4.1	0.9609	0.2110	0.5311	18.1	0.4532	0.5994	0.1264
4.2	-0.0391	0.2110	0.5311	19.1	0.6159	0.4179	0.6930
5.1	0.5999	0.1579	0.4623	20.1	0.2514	0.7778	0.8214
6.1	0.0225	0.5494	0.2271	21.1	0.8377	0.9573	0.2387
6.2	1.0225	0.5494	0.2271	21.2	0.8377	-0.0427	0.2387
7.1	0.2115	0.6650	0.4454	22.1	0.7468	0.5096	0.4134
8.1	0.5333	0.9573	0.2615	23.1	0.2749	-0.0204	0.4718
8.2	0.5333	-0.0427	0.2615	23.2	0.2749	0.9796	0.4718
9.1	0.8482	0.7112	0.6357	24.1	0.3381	0.0435	0.7581
10.1	0.2217	0.8461	0.1420	24.2	0.3381	1.0435	0.7581
11.1	0.4148	0.5998	0.6979	25.1	0.8477	0.1680	0.8617
12.1	0.8687	0.2697	0.2564	26.1	0.5268	0.6638	0.4534
13.1	0.2595	0.3166	0.1302	27.1	1.0213	0.6347	0.8454
14.1	0.8040	0.7010	0.1273	27.2	0.0213	0.6347	0.8454

V0.2Model2

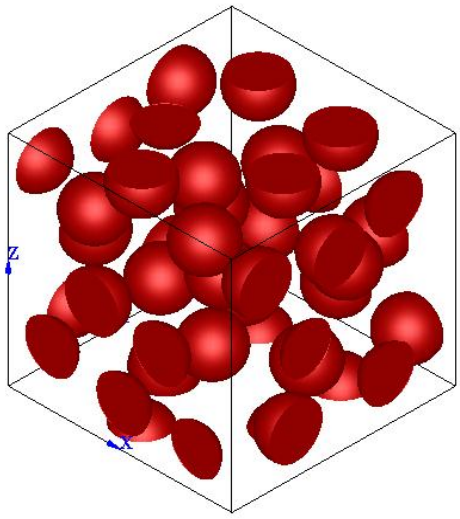

Inclusions	X	Y	Z	Inclusions	X	Y	Z
1.1	0.7750	0.4547	0.9673	14.1	1.0513	0.3337	0.4814
1.2	0.7750	0.4547	-0.0327	14.2	0.0513	0.3337	0.4814
2.1	0.3159	0.8016	0.9490	15.1	0.3728	1.0104	0.5127
2.2	0.3159	0.8016	-0.0510	15.2	0.3728	0.0104	0.5127
3.1	0.8376	0.9490	0.1704	16.1	0.3655	0.5083	0.7500
3.2	0.8376	-0.0510	0.1704	17.1	1.0252	0.7362	0.8490
4.1	0.7179	0.7663	0.9700	17.2	0.0252	0.7362	0.8490
4.2	0.7179	0.7663	-0.0300	18.1	-0.0225	0.2865	0.1763
5.1	0.9723	0.1512	0.8168	18.2	0.9775	0.2865	0.1763
5.2	-0.0277	0.1512	0.8168	19.1	0.5452	0.3671	0.2524
6.1	0.7753	0.5594	0.2123	20.1	0.6952	0.1822	0.8339
7.1	0.5091	0.9646	0.1856	21.1	0.4058	0.6488	0.2630
7.2	0.5091	-0.0354	0.1856	22.1	0.4067	0.8033	0.6862
8.1	0.1722	0.7349	0.4391	23.1	0.1888	0.9607	0.2490
9.1	0.6751	0.9721	0.4628	23.2	0.1888	-0.0393	0.2490
9.2	0.6751	-0.0279	0.4628	24.1	-0.0335	0.4835	0.7734
10.1	0.6206	0.3348	0.5932	24.2	0.9665	0.4835	0.7734
11.1	0.8365	0.6719	0.5666	25.1	0.2854	0.3969	0.3712
12.1	0.3130	0.3887	1.0431	26.1	0.4420	0.1538	0.9511
12.2	0.3130	0.3887	0.0431	26.2	0.4420	0.1538	-0.0489
13.1	0.2535	0.1331	0.7596	27.1	0.0308	0.6980	0.1980
				27.2	1.0308	0.6980	0.1980

V0.2Model3

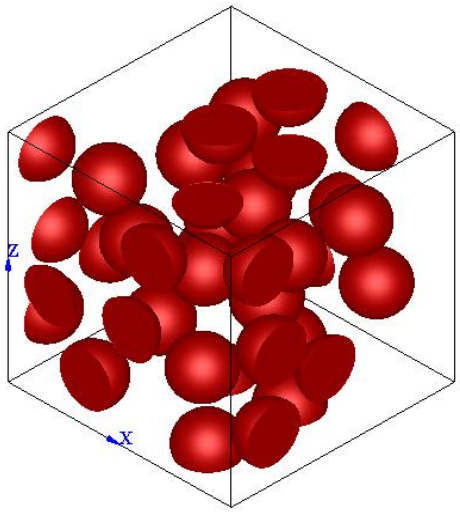

Inclusions	X	Y	Z	Inclusions	X	Y	Z
1.1	0.7257	0.4311	0.4849	16.1	0.2068	0.8562	0.7424
2.1	0.4629	0.7966	-0.0013	17.1	0.4890	0.6703	0.2539
2.2	0.4629	0.7966	0.9987	18.1	0.4473	0.5001	0.9889
3.1	1.0168	0.4365	0.3335	18.2	0.4473	0.5001	-0.0111
3.2	0.0168	0.4365	0.3335	19.1	-0.0304	0.2202	0.4991
4.1	0.8435	0.7140	0.7100	19.2	0.9696	0.2202	0.4991
5.1	0.5389	-0.0239	0.4770	20.1	-0.0300	0.1629	0.8502
5.2	0.5389	0.9761	0.4770	20.2	0.9700	0.1629	0.8502
6.1	0.7259	0.5338	1.0074	21.1	0.2233	0.3527	0.5033
6.2	0.7259	0.5338	0.0074	22.1	0.6250	0.0079	0.7966
7.1	0.3638	0.3131	0.2775	22.2	0.6250	1.0079	0.7966
8.1	0.1355	0.7852	0.1974	23.1	0.1834	-0.0464	0.4370
9.1	0.8019	0.8482	0.3747	23.2	0.1834	0.9536	0.4370
10.1	0.8647	0.3966	0.7393	24.1	0.3467	1.0315	0.1859
11.1	0.6406	0.2380	0.6507	24.2	0.3467	0.0315	0.1859
12.1	0.5222	0.5775	0.6785	25.1	0.2569	0.6975	0.4401
13.1	0.2631	0.5683	0.7537	26.1	0.9809	0.1891	0.1940
14.1	0.2325	0.2209	0.8168	26.2	-0.0191	0.1891	0.1940
15.1	0.7288	0.1649	1.0384	27.1	0.7004	0.1692	0.3246
15.2	0.7288	0.1649	0.0384				

V0.2Model4

- Volume ratio (V): c = 0.3
- Diameter: d = 0.2768

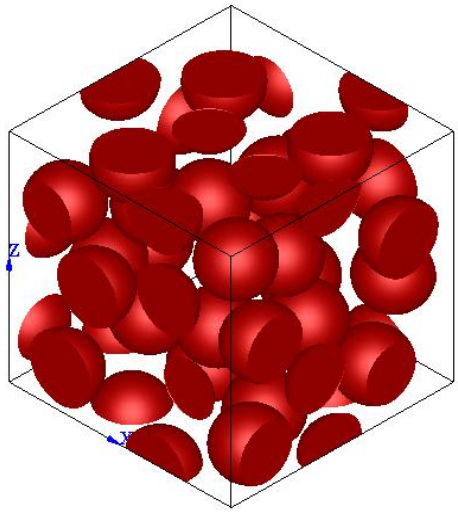

Inclusions	X	Y	Z	Inclusions	X	Y	Z
1.1	0.1818	0.4655	0.5683	14.1	0.8258	0.1951	0.8044
2.1	0.6597	0.0175	-0.0129	15.1	0.2383	0.7936	0.3719
2.2	0.6597	1.0176	-0.0129	16.1	0.7510	0.3982	0.0685
2.3	0.6597	1.0176	0.9871	16.2	0.7510	0.3982	1.0686
2.4	0.6597	0.0175	0.9871	17.1	0.4442	0.4562	1.0696
3.1	0.7795	0.4496	0.6706	17.2	0.4442	0.4562	0.0696
4.1	0.1691	1.0838	0.7609	18.1	0.6541	0.2844	0.4079
4.2	0.1691	0.0837	0.7609	19.1	0.0520	0.3823	0.3214
5.1	0.4512	0.7572	0.6612	19.2	1.0520	0.3823	0.3214
6.1	0.0359	0.4522	1.0012	20.1	0.7328	0.7126	0.9454
6.2	1.0359	0.4522	1.0012	20.2	0.7328	0.7126	-0.0546
6.3	1.0359	0.4522	0.0012	21.1	0.7907	0.5491	0.3716
6.4	0.0359	0.4522	0.0012	22.1	0.9195	0.7179	0.1730
7.1	0.4757	0.4244	0.7488	22.2	-0.0805	0.7179	0.1730
8.1	0.2573	0.7103	0.9711	23.1	0.3511	0.0281	0.5381
8.2	0.2573	0.7103	-0.0289	23.2	0.3511	1.0281	0.5381
9.1	0.5514	0.7512	0.3265	24.1	0.7039	-0.0379	0.6764
10.1	0.2304	0.0108	0.1630	24.2	0.7039	0.9621	0.6764
10.2	0.2304	1.0108	0.1630	25.1	0.9403	0.1958	0.5343
11.1	-0.0339	0.7977	0.6599	25.2	-0.0597	0.1958	0.5343
11.2	0.9661	0.7977	0.6599	26.1	0.3550	0.1984	0.9575
12.1	0.8093	-0.0797	0.3804	26.2	0.3550	0.1984	-0.0425
12.2	0.8093	0.9203	0.3804	27.1	0.9284	0.1570	0.1405
13.1	0.3712	0.2621	0.3309	27.2	-0.0716	0.1570	0.1405

V0.3Model1

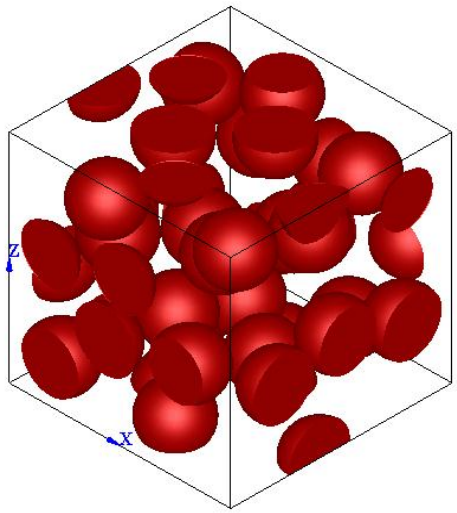

Inclusions	X	Y	Z	Inclusions	X	Y	Z
1.1	0.5721	0.1779	0.0697	15.1	0.5897	0.6123	0.9679
1.2	0.5721	0.1779	1.0697	15.2	0.5897	0.6123	-0.0321
2.1	0.9488	0.5317	0.4028	16.1	0.0008	0.4010	1.0079
2.2	-0.0512	0.5317	0.4028	16.2	1.0008	0.4010	1.0079
3.1	0.4860	0.2705	0.3943	16.3	1.0008	0.4010	0.0079
4.1	0.8323	0.1896	0.8523	16.4	0.0008	0.4010	0.0079
5.1	0.4311	-0.0157	0.3851	17.1	0.1838	0.0518	0.1688
5.2	0.4311	0.9843	0.3851	17.2	0.1838	1.0518	0.1688
6.1	0.3266	0.5520	0.5043	18.1	0.4179	0.6417	0.2355
7.1	-0.0229	0.2389	0.3595	19.1	0.0760	0.7978	0.8293
7.2	0.9771	0.2389	0.3595	19.2	1.0760	0.7978	0.8293
8.1	0.1849	0.6220	1.0580	20.1	0.6226	0.3389	0.6597
8.2	0.1849	0.6220	0.0580	21.1	0.3803	0.8527	-0.0803
9.1	0.8336	0.5289	0.7576	21.2	0.3803	0.8527	0.9197
10.1	0.2856	0.1556	0.7994	22.1	0.3578	0.3820	-0.0256
11.1	0.7523	1.0633	0.4208	22.2	0.3578	0.3820	0.9744
11.2	0.7523	0.0632	0.4208	23.1	0.1950	0.2949	0.5515
12.1	0.9581	0.8221	0.3181	24.1	0.7070	0.4492	0.2408
12.2	-0.0419	0.8221	0.3181	25.1	0.6045	0.6769	0.5678
13.1	0.7505	0.8372	0.7923	26.1	0.5097	-0.0406	0.6659
14.1	0.1811	0.9483	0.6011	26.2	0.5097	0.9594	0.6659
14.2	0.1811	-0.0517	0.6011	27.1	0.6852	0.8494	0.1765

V0.3Model2

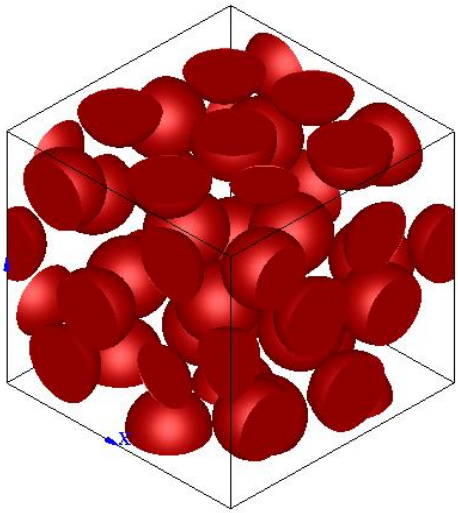

Inclusions	X	Y	Z	Inclusions	X	Y	Z
1.1	0.3589	0.0240	0.4600	14.1	-0.0035	0.3898	0.5604
1.2	0.3589	1.0240	0.4600	14.2	0.9965	0.3898	0.5604
2.1	0.7039	0.6107	0.2601	15.1	0.5536	0.1704	1.0126
3.1	0.5097	0.5037	0.9692	15.2	0.5536	0.1704	0.0126
3.2	0.5097	0.5037	-0.0308	16.1	0.8188	0.7141	0.9850
4.1	1.0467	0.6531	0.7478	16.2	0.8188	0.7141	-0.0150
4.2	0.0467	0.6531	0.7478	17.1	0.7883	0.3628	1.0829
5.1	0.2378	-0.0104	0.1916	17.2	0.7883	0.3628	0.0829
5.2	0.2378	0.9896	0.1916	18.1	0.3295	0.6868	0.3940
6.1	0.7755	0.4947	0.7346	19.1	0.3486	0.7837	0.7546
7.1	0.5104	0.3778	0.2985	20.1	0.3655	0.4377	0.5735
8.1	-0.0106	0.5530	0.1815	21.1	0.2041	1.0470	0.8493
8.2	0.9894	0.5530	0.1815	21.2	0.2041	0.0470	0.8493
9.1	0.9884	-0.0055	0.5517	22.1	0.9428	0.1688	0.2436
9.2	-0.0116	-0.0055	0.5517	22.2	-0.0572	0.1688	0.2436
9.3	-0.0116	0.9945	0.5517	23.1	0.7024	0.9298	0.3798
9.4	0.9884	0.9945	0.5517	23.2	0.7024	-0.0702	0.3798
10.1	0.1768	0.3290	1.0279	24.1	0.5338	0.8319	0.0398
10.2	0.1768	0.3290	0.0279	24.2	0.5338	0.8319	1.0398
11.1	0.7103	0.2351	0.5581	25.1	0.9247	0.2270	0.8012
12.1	0.2506	0.7226	0.0394	25.2	-0.0753	0.2270	0.8012
12.2	0.2506	0.7226	1.0394	26.1	0.9372	0.7302	0.4204
13.1	0.7255	-0.0383	0.8302	26.2	-0.0628	0.7302	0.4204
13.2	0.7255	0.9617	0.8302	27.1	0.1874	0.3554	0.3351

V0.3Model3

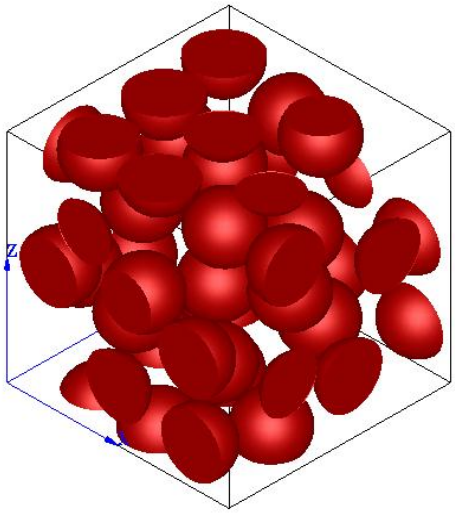

Inclusions	X	Y	Z	Inclusions	X	Y	Z
1.1	-0.0255	0.2956	0.8035	15.1	0.6454	0.3362	0.7743
1.2	0.9745	0.2956	0.8035	16.1	0.3478	-0.0678	0.7727
2.1	1.0581	0.2722	0.3597	16.2	0.3478	0.9322	0.7727
2.2	0.0581	0.2722	0.3597	17.1	0.4906	-0.0332	0.2301
3.1	0.6919	0.2502	0.3031	17.2	0.4906	0.9668	0.2301
4.1	0.8175	0.0210	0.4922	18.1	1.0188	0.5547	0.2450
4.2	0.8175	1.0210	0.4922	18.2	0.0188	0.5547	0.2450
5.1	0.2305	0.1879	-0.0537	19.1	0.8300	0.4460	0.5585
5.2	0.2305	0.1879	0.9463	20.1	0.8300	0.0245	0.1637
6.1	0.6461	0.7672	0.9235	20.2	0.8300	1.0245	0.1637
6.2	0.6461	0.7672	-0.0765	21.1	0.3449	0.6070	0.2741
7.1	0.1585	0.8207	0.3458	22.1	0.2019	0.5059	-0.0219
8.1	0.3682	0.2102	0.3655	22.2	0.2019	0.5059	0.9781
9.1	0.6323	0.6930	0.5671	23.1	0.3828	0.5993	0.7561
10.1	0.1906	0.4241	0.6069	24.1	0.5360	0.0795	0.5874
11.1	0.7450	0.6612	0.2992	24.2	0.5360	1.0795	0.5874
12.1	0.4950	0.4800	1.0514	25.1	0.5290	0.1573	1.0104
12.2	0.4950	0.4800	0.0514	25.2	0.5290	0.1573	0.0104
13.1	0.0309	0.7286	0.6370	26.1	0.1857	0.0491	0.5318
13.2	1.0309	0.7286	0.6370	26.2	0.1857	1.0491	0.5318
14.1	0.1811	0.7971	0.9860	27.1	0.8385	0.3522	1.0722
14.2	0.1811	0.7971	-0.0140	27.2	0.8385	0.3522	0.0722

V0.3Model4

Appendix B: Boundary conditions

A typical *.inp file is presented below, which is the input file of a uniaxial tension simulation with stiffness ratio of 10 for finite element analysis.

```
**----------------------------------------------------------------
*Heading
** Job name: test Model name: Analysis1
**Preprint, echo=NO, model=NO, history=NO, contact=NO
**Part, name=RVE
**----------------------------------------------------------------
**NODES
**----------------------------------------------------------------
*Node, nset=AllNodes, input=Allnodes.txt
**Dummy Nodes
*Node
     1000001,       1.10,         0.5,         0.5
*Node
     1000002,         0.5,       1.10,         0.5
*Node
     1000003,         0.5,         0.5,       1.10
*Nset, nset=refpoint4
 1000001,
*Nset, nset=refpoint5
 1000002,
*Nset, nset=refpoint6
 1000003,
**----------------------------------------------------------------
**ELEMENTS
**----------------------------------------------------------------
*Element, type=C3D10MH, elset=Matrix, input=EleMatrix.txt
*Element, type=C3D10MH, elset=Particle, input=ElePart.txt
**----------------------------------------------------------------
**Node set definitions
**----------------------------------------------------------------
**Node sets: surface (edges not included)
*nset, nset=Xinf, UNSORTED
*include, input=Surf1.txt
*nset, nset=Xsup, UNSORTED
*include, input=Surf2.txt
```

```
*nset, nset=Yinf, UNSORTED
*include, input=Surf3.txt
*nset, nset=Ysup, UNSORTED
*include, input=Surf4.txt
*nset, nset=Zinf, UNSORTED
*include, input=Surf5.txt
*nset, nset=Zsup, UNSORTED
*include, input=Surf6.txt
**Node sets: edge (corners not included)
**----------------------------------------
*nset, nset=Xaxis1, UNSORTED
*include, input=Edge1.txt
*nset, nset=Xaxis2, UNSORTED
*include, input=Edge2.txt
*nset, nset=Xaxis3, UNSORTED
*include, input=Edge3.txt
*nset, nset=Xaxis4, UNSORTED
*include, input=Edge4.txt
*nset, nset=Yaxis1, UNSORTED
*include, input=Edge5.txt
*nset, nset=Yaxis2, UNSORTED
*include, input=Edge6.txt
*nset, nset=Yaxis3, UNSORTED
*include, input=Edge7.txt
*nset, nset=Yaxis4, UNSORTED
*include, input=Edge8.txt
*nset, nset=Zaxis1, UNSORTED
*include, input=Edge9.txt
*nset, nset=Zaxis2, UNSORTED
*include, input=Edge10.txt
*nset, nset=Zaxis3, UNSORTED
*include, input=Edge11.txt
*nset, nset=Zaxis4, UNSORTED
*include, input=Edge12.txt
**----------------------------------------
**Node sets: corner
*nset, nset=Corner1, UNSORTED
*include, input=corner1.txt
*nset, nset=Corner2, UNSORTED
*include, input=corner2.txt
*nset, nset=Corner3, UNSORTED
*include, input=corner3.txt
```

```
*nset, nset=Corner4, UNSORTED
*include, input=corner4.txt
*nset, nset=Corner5, UNSORTED
*include, input=corner5.txt
*nset, nset=Corner6, UNSORTED
*include, input=corner6.txt
*nset, nset=Corner7, UNSORTED
*include, input=corner7.txt
*nset, nset=Corner8, UNSORTED
*include, input=corner8.txt
**----------------------------------------------------------------
**MATERIALS
**----------------------------------------------------------------
** Section: Material1_Section
*Solid Section, elset=Matrix, material=Material1
*Material, name=Material1
*Hyperelastic, neo hooke
 0.5, 0.0
** Section: Material2_Section
*Solid Section, elset=Particle, material=Material2
*Material, name=Material2
*Hyperelastic, neo hooke
 5., 0.0
**----------------------------------------------------------------
** PBC constraints: Equations
**----------------------------------------------------------------
*include, input=EqCorners.txt
*include, input=EqEdges.txt
*include, input=EqSurfaces.txt
**----------------------------------------------------------------
** STEPS: Step-1
**----------------------------------------------------------------
*Step, name=Step-1, nlgeom=YES
*Static
0.05, 1., 1e-03, 0.05
**----------------------------------------------------------------
** BOUNDARY CONDITIONS
**----------------------------------------------------------------
** Name: BC-1 Type: Displacement/Rotation
*Boundary
Corner1, 1, 3
Refpoint4, 2, 3
```

Refpoint5, 3, 3

Refpoint4, 1, 1, 1.0

**----------

** OUTPUT REQUESTS

**

*Restart, write, frequency=0

**

** FIELD OUTPUT: F-Output-1

**

*Output, field

*Node Output

RF, U

*Element Output, directions=YES

EVOL, IVOL, LE, NE, S

**

** HISTORY OUTPUT: H-Output-1

**

*Output, history, variable=PRESELECT

*End Step

Appendix C: Brief introduction of Bass's experiments [81]

In order to evaluate the theory described in section 4.2, experimental results are needed to verify the theoretical analysis. As a matter of fact, experiments carried on biological tissues must follow extremely strict protocols, and require many precise devices and special laboratory, so it is impossible and impractical to repeat the experiments by ourselves.

As mentioned in Chapter 4, the experimental data adopted from Bass et al [81] are in vitro experiment results of uniaxial and biaxial tension of Human Annulus Fibrosus (HAF). In this experiment, specimens from five different human spines were processed and prepared beforehand. In order to make sure that the spines from donors were normal and physiological healthy, certain examinations had been carried out before and after harvest. Bones connected by the annulus were conserved for the sake of maximizing the specimen height and mimicking the physical load state. The original annulus thickness of each specimen was measured and average thickness was calculated and applied in the later analysis. Summary of the specimens' preparation steps is presented below:

1. Harvest, freeze and X-ray the human spines;
2. Separate and section the vertebrae and remove attached soft tissue;
3. Cut thin slices from the front side of the rest of the disc;
4. Cut these slices again in the vertical direction to the previous cutting interface;
5. Remove redundant bones and tissues to obtain the final specimens;
6. Select qualified specimens for the experiments.

The schematic procedure of preparing specimens is shown in Figure C1 (Figure 1 in Bass et al.[81]). During the experiment, the specimens were immersed in physiological saline. The schematic diagram of the biaxial testing devices is shown in Figure C2 (Figure 2 in Bass et al.[81]). Prerequisite loading cycles were necessary for each specimen to eliminate the pseudo-strain and identify a relatively stable initial condition. Two specimens among the five were applied uniaxial tensile loading along the axial directions; for the rest of the specimens, biaxial tensile tests were carried out. Each sample was preloaded with a series of strains ($E_{22} = 0.0, \pm 0.0125, \pm 0.025, +0.0375,$

respectively) on the circumferential directions, and tensile force was measured as the specimen was stretched along the axial direction. Here the circumferential direction is the 2-direction and tensile direction is the 1-direction, which are presented in Figure C1. The specimens were left still for fifteen minutes during every preload strain case, which helped it back to the equilibrium state.

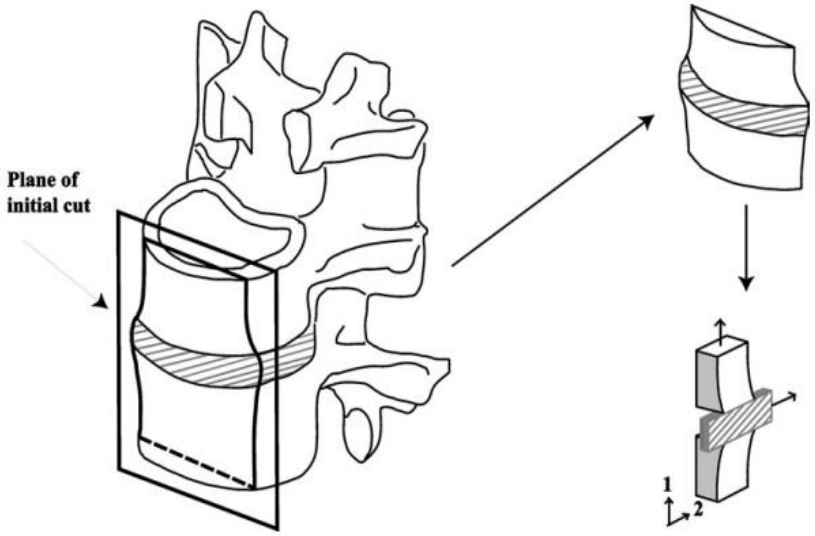

Figure C1 Schematic diagram of specimens' preparation steps

With the help of commercial software Image J (http://rsbweb.nih.gov/ij/), the uniaxial and biaxial tests data were digitalized from the figures shown in the paper and strain energy of the ground matrix with collagen fibres under different stretch ratios, which are later adopted to compare with the FE simulation results to verify the existence of fibre-matrix interaction.

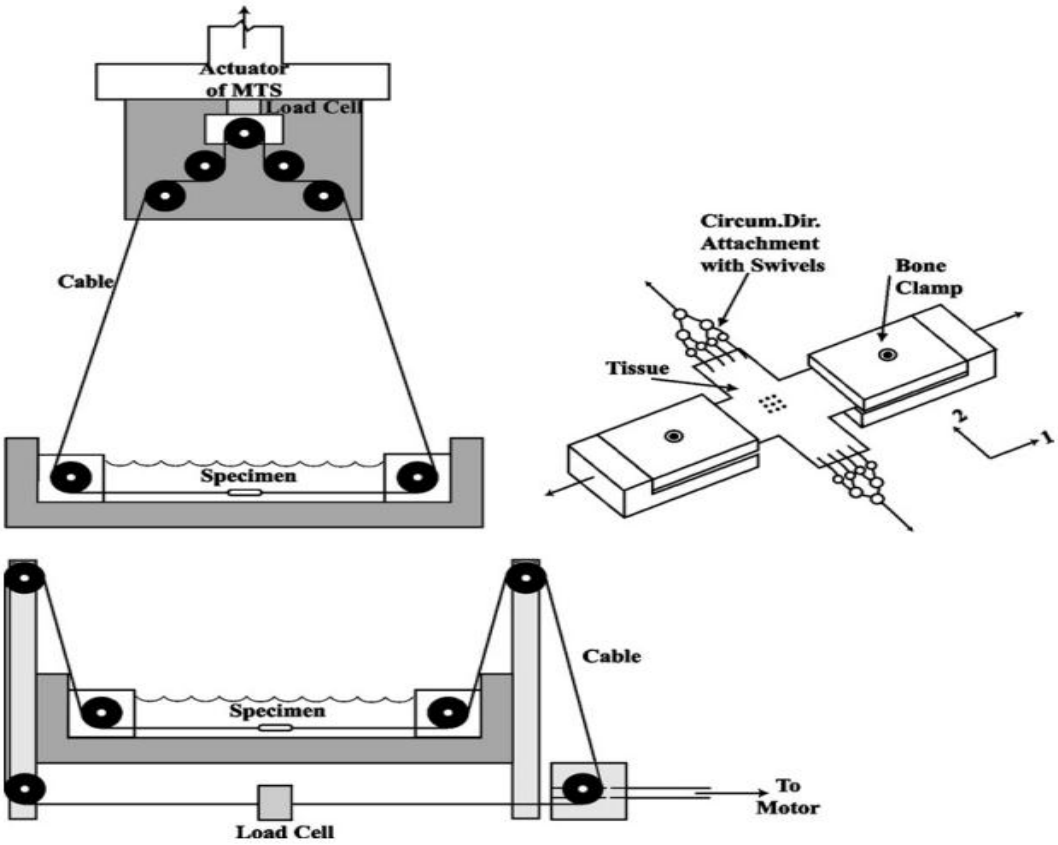

Figure C2 Schematic diagram of biaxial testing device

Reference

1. Daniel, I. and O. Ishai, *Engineering mechanics of composite materials*. 2006: Oxford University Press.
2. Holliday, L., *Composite materials*. 1966: Elsevier Pub. Co.
3. Hu, X. and S. Chen, *Present status of polymer composites & perspective of basalt fiber*. Hi-Tech Fiber & Application, 2005. 30(3): p. 9-12.
4. Guth, E., *Theory of filler reinforcement*.. Journal of Applied Physics, 1945. 16(1): p. 20-25.
5. Hull, D., *An introduction to composite materials*. Cambridge solid state science series, ed. T.W. Clyne. 1981, Cambridge University Press: Cambridge.
6. Guo, Z.Y., X.Q. Peng, and B. Moran, *A composites-based hyperelastic constitutive model for soft tissue with application to the human annulus fibrosus.* Journal of the Mechanics and Physics of Solids, 2006. 54(9): p. 1952-1971.
7. Peng, X.Q., Z.Y. Guo, and B. Moran, *An anisotropic hyperelastic constitutive model with fiber-matrix shear interaction for the human annulus fibrosus.* Journal of Applied Mechanics-Transactions of the Asme, 2006. 73(5): p. 815-824.
8. Paul, B., *Prediction of Elastic Constants of Multiphase Materials.* Transactions of the American Institute of Mining and Metallurgical Engineers, 1960. 218(1): p. 36-41.
9. Hashin, Z. and B.W. Rosen, *The Elastic Moduli of Fiber Reinforced materials.* Journal of Applied Mechanics, 1964. 31: p. 223-232.
10. Hashin, Z. and S. Shtrikman, *A variational approach to the theory of the elastic behaviour of multiphase materials.* Journal of the mechanics and physics of solids, 1963. 11(2): p. 127-140.
11. Milton, G.W. and R.V. Kohn, *Variational bounds on the effective moduli of anisotropic composites.* Journal of the mechanics and physics of solids, 1988. 36(6): p. 597-629.
12. Hill, R., *Theory of Mechanical Properties of Fibre-Strengthened Materials .3. Self-Consistent Model.* Journal of the Mechanics and Physics of Solids, 1965. 13(4): p. 189-198.
13. Hill, R., *A Self-Consistent Mechanics of Composite Materials.* Journal of the Mechanics and Physics of Solids, 1965. 13(4): p. 213-222.

14. Hill, R., *Elastic Properties of Reinforced Solids - Some Theoretical Principles.* Journal of the Mechanics and Physics of Solids, 1963. 11(5): p. 357-372.
15. Hill, R., *Theory of Mechanical Properties of Fibre-Strengthened Materials .1. Elastic Behaviour.* Journal of the Mechanics and Physics of Solids, 1964. 12(4): p. 199-212.
16. Hill, R., *Theory of Mechanical Properties of Fibre-Strengthened Materials .2. Inelastic Behaviour.* Journal of the Mechanics and Physics of Solids, 1964. 12(4): p. 213-218.
17. Whitney, J.M. and M.B. Riley, *Elastic properties of fibre reinforced composite materials Materials.* Aiaa Journal, 1966. 4(9): p. 1537.
18. Christensen, R.M. and K.H. Lo, *Solutions for effective shear properties in three phase sphere and cylinder models.* Journal of the mechanics and physics of solids, 1979. 27(4): p. 315-330.
19. Christensen, R.M. and K.H. Lo, *Erratum: Solutions for effective shear properties in three phase sphere and cylinder models.* Journal of the mechanics and physics of solids, 1986. 34(6): p. 639-639.
20. Mori, T. and K. Tanaka, *Average stress in matrix and average elastic energy of materials with misfitting inclusions.* Acta Metallurgica, 1973. 21(5): p. 571-574.
21. Theocaris, P.S. and E. Sideridis, *The elastic moduli of particulate-filled polymers.* Journal of Applied Polymer Science, 1984. 29(10): p. 2997-3011.
22. Ravichandran, K.S., *Elastic properties of 2-phase composites.* Journal of the American Ceramic Society, 1994. 77(5): p. 1178-1184.
23. Bourkas, G., Prassianakis, I., Kytopoulos, V., Sideridis, E. and Younis, C., *Estimation of Elastic Moduli of Particulate Composites by New Models and Comparison with Moduli Measured by Tension, Dynamic, and Ultrasonic Tests.* Advances in Materials Science and Engineering, 2010.
24. Torquato, S., *Effective stiffness tensor of composite media .1. Exact series expansions.* Journal of the mechanics and physics of solids, 1997. 45(9): p. 1421-1448.
25. Torquato, S., *Effective stiffness tensor of composite media: II. Applications to isotropic dispersions.* Journal of the mechanics and physics of solids, 1998. 46(8): p. 1411-1440.
26. Jiang, C.P., Z.H. Tong, and Y.K. Cheung, *A generalized self-consistent method accounting for fiber section shape.* International journal of solids and structures, 2003. 40(10): p. 2589-2609.

27. Ju, J.W. and K. Yanase, *Micromechanics and effective elastic moduli of particle-reinforced composites with near-field particle interactions.* Acta Mechanica, 2010. 215(1-4): p. 135-153.
28. Halpin, J.C. and J.L. Kardos, *Halpin-Tsai Equations - Review.* Polymer Engineering and Science, 1976. 16(5): p. 344-352.
29. Jaensson, B.O. and Sundstro.Bo, *Determination of Young's Modulus and Poission's Ratio for WC-CO alloys by finite element method.* Materials Science and Engineering, 1972. 9(4): p. 217.
30. Tessier-Doyen, N., J.C. Glandus, and M. Huger, *Experimental and numerical study of elastic behavior of heterogeneous model materials with spherical inclusions.* Journal of Materials Science, 2007. 42(14): p. 5826-5834.
31. Segurado, J. and J. Llorca, *A numerical approximation to the elastic properties of sphere-reinforced composites.* Journal of the Mechanics and Physics of Solids, 2002. 50(10): p. 2107-2121.
32. Hill, R., *The essential structure of constitutive laws for metal composites and polycrystals.* Journal of the mechanics and physics of solids, 1967. 15(2): p. 79-95.
33. Drugan, W.J. and J.R. Willis, *A micromechanics-based nonlocal constitutive equation and estimates of representative volume element size for elastic composites.* Journal of the mechanics and physics of solids, 1996. 44(4): p. 497-524.
34. Drugan, W.J., *Micromechanics-based variational estimates for a higher-order nonlocal constitutive equation and optimal choice of effective moduli for elastic composites.* Journal of the mechanics and physics of solids, 2000. 48(6-7): p. 1359-1387.
35. Tarnopolskii, Y.M. and T. Kincis, *Static test methods for composites*. 1985: Van Nostrand Reinhold. xvii,301p.
36. Hodgkinson, J.M., *Mechanical testing of advanced fibre composites*. 2000: CRC Press.
37. Adams, D.F., L.A. Carlsson, and R.B. Pipes, *Experimental characterization of advanced composite materials*. 2003: CRC Press.
38. *The composite materials handbook-MIL 17*. 1998, Lancaster, Pa.: Technomic. 1 computer optical disc.
39. Murray, M.J., *Fracture of WC-CO alloys-example of spatially Constrained crack tip opening displacement.* Proceedings of the Royal Society of London

Series a-Mathematical Physical and Engineering Sciences, 1977. 356(1687): p. 483-508.

40. Doi, H., Fujiwara, Y., Miyake, K. and Ossawa, Y., *A systematic investigation of elastic moduli of WC-CO alloys.* Metallurgical Transactions, 1970. 1(5): p. 1417.
41. Braem, M., Vandoren, V. E., Lambrechts, P. and Vanherle, G., *Determination of Young's Modulus of dental composites - a phenomenological model.* Journal of Materials Science, 1987. 22(6): p. 2037-2042.
42. Ibrahim, I.A., F.A. Mohamed, and E.J. Lavernia, Particulate *reinforced mental matrix composites - a review.* Journal of Materials Science, 1991. 26(5): p. 1137-1156.
43. Smith, J.C., *Elastie-constants of a particulate-filled glassy polymer - comparison of experimental values with theoretical predictions.* Polymer Engineering and Science, 1976. 16(6): p. 394-399.
44. Smith, J.C., *Experimental values for elastic-constants of a particulate-filled glassy polymer.* Journal of Research of the National Bureau of Standards Section a-Physics and Chemistry, 1976. 80(1): p. 45-49.
45. Hasselma.Dp and R.M. Fulrath, *Effect of alumina dispersions on Young's Modulus of a glass.* Journal of the American Ceramic Society, 1965. 48(4): p. 218.
46. Hasselma.Dp and R.M. Fulrath, *Effect of spherical tungsten dispersions on Young's Modulus of a glass.* Journal of the American Ceramic Society, 1965. 48(10): p. 548.
47. Ishai, O. and L.J. Cohen, *Elastic properties of filled and porous epoxy composites.* International Journal of Mechanical Sciences, 1967. 9(8): p. 539-546.
48. Tsai, C.L. and I.M. Daniel, *Method for thermo-mechanical characterization of single fibers.* Composites Science and Technology, 1994. 50(1): p. 7-12.
49. Singh, R.N. and M. Sutcu, *Determination of fibre-matrix interfacial properties in ceramic-matrix composites by a fibre push-out technique.* Journal of Materials Science, 1991. 26(9): p. 2547-2556.
50. Hill, R., *Constitutive macro-variables for heterogeneous solids at finite strain.* Proceedings of the Royal Society of London Series a-Mathematical and Physical Sciences, 1972. 326(1565): p. 131.
51. Ogden, R., *Large Deformation Isotropic Elasticity - On the Correlation of Theory and Experiment for Incompressible Rubberlike Solids.* Proceedings of

the Royal Society of London. Series A, Mathematical and Physical Sciences (1934-1990), 1972. 326(1567): p. 565-584.

52. Hashin, Z., *Large Isotropic Elastic-Deformation of Composites and Porous-Media.* International Journal of Solids and Structures, 1985. 21(7): p. 711-720.
53. Castaneda, P.P., *The overall constitutive behavior of nonlinearly elastic composites.* Proceedings of the Royal Society a-Mathematical Physical and Engineering Sciences, 1989. 422(1862): p. 147-171.
54. Imam, A., G.C. Johnson, and M. Ferrari, *Determination of the overall moduli in second-order incompressible elasticity.* Journal of the mechanics and physics of solids, 1995. 43(7): p. 1087-1104.
55. Castaneda, P.P. and E. Tiberio, *Homogenization estimates for hyperelastic composites and particle-reinforced rubbers.* Comptes Rendus De L Academie Des Sciences Serie Ii Fascicule B-Mecanique Physique Astronomie, 1999. 327(13): p. 1297-1304.
56. Lopez-Pamies, O. and P.P. Castaneda, *Second-order estimates for the large-deformation response of particle-reinforced rubbers.* Comptes Rendus Mecanique, 2003. 331(1): p. 1-8.
57. Lopez-Pamies, O. and P.P. Castaneda, *Second-order homogenization estimates incorporating field fluctuations in finite elasticity.* Mathematics and Mechanics of Solids, 2004. 9(3): p. 243-270.
58. Lopez-Pamies, O. and P. Ponte Castaneda, *Second-order estimates for the macroscopic response and loss of ellipticity in porous rubbers at large deformations.* Journal of Elasticity, 2004. 76(3): p. 247-287.
59. Lopez-Pamies, O. and P.P. Castaneda, *On the overall behavior, microstructure evolution, and macroscopic stability in reinforced rubbers at large deformations: I - Theory.* Journal of the Mechanics and Physics of Solids, 2006. 54(4): p. 807-830.
60. Lopez-Pamies, O. and P.P. Castaneda, *On the overall behavior, microstructure evolution, and macroscopic stability in reinforced rubbers at large deformations: II - Application to cylindrical fibers.* Journal of the Mechanics and Physics of Solids, 2006. 54(4): p. 831-863.
61. Moraleda, J., J. Segurado, and J. Llorca, *Finite deformation of incompressible fiber-reinforced elastomers: A computational micromechanics approach.* Journal of the mechanics and physics of solids, 2009. 57(9): p. 1596-1613.

62. Bergstrom, J.S. and M.C. Boyce, *Mechanical behavior of particle filled elastomers.* Rubber Chemistry and Technology, 1999. 72(4): p. 633-656.
63. Khisaeva, Z.F. and M. Ostoja-Starzewski, *On the size of RVE in finite elasticity of random composites.* Journal of elasticity, 2006. 85(2): p. 153-173.
64. Chen, C., T.J. Lu, and N.A. Fleck, *Effect of imperfections on the yielding of two-dimensional foams.* Journal of the mechanics and physics of solids, 1999. 47(11): p. 2235-2272.
65. Einstein, A. and R. Fürth, *Investigation on Theory of Brownian Motion.* Dover Publications, inc., 1956.
66. Smallwood, H., *Limiting Law of the Reinforcement of Rubber.* J. Appl. Phys., 1944. 15(11): p. 758.
67. Eshelby, J.D., *The Determination of the Elastic Field of an Ellipsoidal Inclusion, and Related Problems.* Proceedings of the Royal Society of London. Series A. Mathematical and Physical Sciences, 1957. 241(1226): p. 376-396.
68. Kerner, E.H., *The Elastic and Thermo-elastic Properties of Composite Media.* Proceedings of the Physical Society. Section B, 1956. 69(8): p. 808.
69. Michel, J.C., H. Moulinec, and P. Suquet, *Effective properties of composite materials with periodic microstructure: a computational approach.* Computer Methods in Applied Mechanics and Engineering, 1999. 172(1-4): p. 109-143.
70. Ball, J.M., *Constitutive inequalities and existence theorems in nonlinear elastostatics*, in *Nonlinear analysis and mechanics: Heriot-Watt Symposium (Edinburgh, 1976), Vol. I*. 1977, Pitman.
71. Dacorogna, B., *Remarques sur les Notions de Polyconvexité, Quasi- Convexité et Convexité de Rang.* J. Math. Pures Appl., 1985. 64: p. 403-438.
72. Kohn, R.V. and G. Strang, *Optimal design and relaxation of variational problems, I.* Communications on Pure and Applied Mathematics, 1986. 39(1): p. 113-137.
73. Mullins, L. and N.R. Tobin, *Stress softening in rubber vulcanizates. Part i. use of a strain amplification factor to describe the elastic behavior of filler-reinforced vulcanized rubber.* J. Appl. Polym. Sci., 1957. 9: p. 2993-3009.
74. Smallwood, H.M., *Llimiting law of the reinforcement of rubber.* J. Appl. Phys., 1944. 15: p. 758-766.
75. Einstein, A., *Eine neue Bestimmung der Molekul-dimensionen.* Ann. d. Physik, 1906. 19: p. 289.

76. Guth, E. and O. Gold, *On the hydrodynamical theory of the viscosity of suspensions.* Phys. Rev., 1938. 53: p. 322.
77. Govindjee, S. and J. Simo, *A micro-mechanically based continuum damage model for carbon black-filled rubbers incorporating mullins effect.* Journal of the mechanics and physics of solids, 1991. 39(1): p. 87-112.
78. Fung, Y.C., K. Fronek, and P. Patitucci, *Pseudoelasticity of Arteries and the Choice of Its Mathematical Expression.* American Journal of Physiology, 1979. 237(5): p. H620-H631.
79. Federico, S., Grillo, A., Giaquinta, G. and Herzog, W., *Convex Fung-type potentials for biological tissues.* Meccanica, 2008. 43(3): p. 279-288.
80. Walton, J.R. and J.P. Wilber, *Sufficient conditions for strong ellipticity for a class of anisotropic materials.* International Journal of Non-Linear Mechanics, 2003. 38(4): p. 441-455.
81. Bass, E.C., Ashford, F. A., Segal, M. R. and Lotz, J. C., *Biaxial testing of human annulus fibrosus and its implications for a constitutive formulation.* Annals of Biomedical Engineering, 2004. 32(9): p. 1231-1242.
82. Criscione, J.C., A.S. Douglas, and W.C. Hunter, *Physically based strain invariant set for materials exhibiting transversely isotropic behavior.* Journal of the Mechanics and Physics of Solids, 2001. 49(4): p. 871-897.
83. Holzapfel, G.A., T.C. Gasser, and R.W. Ogden, *A new constitutive framework for arterial wall mechanics and a comparative study of material models.* Journal of Elasticity, 2000. 61(1-3): p. 1-48.
84. Quapp, K.M. and J.A. Weiss, *Material characterization of human medial collateral ligament.* Journal of Biomechanical Engineering-Transactions of the Asme, 1998. 120(6): p. 757-763.
85. Gasser, C.T., R.W. Ogden, and G. Holzapfel, *Hyperelastic modelling of arterial layers with distributed collagen fibre orientations.* Journal of the Royal Society interface, 2006. 3(6): p. 15-35.
86. Blemker, S.S., P.M. Pinsky, and S.L. Delp, *A 3D model of muscle reveals the causes of nonuniform strains in the biceps brachii.* Journal of Biomechanics, 2005. 38(4): p. 657-665.
87. Spencer, A.J.M., *Continuum theory of the mechanics of fibre-reinforced composites*. Courses and lectures / International Centre for Mechanical Sciences ; no. 282. 1984, Wein ; New York: Springer-Verlag. viii, 284.

88. Holzapfel, G.A., Schulze-Bauer, C. A. J., Feigl, G. and Regitnig, P., *Single lamellar mechanics of the human lumbar anulus fibrosus.* Biomechanics and Modeling in Mechanobiology, 2005. 3(3): p. 125-140.
89. Caner, F.C., Guo, Z., Moran, B., Bazant, Z. P. and Carol, I., *Hyperelastic anisotropic microplane constitutive model for annulus fibrosus.* Journal of Biomechanical Engineering-Transactions of the Asme, 2007. 129(5): p. 632-641.
90. deBotton, G., I. Hariton, and E.A. Socolsky, *Neo-Hookean fiber-reinforced composites in finite elasticity.* Journal of the Mechanics and Physics of Solids, 2006. 54(3): p. 533-559.
91. Guo, Z.Y., X.Q. Peng, and B. Moran, *Large deformation response of a hyperelastic fibre reinforced composite: Theoretical model and numerical validation.* Composites Part a-Applied Science and Manufacturing, 2007. 38(8): p. 1842-1851.
92. Kouznetesova, V., *Computational homogenization for the multi-scale analysis of multi-phase materials*. 2002, Eindhoven University of Technology.
93. Adams, M.A. and T.P. Green, *Tensile properties of the annulus fibrosus.* Europe Spine Journal, 1993. 2: p. 203-208.
94. Cohen, I., *Simple algebraic approximations for the effective elastic moduli of cubic arrays of spheres.* Journal of the mechanics and physics of solids, 2004. 52(9): p. 2167-2183.
95. Ogden, R.W., *Overall moduli of nonlinear elastic composit-materials.* Journal of the mechanics and physics of solids, 1974. 22(6): p. 541-553.
96. Lopez-Pamies, O., *An Exact Result for the Macroscopic Response of Particle-Reinforced Neo-Hookean Solids.* Journal of Applied Mechanics, 2010. 77(2): p. 021016.
97. Guo, Z.Y., Caner, F., Peng, X. Q. and Moran, B., *On constitutive modelling of porous neo-Hookean composites.* Journal of the mechanics and physics of solids, 2008. 56(6): p. 2338-2357.
98. Moraleda, J., J. Segurado, and J. Llorca, *Finite deformation of porous elastomers: a computational micromechanics approach.* Philosophical Magazine, 2007. 87(35): p. 5607-5627.
99. Hohe, J. and W. Becker, *Geometrically nonlinear stress-strain behavior of hyperelastic solid foams.* Computational Materials Science, 2003. 28(3-4): p. 443-453.

100. Demiray, S., W. Becker, and J. Hohe, *Analysis of two- and three-dimensional hyperelastic model foams under complex loading conditions.* Mechanics of Materials, 2006. 38(11): p. 985-1000.
101. ABAQUS, *Analysis User's Manual, Version 6.10*. 2010: SIMULIA Inc.
102. Segurado, J. and J. LLorca, *Computational micromechanics of composites: The effect of particle spatial distribution.* Mechanics of Materials, 2006. 38(8-10): p. 873-883.
103. Segurado, J. and J. Llorca, *A computational micromechanics study of the effect of interface decohesion on the mechanical behavior of composites.* Acta Materialia, 2005. 53(18): p. 4931-4942.
104. Miehe, C., J. Schroder, and M. Becker, *Computational homogenization analysis in finite elasticity: material and structural instabilities on the micro- and macro-scales of periodic composites and their interaction.* Computer Methods in Applied Mechanics and Engineering, 2002. 191(44): p. 4971-5005.
105. Stokes, I.A.F. and J.C. Iatridis, *Mechanical conditions that accelerate intervertebral disc degeneration: Overload versus immobilization.* Spine, 2004. 29(23): p. 2724-2732.
106. Wu, H.C. and R.F. Yao, *Mechanical-Behavior of Human Annulus Fibrosis.* Journal of Biomechanics, 1976. 9(1): p. 1-7.
107. Galante, J.O., *Tensile Properties of Human Lumbar Annulus Fibrosus.* Acta Orthopaedica Scandinavica, 1967: p. Suppl 100:1-91.
108. Rao, A.A. and G.A. Dumas, *Influence of Material Properties on the Mechanical-Behavior of the L5-S1 Intervertebral-Disk in Compression - a Nonlinear Finite-Element Study.* Journal of Biomedical Engineering, 1991. 13(2): p. 139-151.
109. Tong, P. and Y.C. Fung, *Stress-Strain Relationship for Skin.* Journal of Biomechanics, 1976. 9(10): p. 649-657.
110. Wilber, J.P. and J.R. Walton, *The convexity properties of a class of constitutive models for biological soft issues.* Mathematics and Mechanics of Solids, 2002. 7(3): p. 217-235.
111. Weiss, J.A. and J.C. Gardiner, *Computational modeling of ligament mechanics.* Critical Reviews in Biomedical Engineering, 2001. 29(3): p. 303-371.
112. Humphrey, J.D., *Continuum biomechanics of soft biological tissues.* Proceedings of the Royal Society of London Series a-Mathematical Physical and Engineering Sciences, 2003. 459(2029): p. 3-46.

113. Carol, I., M. Jirasek, and Z.P. Bazant, *A framework for microplane models at large strain, with application to hyperelasticity.* International Journal of Solids and Structures, 2004. 41(2): p. 511-557.
114. Caner, F.C. and I. Carol, *Microplane constitutive model and computational framework for blood vessel tissue.* Journal of Biomechanical Engineering-Transactions of the Asme, 2006. 128(3): p. 419-427.
115. Fujita, Y., Wagner, D. R., Biviji, A. A., Duncan, N. A. and Lotz, J. C., *Anisotropic shear behavior of the annulus fibrosus: effect of harvest site and tissue prestrain.* Medical Engineering & Physics, 2000. 22(5): p. 349-357.
116. deBotton, G. and I. Hariton, *Out-of-plane shear deformation of a neo-Hookean fiber composite.* Physics Letters A, 2006. 354(1-2): p. 156-160.
117. Guo, Z.Y., X.Q. Peng, and B. Moran, *Mechanical response of neo-Hookean fiber reinforced incompressible nonlinearly elastic solids.* International Journal of Solids and Structures, 2007. 44(6): p. 1949-1969.
118. Sacks, M.S., *Biaxial mechanical evaluation of planar biological materials.* Journal of Elasticity, 2000. 61(1-3): p. 199-246.
119. Wagner, D.R. and J.C. Lotz, *Theoretical model and experimental results for the nonlinear elastic behavior of human annulus fibrosus.* Journal of Orthopaedic Research, 2004. 22(4): p. 901-909.
120. Weiss, J.A., J.C. Gardiner, and C. Bonifasi-Lista, *Ligament material behavior is nonlinear, viscoelastic and rate-independent under shear loading.* Journal of Biomechanics, 2002. 35(7): p. 943-950.
121. Eberlein, R., G.A. Holzapfel, and M. Frohlich, *Multi-segment FEA of the human lumbar spine including the heterogeneity of the annulus fibrosus.* Computational Mechanics, 2004. 34(2): p. 147-163.
122. Baer, E., J.J. Cassidy, and A. Hiltner, *Hierarchical Structure of Collagen Composite Systems - Lessons from Biology.* Pure and Applied Chemistry, 1991. 63(7): p. 961-973.
123. Elliott, D.M. and L.A. Setton, *Anisotropic and inhomogeneous tensile behavior of the human anulus fibrosus: Experimental measurement and material model predictions.* Journal of Biomechanical Engineering-Transactions of the Asme, 2001. 123(3): p. 256-263.
124. Acaroglu, E.R., Iatridis, J. C., Setton, L. A., Foster, R. J., Mow, V. C. and Weidenbaum, M., *Degeneration and aging affect the tensile behavior of human lumbar anulus fibrosus.* Spine, 1995. 20(24): p. 2690-2701.

125. Schroeder, Y., Elliott, D. M., Wilson, W., Baaijens, F. P. T. and Huyghe, J. M., *Experimental and model determination of human intervertebral disc osmoviscoelasticity.* Journal of Orthopaedic Research, 2008. 26(8): p. 1141-1146.

126. Humphrey, J.D., R.L. Barazotto, and W.C. Hunter, *Finite Extension and Torsion of Papillary-Muscles - a Theoretical Framework.* Journal of Biomechanics, 1992. 25(5): p. 541-547.